The RESEARCH LABORATORY

of

ELECTRONICS

at the

MASSACHUSETTS INSTITUTE OF TECHNOLOGY
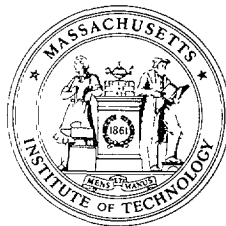CAMBRIDGE, MASSACHUSETTS 02139

Touch Lab Report 9

**Identification and Control of Haptic Systems:
A Computational Theory**

Steingrimur Pall Karason, Anurudha M. Annaswamy,
and Mandayam A. Srinivasan

RLE Technical Report No. 621

January 1998

Touch Lab Report 9

Identification and Control of Haptic Systems:
A Computational Theory

Steingrimur Pall Karason, Anurudha M. Annaswamy,
and Mandayam A. Srinivasan

RLE Technical Report No. 621

January 1998

The Research Laboratory of Electronics
MASSACHUSETTS INSTITUTE OF TECHNOLOGY
CAMBRIDGE, MASSACHUSETTS 02139-4307

Identification and Control of Haptic Systems :
A Computational Theory

by

Steingrímur Páll Kárason

Submitted to the Department of Mechanical Engineering
on February 5th, 1997, in partial fulfillment of the
requirements for the degree of
Doctor of Science

Abstract

This thesis provides a theoretical framework for haptics, the study of exploration and manipulation using hands. Be it human or robotic research, an understanding of the nature of contact, grasp, exploration, and manipulation is of singular importance. In human haptics the objective is to understand the mechanics of hand actions, sensory information processing, and motor control. While robots have lagged behind their human counterparts in dexterity, recent developments in tactile sensing technology have made it possible to build sensor arrays that in some way mimic human performance. We believe that a computational theory of haptics, that investigates what kind of sensory information is necessary and how it has to be processed is beneficial to both human and robotic research.

Human and robot tactile sensing can be accomplished by arrays of mechanosensors embedded in a deformable medium. When an object comes in contact with the surface of the medium, information about the shape of the surface of the medium and the force distribution on the surface is encoded in the sensor signals. The problem for the central processor is to reliably and efficiently infer the object properties and the contact state from these signals. In the first part of the thesis we discuss the surface signal identification problem: the processing of sensor signals resulting in algorithms and guidelines for sensor design that give optimal estimates of the loading and displacement distributions on the surface of the fingerpad.

In the second part of the thesis we focus on how the information obtained from such optimal sensing can be used for exploration of objects. We argue that an accurate reconstruction of object properties can occur using two basic building blocks of Exploration Strategy and Finger Control. Exploration Strategy pertains to the problem of inferring object properties such as shape, texture and compliance and interface properties such as state of contact, from the estimated surface signals. This involves determining, in each case, what kind of sensor information and what kind of action is needed. Finger Control refers to the transformation of the action needed into a command trajectory for the fingerpad, which defines the desired direction of movement for manipulation. We define and anlyze the components of both these blocks, provide explicit mathematical formulation, and give numerical examples where appropriate. Our formulation of this computational theory of haptics is independent of implementation so that it is applicable to both robots and humans.

Thesis Supervisor: Anuradha M. Annaswamy
Title: Associate Professor

4

Contents

List of Figures

9

List of Tables

Chapter 1

Introduction

Compared to vision and hearing, we might attach less importance to the sense of touch, primarily because the former senses can easily be temporarily occluded and we are therefore more aware of their presence. We therefore tend to underestimate the importance of the sense of touch but on second thought we realize that without it, our life would be much harder and possibly more difficult than without vision or hearing [48]. We apply touch for almost any activity involving direct interaction with our environment and in robotic research it has been observed that controlling this interaction is very difficult without tactile information. The research into the nature of tactile sensing has been conducted more or less separately in the fields of robotics and physiology, but the primary difference between these fields lies only the implementation. We however believe that a common framework and theory can be constructed, revealing the limitations and possibilities of touch and manipulation and further explicitly formulating the information processing involved.

The use of the word *Haptics* used in the title of this thesis is primarily confined to a circle of people working on tactile sensing research and in other related areas. The term refers to the mechanics and the information processing involved in tactual exploration, manipulation and perception, and it is used in robotic as well as physiological circles. A computational theory of haptics is then a formulation of the relevant information transfer and processing and will necessary include mechanistic as well as signal processing models. This formulation is the primary subject of this thesis. The problems we concentrate on, are (i) the mechanical modeling of compliant fingerpads, (ii) the information processing of signals from strain or stress sensors embedded in the fingerpad, (iii) the inference of object and environment properties from these signals, and finally (iv) the relation of the above to the movement of hands and fingers during haptic exploration.

The contributions of this thesis can be summarized as the presentation of a computational

theory of touch, which we can itemize as:

1. A complete solution for a 3D linear model of the fingerpad with general normal and shear loading distributions, also including elastic, viscous and inertial effects.

2. Transfer function formulation of the above solution, an approach that provides access to well developed and effective signal processing tools such as the Fast Fourier Transform (FFT) and the Kalman and Wiener filters which we evoke to decode surface signals from subsurface sensor signals.

3. We present an optimal set of sensors selected from all linear strains and stresses. So as to obtain maximum spatial bandwidth in the sensor signals without a directional bias.

4. A detailed framework delineating definitions and providing consistent formulation of exploratory procedures and control strategies that can be used for the identification of object properties such as shape, texture and compliance.

The thesis is composed of four, largely independent chapters in addition to appendices, each discussing a specific aspect of the above problem. The chapters are designed so that they can read as independent papers. Therefore, a more detailed introduction and background information such as literature review, are to be found in the introduction part of each chapter, and we refer the reader to those sections for that information. Chapter 2 is slightly different, in that it concentrates on giving tutorial information, primarily on the mathematical methods and tools used in subsequent chapters. Some parts of that chapter may therefore be repeated later in the thesis, but then in order to preserve the continuity within and independence of each chapter.

Chapterwise the thesis is organized as follows: Chapter 2 contains a tutorial on the mathematical methods applied in the subsequent chapters. In chapter 3 we present a model valid under static or quasi-static conditions and where we further show how our methods can be applied to predict the onset of slip before the finger starts to slide. In chapter 4 we delineate a dynamic version of the fingerpad model including viscoelastic and inertial effects. We further analyze the solution and derive conditions, under which the inertial effects can be ignored but that considerably simplifies the solution. In chapter 5 we discuss exploration strategies, connecting object properties, sensors, signal processing and hand or fingerpad movements. Finally, in appendices A-F we give detailed derivations as well as some mathematical manipulations and observations regarding the solutions presented in the chapters delineated above.

Chapter 2

Mathematical Preliminaries

1. Introduction

Most people working on mechanical systems are aware of integral transforms, such as Fourier and Laplace transforms, as tools used to solve differential equations or the analysis of measurement data. The general attitude however differs widely, depending mostly on the discipline people belong to. Control engineers work extensively with integral transforms and are in general quite comfortable in expressing the solutions in the form of a transform. In many cases the answer would be a transfer function describing a system without the input being prescribed. A mechanics engineer, on the other hand, is more likely to bring the solution one step further by prescribing some specific input (boundary conditions) and then go through effort of obtaining the actual solution to that input. Both approaches have their merit, but ideally one would apply both and use specific solutions as well as transfer functions to explain or predict the systems response to generic inputs.

In this chapter we will attempt to bring these two above-mentioned disciplines closer together in the application of integral transforms to contact problems. We will first give the basic theory of integral transforms and then apply it to several structures of differing complexity. The structures we will analyze, will vary from the statically loaded spring (Winkler) foundation to the dynamic loading of the semi-infinite elastic halfspace. By going from the simple structures to the more complex and by looking at static loading before dynamic, we hope to introduce various modeling details and their consequences separately. Through the analysis of the transfer function solution for each structure and by comparing that solution to some of the available solutions we hope that in the end, the reader will be well acquainted and comfortable with both forms of solutions.

The use of integral transforms in contact mechanics has mainly been promoted by Sneddon and for a detailed discussion cf. [70, 71], but more applications, models, and solution methods are given in [15, 61, 51]. Finally, for a general reference on contact mechanics cf. [36], but on viscoelasticity cf. [83].

This chapter is organized as follows: In section 2, we give the definition and some basic properties of Fourier (1D and 2D), and Laplace transforms. We also discuss briefly, some variants of the Fourier transforms, namely the finite and discrete Fourier transforms. Section 3 is devoted to static contact problems, and section 4 to dynamic problems. We conclude by summarizing our conclusions in section 5.

2. Integral Transforms

The use of integral transforms for the solution of partial differential equations (PDE) is based on the method of separation of variables introduced by d'Alembert, Bernoulli and Euler in the mid-eighteenth century [71]. The transform concept becomes convenient when the solutions are parameterized by the separation constants that characterize the method.

Example: When using the method of separation of variables to obtain a solution of Laplace's equation in Cartesian coordinates

$$\frac{\partial^2 \phi}{\partial x^2} + \frac{\partial^2 \phi}{\partial y^2} + \frac{\partial^2 \phi}{\partial z^2} = 0 \tag{2.1}$$

the usual procedure is to assume that the solution can be expressed as

$$\phi = X(x)Y(y)Z(z).$$

Substituting this into Eq. (2.1) and dividing by $X(x)Y(y)Z(z)$ we obtain

$$\frac{X''(x)}{X(x)} + \frac{Y''(y)}{Y(y)} + \frac{Z''(z)}{Z(z)} = 0.$$

We observe that the first term is a function of x only, the second of y only and the third of only z. They must therefore each be a constant. Let

$$\frac{X''}{X} = -a_x \qquad \frac{Y''}{Y} = -a_y \text{ then } \frac{Z''}{Z} = a_x + a_y,$$

where a_x and a_y can be any constants, complex or real. We then have that

$$X = e^{\pm jx\sqrt{a_x}} \qquad Y = e^{\pm jy\sqrt{a_y}} \qquad Z = e^{\pm z\sqrt{a_x + a_y}}$$

and that

$$\phi = e^{\pm jx\sqrt{a_x} \pm jy\sqrt{a_y}} e^{\pm z\sqrt{a_x + a_y}}$$

is a solution of Eq. (2.1) for all a_x, a_y.

This solution method can be applied to a wide variety of PDEs and we will now discuss how it can generally be developed to solve PDEs with prescribed boundary conditions.

Suppose that we have to determine a displacement field u, the solution of a homogeneous PDE of the form

$$L\left[u(r)\right] = 0 \qquad r \in D$$

in which $r = (x_1, x_2, x_3)$ is the position vector of a field point in a domain D, and $L[\cdot]$ is a linear differential operator in the variables x_1, x_2, and x_3. The set which the domain D is a part of is in most cases prescribed by the geometry and we will assume here, for the sake of clarity, that $D \subset \mathbb{R}^3$ and the operator therefore given in Cartesian coordinates. The discussion given here will also apply to other coordinate systems, such as cylindrical, spherical and others and we will, where applicable, give special comments regarding to them.

Assuming that the method of separation of variables enables us to find a solution $\eta(r, \alpha_1, \alpha_2)$ involving 2 arbitrary (separation) constants (α_1, α_2), whose values are taken from a set Ω. Since the operator $L[\cdot]$ is linear, the function

$$u(r) = \int_\Omega \eta(r, \alpha_1, \alpha_2) F(\alpha_1, \alpha_2) d\alpha_1 d\alpha_2$$

will also be a solution for a class of functions $F(\cdot)$. If we in addition have the boundary condition[1]

$$u(x_1, x_2, x_3 = X_3) = f(x_1, x_2)$$

X_3 being a constant, then we must choose $\bar{f}(\alpha_1, \alpha_2)$ such that

$$f(x_1, x_2) = \int_\Omega K(x_1, x_2, \alpha_1, \alpha_2) \bar{f}(\alpha_1, \alpha_2) d\alpha_1 d\alpha_2 \qquad (x_1, x_2) \in D \cap \{x_3 = X_3\}$$

where $K(x_1, x_2, \alpha_1, \alpha_2) = \eta(x_1, x_2, x_3 = X_3, \alpha_1, \alpha_2)$. We now adopt the convention of saying that $f(\cdot)$ is the integral transform of the function $\bar{f}(\cdot)$ by the kernel $K(\cdot)$. The factors that determine the form of the kernel and hence the type of transform are differential operator L and the coordinate system, which in turn is in most cases determined by the geometry of the boundary. The problems we are interested in here, is in mechanics and then $L[\cdot]$ is, in general,

---

[1] We assume simple boundary conditions, where only u is prescribed at the boundary. Other types of boundary conditions, involving derivatives of u can be treated similarly.

the Navier's operator:

$$L[u] = (\lambda + \mu)\Delta u + \mu \nabla \times \nabla \times u - \rho\ddot{u} = 0 \qquad u \in D, \tag{2.2}$$

where λ, μ and ρ are material constants defined later. We restrict us now to homogeneous materials and for the time being make the following assumptions on boundary conditions:

1. The boundary conditions are static, so dynamical effects can be ignored, ($\ddot{u} = 0$).

2. They are prescribed in Cartesian coordinates, then $L[\cdot]$ will have constant coefficients, and we write $(x_1, x_2, x_3) = (x, y, z)$, .

3. Specifically, let the boundary conditions be $u(x, y, 0) = f(x, y)$ and $z \in \mathbb{R}^{0+}$, i.e. the problem of a semi-infinite solid or a halfspace loaded on the boundary.

The method of separation of variables then gives us that Eq. 2.2 has a solution $u = \exp(j(\omega_x x + \omega_y y)) \exp\left(-z\sqrt{\omega_x^2 + \omega_y^2}\right)$ which is valid for all real (ω_x, ω_y). From which we obtain the kernel $K = \exp\left(j(\omega_x x + \omega_y y)\right)$ and hence recognize the integral transform as being the inverse Fourier transform and the separation constants (ω_x, ω_y) as being the corresponding spatial frequencies.

We will now explore some the properties of the Fourier transform and some of its relatives.

2.1 The Fourier Transform

The Fourier transform is useful when when the DE has constant coefficients and the domain of the solution extends to infinity in both directions ($D = \mathbb{R}$). It is defined as

$$\bar{f}(\omega_x) = \mathcal{F}[f] = \int_{-\infty}^{+\infty} f(x)e^{-j\omega_x x} dx. \tag{2.3}$$

Its inverse is,

$$f(x) = \mathcal{F}^{-1}[\bar{f}] = \frac{1}{2\pi}\int_{-\infty}^{+\infty} \bar{f}(\omega_x)e^{j\omega_x x} d\omega_x. \tag{2.4}$$

Convolution Theorem

The convolution theorem is a powerful theorem which states that the transform of a convolution of two functions is the product of the transforms of each function, i.e.

$$\mathcal{F}\left[\int_{-\infty}^{+\infty} f(u)g(x-u)du\right] = \mathcal{F}[f(x)]\,\mathcal{F}[g(x)] = \bar{f}(\omega_x)\bar{g}(\omega_x) \tag{2.5}$$

18

Transfer Functions: This theorem is very useful when applied in conjunction with the superposition principle. Convolution can be viewed as a expression that is obtained when the principle is applied to a shift invariant system in order to obtain the solution for a general boundary condition from a solution obtained by describing the boundary conditions as an Dirac's impulse function $\delta(x)$. The power of this concept lies in the fact that one only has to solve the problem for one type of boundary conditions, the impulse function, which is often relatively simple. A general solution can then be obtained from the impulse response using convolution, which becomes a simple product in the frequency domain. The Fourier transform of the impulse response is defined as being a *Transfer Function*[2] a term which we will use frequently.

Properties

The relation between the behavior of a function and its Fourier transform is in many ways interesting and several theorems exist describing that. However, here we will only detail the relations most relevant to subsequent analysis.

Oddness and Evenness: The function symmetry properties around the origin have some significance as for real functions the following applies,

If $f(x)$ is real and even $\quad\Leftrightarrow\quad \bar{f}(\omega_x)$ is real and even

If $f(x)$ is real and odd $\quad\Leftrightarrow\quad \bar{f}(\omega_x)$ is imaginary and odd

Derivatives: Differentiating Eq (2.4) wrt. x. a relation for the Fourier transform of derivatives is obtained as

$$\mathcal{F}\left[\frac{\partial^n f}{\partial x^n}\right] = (j\omega_x)^n \mathcal{F}[f] = (j\omega_x)^n \bar{f}(\omega_x) \tag{2.6}$$

Scaling: The similarity theorem describes how scaling of original function's variable translates into frequency space. and it states that

$$\mathcal{F}[f(ax)] = \frac{1}{a}\bar{f}(\frac{\omega_x}{a}). \tag{2.7}$$

In plain english this means that a function that is 'flat' has a Fourier transform that is 'sharp' in frequency space, and reverse, as is illustrated in Fig. 2-1.

---

[2]For spatial systems (not dynamic) the impulse response is frequently called *point spread function* and the Fourier transform of that the *modulation transfer function* [27].
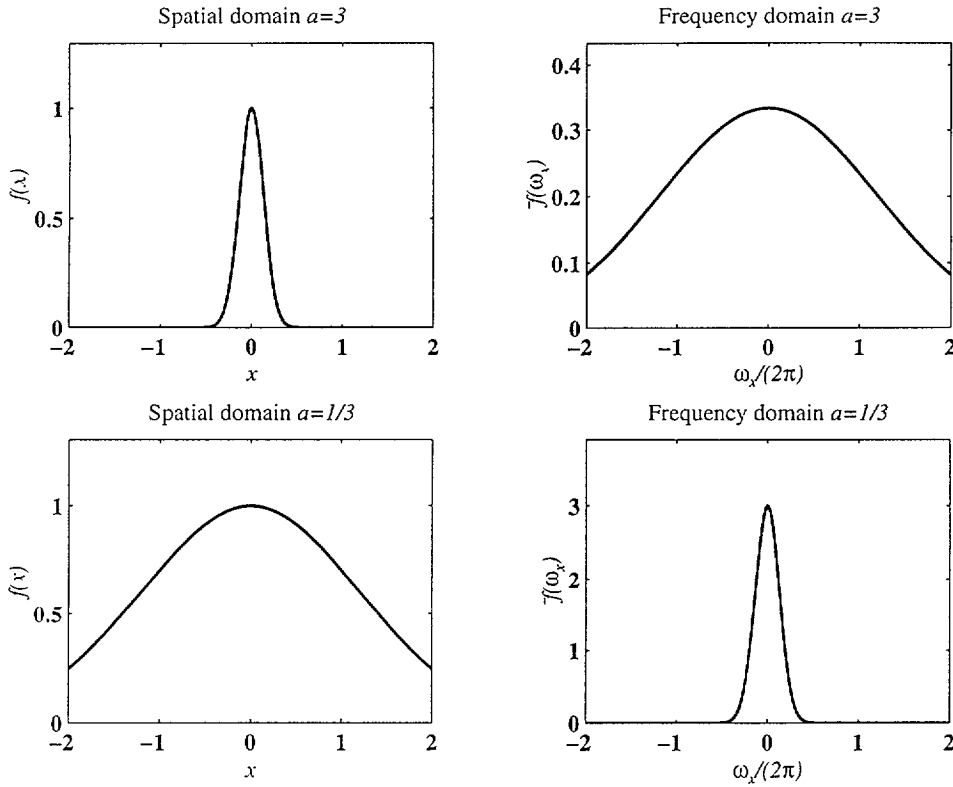
Figure 2-1: Illustrating the effects of scaling on the relationship between a function and its Fourier transform. The figures on the left are the scaled functions in the spatial domain, i.e. $f(ax)$ where $f(x) = \exp(-\pi x^2)$ and the figures on the right and side are the corresponding Fourier transforms, which are obtained using, $\mathcal{F}(f) = \exp(-\pi \omega_x^2)$. The Fourier transform is then scaled in the frequency domain according to Eq. (2.6). which gives us that $\mathcal{F}(f(ax)) = |a|^{-1} \bar{f}(\omega_x/|a|) = |a|^{-1} \exp(-\pi(\omega_x/a)^2)$.

2.2 The 2-D Fourier Transform

The 2-D Fourier transform is a generalization of the 1-D version above, and is mainly applicable to partial differential equations (PDE). It and its inverse are defined as

$$\bar{f}(\omega_x, \omega_y) = \mathcal{F}_{2D}\,[f] = \int\!\!\int_{-\infty}^{+\infty} f(x,y)e^{-j(\omega_x x + \omega_y y)}dxdy$$

$$f(x,y) = \mathcal{F}_{2D}^{-1}\,[f] = \frac{1}{4\pi^2} \int\!\!\int_{-\infty}^{+\infty} \bar{f}(\omega_x, \omega_y)e^{j(\omega_x x + \omega_y y)}d\omega_x d\omega_y.$$

(2.8)

Properties

The theorems and properties delineated for the 1-D Fourier transform above can be generalized for the 2-D transform and are in brief:

Oddness and Evenness:

20

Spatial domain *a=3/2 b=2/3*   Frequency domain *a=3/2 b=2/3*
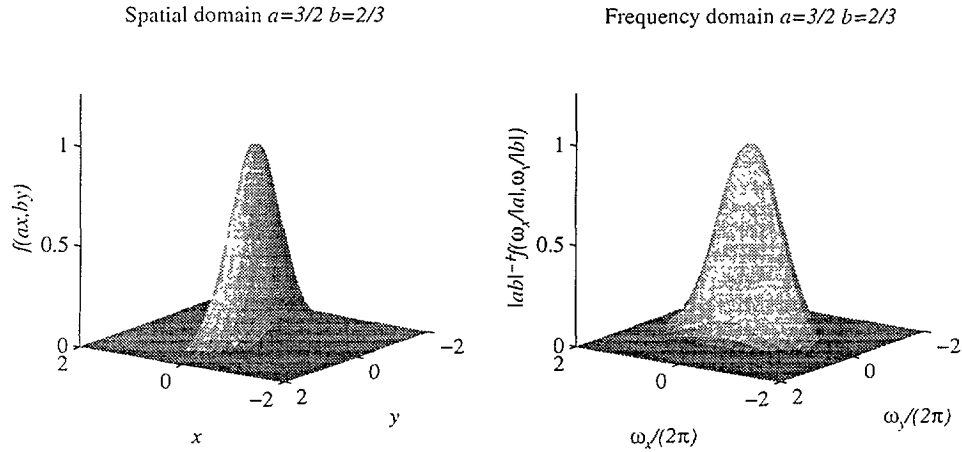
Figure 2-2: Illustrating the relationship between an asymmetric distribution and its 2D-Fourier transform. The figure on the left is the distribution in the spatial domain, i.e. $f(x,y) = \exp(-\pi(a^2x^2 + b^2y^2))$ with $a = 3/2$ and $b = 2/3$. The figure on the right hand side is the corresponding Fourier transform, which is $\mathcal{F}_{\in\mathcal{D}}(f) = \exp(-\pi(\omega_x^2/a^2 + \omega_y^2/b^2))/|ab|$.

If $f(x,y)$ is real and even $\quad\Leftrightarrow\quad$ $\bar{f}(\omega_x,\omega_y)$ is real and even

If $f(x,y)$ is real and odd $\quad\Leftrightarrow\quad$ $\bar{f}(\omega_x,\omega_y)$ is imaginary and odd [3]

Derivatives:

$$\mathcal{F}_{2D}\left[\frac{\partial^n}{\partial x^n}\frac{\partial^m f}{\partial y^m}\right] = (j\omega_x)^n(j\omega_y)^m \mathcal{F}[f] = (j\omega_x)^n(j\omega_y)^m\bar{f}(\omega_x,\omega_y) \tag{2.9}$$

Scaling: The two-dimensional version of the Similarity theorem states that

$$\mathcal{F}_{2D}[f(ax,by)] = \frac{1}{|ab|}\bar{f}(\frac{\omega_x}{a},\frac{\omega_y}{b}). \tag{2.10}$$

Again, this means that a function which is concentrated along some preferred direction has a Fourier transform, which preferred direction in frequency space, is generally at right angles to that direction (see Fig. 2-2).

2.3   The Laplace Transform

Related to the Fourier transform is the Laplace transform, and it is applicable when the domain D of the solution extends to infinity in only one direction, i.e. $D = \mathbb{R}^{0+}$ and it is primarily

---

[3]By 'odd' we mean that $f(x,y)$ has the same sign as xy, i.e. positive in 1st and 3rd quadrants but negative in 2nd and 4th quadrants.

used on dynamic DE when the effects of transients are included. It is defined as

$$F(s) = \mathcal{L}[f] = \int_0^\infty f(t)e^{-st}dt \tag{2.11}$$

Its inverse is,

$$f(t) = \mathcal{L}^{-1}[F] = \frac{1}{j2\pi} \int_{c-j\infty}^{c+j\infty} F(s)e^{st}ds \tag{2.12}$$

Properties

The only property of the Laplace transform that we will detail here is how derivatives get transformed, which assuming zero initial conditions is:

Derivatives:

$$\mathcal{L}\left[\frac{\mathrm{d}^n f}{\mathrm{d}t^n}\right] = s^n \mathcal{L}[f] = s^n F(s). \tag{2.13}$$

2.4 Other Transforms

Finite and Discrete Fourier Transform

One of the properties of the semi-infinite halfspace is that the frequency spectrum[4] of its solutions is continuous. Conversely, if the domain D is finite, say $x \in [-L/2, L/2]$, the spectrum becomes discrete as then the solution will only be valid for discrete values of ω_x. The inversion formula (Eq. 2.4) therefore becomes

$$\hat{f}(x) = \sum_{n=-\infty}^{+\infty} \bar{f}(n2\pi/L)e^{j\frac{n2\pi x}{L}} \tag{2.14}$$

and the limits of integration in Eq. (2.3) become finite ($[-L/2, L/2]$).

If we, additionally, assume that we have only available sampled values , i.e. discrete in x, the transform in Eq. (2.3) becomes a finite series and the series in Eq. (2.14) also becomes finite, i.e.

$$f(kd_s) = \sum_{n=0}^{N-1} \bar{f}(n/d_s)e^{j2\pi\frac{kn}{N}} \qquad \bar{f}(n/d_s) = \sum_{k=0}^{N-1} f(kd_s)e^{-j2\pi\frac{kn}{N}} \tag{2.15}$$

where d_s is the sampling period.

One can also derive derivative, scaling, convolution theorems, similar to Eqs. (2.6), (2.7), and (2.5) for the finite and discrete Fourier transforms and also a discrete and finite 2D-

---

[4]Spectrum is defined as being the set of frequencies for which a solution is valid.

Fourier transform [5]. The derivations are straightforward and the behavior is similar, as in the continuous case, except for the convolution theorem, where the effects of aliasing appear. Care has to be taken and one has to be aware of the effects of aliasing when results given here are being implemented or simulated with a computer.

Cylindrical and Spherical Geometries

When the geometry is such that the equilibrium equations are most suitably expressed in cylindrical or spherical coordinates, the same solution procedure can be applied.

Cylindrical: In the case of cylindrical geometry, the solution can be expressed as a combination of a Fourier and a finite Fourier transform and a series involving Bessel functions, e.g.

$$u(r, \theta, z) = \sum_{n=0}^{\infty} \int_{-\infty}^{+\infty} \bar{T}(r, n, \omega_z) J_n(\omega_z r) \bar{f}(n, \omega_z) e^{jn\theta + j\omega_z z} d\omega_z \tag{2.16}$$

where $J_n(\cdot)$ is a Bessel function of the first kind, of order n, $\bar{f}(\cdot)$ is determined by the boundary conditions, and $T(\cdot)$ can be viewed as having the role of a transfer function.

Spherical: When the equilibrium equations are expressed in spherical coordinates (r, θ, ϕ), the solution can be expressed as a series involving Legendre polynomials, e.g.

$$u(r, \theta, \phi) = \sum_{n=0}^{\infty} \sum_{m=-\infty}^{\infty} T(r, n, m) P_n^m(cos\theta) e^{jm\varphi} \bar{f}(n, m) \tag{2.17}$$

where

$$P_n^m(\mu) = \frac{1}{2^n n!} (1 - \mu^2)^{m/2} \frac{d^{m+n}(\mu^2 - 1)^n}{d\mu^{m+n}}$$

is the Rodriguez's formula for the associated Legendre polynomials and, as before. $\bar{f}(n, m)$. is determined by the boundary conditions and $T(\cdot)$ can similarly be viewed as a transfer function.

3. Static Indentation Problems

In this section we will demonstrate how the mathematical tools developed in the last section can be applied to obtain solutions for static contact problems. We start by giving examples of simple system, but gradually make the models more detailed. By this, we hope to give the reader a feel for the role of each term in the solution and that in turn will make the final solution less obscure and more believable. Having achieved that, we believe that we have demonstrated the power of transfer functions and integral transforms to provide understanding of the qualitative behavior of the solutions to contact problems by viewing them as the output from a system
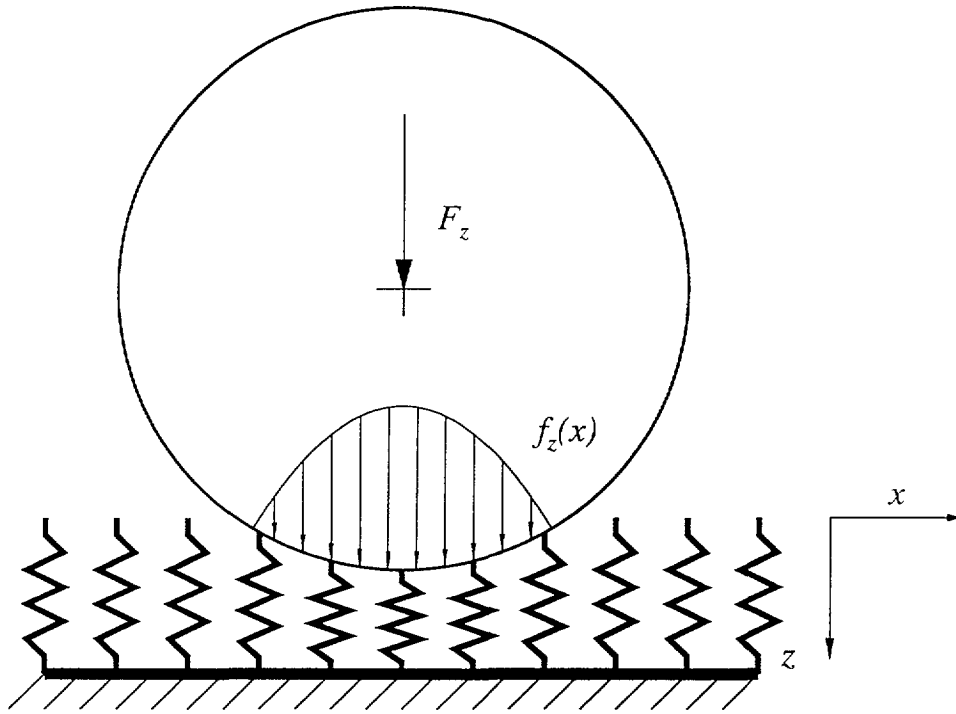
Figure 2-3: Shows a schematic diagram of the Winkler elastic foundation. The foundation shown, is being indented with a rigid object with a total load force F_z, resulting in a load distribution $f_z(x)$. The material is modeled as a collection of non-interconnected springs. The loading at each point on the surface contributes therefore only to the displacement at that location and does not extend beyond the contact region.

which has the boundary conditions as inputs.

3.1   Winkler Foundation

A very simple way of modeling a compliant material is the Winkler foundation, where the material is modeled as a collection of non-interconnected identical springs, (see Fig. 2-3) and the effects of shear are ignored. The force displacement relations we obtain are simply

$$\text{1D}: \ u_z(x) = \frac{1}{k_w} f_z(x), \qquad \text{2D}: \ u_z(x, y) = \frac{1}{k_w} f_z(x, y) \tag{2.18}$$

where u_z is the displacement in the z direction, k_w the stiffness per unit length (1D) or area (2D) of the foundation, and f_z is the normal loading per unit length (1D) or area (2D). The relations in transfer function form are identical.

3.2 Strings and Beams under Tension on a Winkler Foundation

The Winkler foundation model has the advantage of being simple, but the fact that any material deforms continuously, and that the deformations are therefore not independent is neglected. The springs should therefore somehow be interconnected. One way to include this effect is to model the material as a string under tension, S, lying on a Winkler foundation. We assume that the nature of the string is such that it can only resist load along its length[5]. The energy stored is related to the elongation of the string which is related to the first derivative of the surface deformation and the principle of virtual displacements gives us the equilibrium equation [61]:

$$-S\frac{\mathrm{d}^2 u_z}{\mathrm{d}x^2} + k_w u_z = f_z \tag{2.19}$$

which in transfer function form is

$$\bar{u}_z(\omega_x) = \frac{1}{S\omega_x^2 + k_w}\bar{f}_z(\omega_x), \tag{2.20}$$

where S is the string tension. The above can be generalized further to include higher order derivatives of u_z and if we model the medium as a beam under tension S with bending stiffness EI, resting on a Winkler foundation; then using similar methods we obtain the transfer function relation

$$\bar{u}_z(\omega_x) = \frac{1}{EI\omega_x^4 + S\omega_x^2 + k_w}\bar{f}_z(\omega_x). \tag{2.21}$$

3.3 Membranes and Plates under Tension on a Winkler Foundation

The above models can readily be generalized to describe the deformations of a surface subjected to two-dimensional loading where a string corresponds to a stretched membrane, and a beam corresponds to a plate under tension S, having flexural stiffness N. In that case the corresponding equilibrium equations are PDEs in x and y and hence we use Eq. (2.9) to obtain the solution in a transfer function form.

$$\bar{u}_z(\omega_x, \omega_y) = \frac{1}{S\Omega^2 + k_w}\bar{f}_z(\omega_x, \omega_y), \tag{2.22}$$

and

$$\bar{u}_z(\omega_x, \omega_y) = \frac{1}{N\Omega^4 + S\Omega^2 + k_w}\bar{f}_z(\omega_x, \omega_y), \tag{2.23}$$

where $\Omega = \sqrt{\omega_x^2 + \omega_y^2}$

---

[5]The string is therefore equivalent to having the load points connected to its nearest neighbor with a spring in tension.

Remark: That we express the above results in terms of transfer function enables us to interpret the relation between the normal loading and displacement as spatial low-pass filtering. The bandwidth of the filter is then prescribed by the stiffness and the tension; higher stiffness or tension translating to lower bandwidth and therefore smoother deformations.

3.4 Infinite Half-space

In the above we have only obtained expressions for the surface deformations of the medium, subjected to normal load. Since, we will in the chapters to follow need a model that can be used for the analysis of the response of sub-surface sensors we need to extend our model to include sub-surface deformations and also take into account tangential or shear loads. We therefore model the medium now as being homogeneous and extending to infinity[6] in the z direction.

In the case of a continuum model, the solution are not obtained as directly and easily as for the simple foundation problem treated above, and we resort to the following procedure[7]:

Solution Procedure

1. The starting point is the equilibrium equations and the stress-strain relations (generalized Hooke's law).

2. We then combine the two sets of equations to eliminate the stresses and obtain coupled second order PDE's in terms of the displacements only, effectively writing out the transformed Navier's equation.

3. We then transform the PDEs using the Fourier transform with respect to the appropriate variables (in general x, y). The PDEs are then[8] transformed into a system of coupled ODEs in z.

4. The ODE system is solved using standard methods with prescribed surface loading or displacements as boundary conditions.

---

[6] The solution method used here can also be extended to aelotropic (layered) and finite thickness materials, but the solutions quickly become quite complicated and opaque and further discussion will therefore not be given here.

[7] For the sake of simplicity, we assume here that the solution domain is the semi-infinite half-space, and therefore most easily described using Cartesian coordinates. Solution methods for other domains can be obtained similarly, e.g. as shown in section (2.4).

[8] Steps 2 and 3 can be interchanged.

Plane Strain (Line Load)

Example: We will show how the solution for an elastic half-space loaded over a narrow strip, so that the loading can be considered a distribution of line loads. We choose our coordinate system so that the boundary surface coincides with the xy plane and the z-axis is directed into the solid. The tractions (normal and tangential) are assumed not to vary along the y-dimension and hence be functions of x only. We shall assume that that under these conditions, a state of plane strain ($\varepsilon_{yy} = 0$) is produced in the half-space.

Stepping through the procedure introduced above we obtain:

Step 1: Under the simplifying plane strain assumption, the equilibrium equations become:

$$\frac{\partial \sigma_{xx}}{\partial x} + \frac{\partial \sigma_{xz}}{\partial z} = 0$$
$$\frac{\partial \sigma_{zx}}{\partial x} + \frac{\partial \sigma_{zz}}{\partial z} = 0 \tag{2.24}$$

and the stress-strain relationships:

$$\sigma_{xx} = (\lambda + 2\mu)\varepsilon_{xx} + \lambda\varepsilon_{zz}, \quad \sigma_{zz} = (\lambda + 2\mu)\varepsilon_{zz} + \lambda\varepsilon_{xx}, \quad \sigma_{xz} = 2\mu\varepsilon_{xz} \tag{2.25}$$

where

$$\lambda = \frac{E\nu}{(1+\nu)(1-2\nu)} \quad \text{and} \quad \mu = \frac{E}{2(1+\nu)} \tag{2.26}$$

are the Lamé constants (bulk and shear modulus) with E and ν denoting Young's modulus and the Poisson ratio, respectively.

$$\varepsilon_{xx} = \frac{\partial u_x}{\partial x}, \quad \varepsilon_{zz} = \frac{\partial u_z}{\partial z}, \quad \varepsilon_{xz} = \frac{1}{2}\left(\frac{\partial u_x}{\partial z} + \frac{\partial u_z}{\partial x}\right) \tag{2.27}$$

Step 2+3 Carrying steps 2 and 3 out simultaneously we get the system of equations

$$\begin{bmatrix} D^2 - \omega_x^2 & j(\beta^2-1)D\omega_x \\ j(\beta^2-1)D\omega_x & \beta^2 D^2 - \omega_x^2 \end{bmatrix} \begin{bmatrix} u_x \\ u_x \end{bmatrix} = \begin{bmatrix} 0 \\ 0 \end{bmatrix} \tag{2.28}$$

where $\beta^2 = (\lambda + 2\mu)/\mu$ and $D = \dfrac{d}{dz}$.

Step 4: The determinant of the system in Eq. (2.28) is $\Delta = \beta^2(D^2 - \omega_x^2)^2$, and a non-trivial solution will therefore be of the form

$$u_x = (A_x + B_x z)e^{-|\omega_x|z}$$
$$u_z = (A_z + B_z z)e^{-|\omega_x|z}, \tag{2.29}$$

which has 4 unknown coefficients. Two of them can be eliminated by substituting Eq. (2.29) back into

Eq. (2.28) which gives:

$$B_x = -j\mathrm{sgn}(\omega_x)B_z, \quad A_z = j\mathrm{sgn}(\omega_x)A_x + \frac{\beta^2+1}{\beta^2-1}B_z,$$

where sgn is the sign function with $\mathrm{sgn}(0) \triangleq 0$. The two remaining coefficients are decided by the boundary conditions, which we assume are in the form of prescribed tractions on the boundary surface $(z=0)$. The equations relating the coefficients to the tractions are obtained by substituting Eq. (2.29) into Eqs. (2.25) and (2.27) and identifying $\sigma_{zz}(z=0)$ as the normal traction and $\sigma_{xz}(z=0)$ as the tangential traction. We then get the relations

$$2\mu\left((1-2\nu)\mathrm{sgn}(\omega_x)B_z - |\omega_x|A_x\right) = \bar{f}_x$$

$$2\mu\left((2-2\nu)B_z - j\omega_x A_x\right) = \bar{f}_z.$$

Solving for A_z and B_z and substituting back into Eq. (2.29) gives

$$\bar{u}_x = \frac{1}{2\mu}\frac{(2-2\nu-|\omega_x|z)}{|\omega_x|}e^{-|\omega_x|z}\bar{f}_x + \frac{1}{2\mu}j\frac{(1-2\nu-|\omega_x|z)}{\omega_x}e^{-|\omega_x|z}\bar{f}_z = T_{u_xf_x}\bar{f}_x + T_{u_xf_z}\bar{f}_z$$

$$\bar{u}_z = -\frac{1}{2\mu}j\frac{(1-2\nu+|\omega_x|z)}{\omega_x}e^{-|\omega_x|z}\bar{f}_x + \frac{1}{2\mu}\frac{(2-2\nu+|\omega_x|z)}{|\omega_x|}e^{-|\omega_x|z}\bar{f}_z = T_{u_zf_x}\bar{f}_x + T_{u_zf_z}\bar{f}_z,$$

(2.30)

where $T_{u_xf_x}$ and $T_{u_zf_x}$ are the transfer function for the displacements u_x and u_z, resulting from the tangential load f_x, and similarly $T_{u_xf_z}$ and $T_{u_zf_z}$ are the transfer functions for the same displacements displacements, resulting from the normal load f_z.

We express this solution compactly using a Transfer Function Matrix (TFM). i.e.

$$\bar{u} = T_{uf}\bar{f}, \tag{2.31}$$

where $u = [u_x, u_z]^T$, $f = [f_x, f_z]^T$, and

$$T_{uf} = \begin{bmatrix} T_{u_xf_x} & T_{u_xf_z} \\ T_{u_zf_x} & T_{u_zf_z} \end{bmatrix} = \frac{e^{-|\omega_x|z}}{2\mu}\begin{bmatrix} \dfrac{2-2\nu-|\omega_x|z}{|\omega_x|} & j\dfrac{1-2\nu-|\omega_x|z}{\omega_x} \\ -j\dfrac{1-2\nu+|\omega_x|z}{\omega_x} & \dfrac{2-2\nu+|\omega_x|z}{|\omega_x|} \end{bmatrix}$$

Assuming that $f_z(x)$ is an even function, we observe that the resulting $\bar{u}_x(\omega_x)$ is imaginary and odd, indicating that $u_x(x)$ is odd and similarly we conclude that the $u_z(x)$ resulting from an even f_z is also even.

Symmetry: The terms in the TFMs appear similar but there are subtle differences so they are not completely symmetric in ω_x and z. This can be expected, mainly because ω_x is a

28

frequency variable but z is a spatial variable. Also since the domains of each are different ($\omega_x \in [-\infty, +\infty]$, but $z \in [0, +\infty]$).

The strains and stresses can then be obtained using Eqs. (2.25) and (2.27) respectively, giving:

$$
\begin{bmatrix} \bar{\varepsilon}_{xx} \\ \bar{\varepsilon}_{zz} \\ \bar{\varepsilon}_{xz} \end{bmatrix} = \frac{e^{-|\omega_x|z}}{2\mu} \begin{bmatrix} j\,\mathrm{sgn}(\omega_x)(2 - 2\nu + |\omega_x|\,z) & 1 - 2\nu - |\omega_x|\,z \\ j\,\mathrm{sgn}(\omega_x)(2\nu - |\omega_x|\,z) & 1 - 2\nu + |\omega_x|\,z \\ 1 - |\omega_x|\,z & -j\omega_x z \end{bmatrix} \begin{bmatrix} \bar{f}_x \\ \bar{f}_z \end{bmatrix} \tag{2.32}
$$

and

$$
\begin{bmatrix} \bar{\sigma}_{xx} \\ \bar{\sigma}_{zz} \\ \bar{\sigma}_{xz} \end{bmatrix} = e^{-|\omega_x|z} \begin{bmatrix} -j\,\mathrm{sgn}(\omega_x)(2 - |\omega_x|\,z) & 1 - |\omega_x|\,z \\ -j\omega_x z & 1 + |\omega_x|\,z \\ 1 - |\omega_x|\,z & -j\omega_x z \end{bmatrix} \begin{bmatrix} \bar{f}_x \\ \bar{f}_z \end{bmatrix} \tag{2.33}
$$

Mean normal Stress: A stress combination that becomes particularly important for incompressible materials is the mean normal stress, defined as

$$
p_n \overset{\triangle}{=} \frac{1}{3}\left(\sigma_{xx} + \sigma_{yy} + \sigma_{zz}\right).
$$

Its importance lies in that, for incompressible materials, it does not contribute to any strains, (an incompressible body subjected to uniform pressure does not deform at all). This means that strains cannot be used solely as a sensor signal, if one wants to use incompressible materials as a cover for tactile sensors, as then the sensors would not be able to sense the mean normal stress component of the stress signal.

For the line-load case we get that $p_n = \dfrac{1 + \nu}{3}\left(\sigma_{xx} + \sigma_{zz}\right)$ since then $\sigma_{yy} = \nu(\sigma_{xx} + \sigma_{zz})$ and using Eq. (2.33) we get the TFM for p_n as

$$
T_{p_n f} = \frac{2(1 + \nu)e^{-|\omega_x|z}}{3}\begin{bmatrix} -j\,\mathrm{sgn}(\omega_x), & 1 \end{bmatrix}
$$

Other Structures: Comparing the solution for the z-displacements (u_z) on the surface ($z = 0$) of the halfspace subjected to distributed normal load to those obtained for the Winkler foundation and the string we observe that:

$$
\bar{u}_{\text{Winkler}} \propto f_z \qquad \bar{u}_{\text{Halfspace}} \propto \frac{1}{|\omega_x|}f_z \qquad \bar{u}_{\text{String}} \propto \frac{1}{\omega_x^2}f_z
$$

29
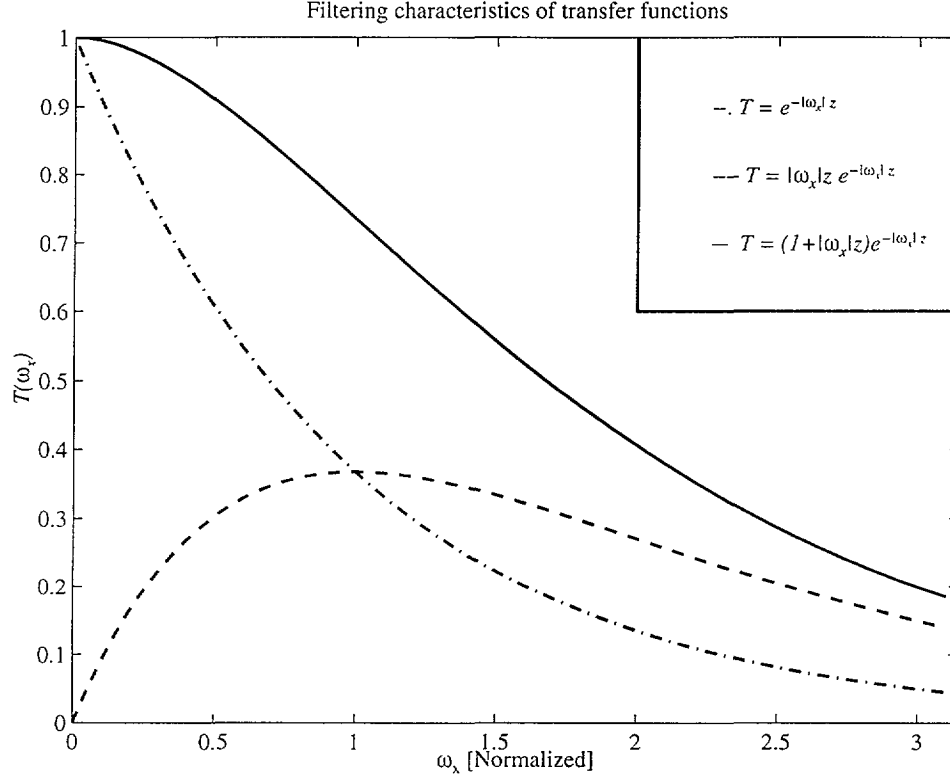
Figure 2-4: Illustrating the shape of typical terms in the transfer functions. The dash-dot curve (i) plots $T = \exp(-|\omega_x|z) = T_{p_n f_z}$ which has lowpass characteristics. The dashed line (ii) plots $T \propto |\omega_x|z\exp(-|\omega_x|z) = T_{\varepsilon_{zz}f_z}$ which has bandpass characteristics. The solid line (iii) plots these two added or $T = (1+|\omega_x|z)\exp(-|\omega_x|z) = T_{\sigma_{zz}f_z}$ which has increased bandwidth over (i)

The relative degree of the transfer function, tells us how localized the resulting deformations will be. The Winkler foundation deforms only directly under the load and that is reflected in a flat spectrum, indicating a very sharp impulse response. The surface displacements of the halfspace spread away from the loading area, because the transfer function goes to zero for higher frequencies the medium must therefore deform gradually. The string has an even sharper transfer function so its displacements must spread out even further. The semi-infinite halfspace therefore behaves, in terms of its surface displacement profile response to distributed normal loading, as something that is between a Winkler foundation and a string under tension.

Spatial Filtering: The exponential term represents spatial lowpass filtering which bandwidth decreases exponentially with depth. For the linear strains and stresses, two main variants of terms can be identified in Eqs (2.32) and (2.33): i) $e^{-|\omega_x|z}$, (p_n) ii) $z|\omega_x|e^{-|\omega_x|z}$, (ε_{zz}). The shapes of each are plotted in Fig. 2-4. There we see that (i) corresponds to a low pass filter but, (ii) a bandpass filter. The combination of (i) and (ii) $(1 + z|\omega_x|)e^{-|\omega_x|z}$ is also plotted as a solid curve and it is seen that it covers both the low and high frequency bands.

30
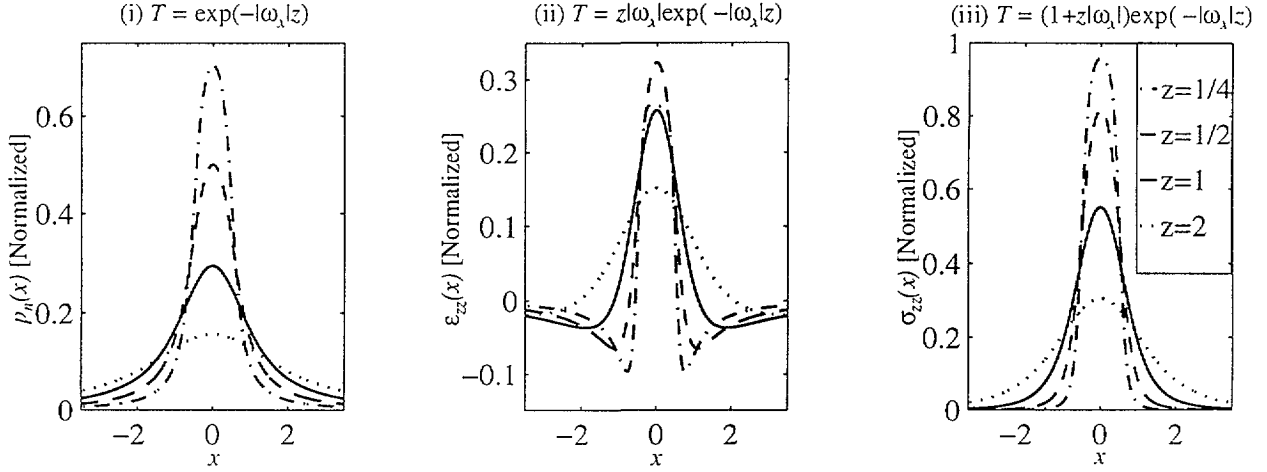
Figure 2-5: Shows the response in the spatial domain, of each of the transfer functions, (i)-(iii) to uniform normal loading in $x \in [-1/2, 1/2]$. In the leftmost figure is the mean normal pressure $p_n = -(\sigma_{xx} + \sigma_{zz})/2$ is plotted. It has the transfer function $T = \exp(-|\omega_x| z)$. In the middle figure the ε_{zz} normal strain is plotted, it has transfer function $T = z |\omega_x| \exp(-|\omega_x| z)$. In the rightmost figure the σ_{zz} normal stress is plotted. It has transfer function $T = (1 + z |\omega_x|) \exp(-|\omega_x| z)$.

For the spatial domain, the effects of the different filtering functions are shown in Fig. 2-5 and there we see that (i) and (iii) are similar, but (i) is more flat. The (ii) terms on the other hand show typical bandpass characteristics such as sign changes near the edge of the contact region ($x = \pm 1/2$).

Sampling period vs. Sensor Depth: We also note the inverse relationship between z and ω_x which becomes quite important when one considers the consequences of using discrete sensors and hence the effects of sampling. It turns out that it has an equivalent effect on the bandwidth of the transfer function, to either place the sensors further apart or further beneath the surface. This indicates a tradeoff between sensor depth and sensor spacing which becomes important when sensor arrays are designed.

General 3D Solution

Exactly the same procedure can be applied when the plane strain assumption is dropped and general loading conditions are considered. That the tractions vary also along the y-dimension is accommodated by using the 2D Fourier transform defined in Eq. (2.8). The solution can similarly be presented using TFMs with full dimensions of the displacement, traction and

31

stress/strain vectors, i.e.

$$u = [u_x, u_y, u_z]^T, \quad \varepsilon = [\varepsilon_{xx}, \varepsilon_{yy}, \varepsilon_{zz}, \varepsilon_{xy}, \varepsilon_{xz}, \varepsilon_{yx}]$$

$$f = [f_x, f_y, f_z]^T, \quad \sigma = [\sigma_{xx}, \sigma_{yy}, \sigma_{zz}, \sigma_{xy}, \sigma_{xz}, \sigma_{yx}].$$

The details of the TFMs will be omitted here but the full solution can be found in chapter 3. All the comments made above regarding the plane strain solutions apply directly to the general 3D solution. Although one has to keep in mind, when transferring the concept of bandwidth over to the 2D transfer functions, that the frequency space is two-dimensional. The bandwidth of transfer functions will therefore in general be dependent on the direction also.

4. Dynamic Problems

The problems we have discussed so far have assumed static loading, i.e. we have ignored both the effects of rate dependent material laws (viscosity) and also the effects of inertia, but we can treat these two phenomena separately. The effects of inertia and wave mechanics will be discussed separately for each structure and we will also assess when inertial effects can be ignored. That will simplify our solution significantly, especially in the case of a semi-infinite solid. The viscoelastic behavior is modeled by modifying the material laws and making them rate dependent.

The effects of inertia ρ are included by adding d'Alemberts force $f_A = \rho \ddot{u}_z$ to the right hand side of the equilibrium equations. Using Laplace transform, the double time derivative can be replaced with a multiplication by s^2 and the only addition to the static solution for the foundation models is a extra term of ρs^2 in the denominator of the transfer function. We will discuss the effects of inertia on the solution to the structures analyzed in sections 3.1-3.3 in the sections 4.1-4.3. The inertia terms have more complex effects on the semi-infinite halfspace solution and we will take a look at those in section 4.4. How viscoelasticity can be included in the transfer function formulation will finally be discussed in section 4.5.

4.1 Winkler Foundation

For this simple case the solution now becomes:

$$\bar{u}_z = \frac{1}{\rho} \frac{1}{\omega_0^2 + s^2} \bar{f}_z, \tag{2.34}$$

where ρ is the density, and $\omega_0^2 = k_w/\rho$ is the resonance frequency of the foundation.

4.2 The String and the Membrane

For the string the solution is:

$$\bar{u}_z = \frac{1}{\rho} \frac{1}{c_2^2 \omega_x^2 + s^2} \bar{f}_z$$

and for the membrane:

$$\bar{u}_z = \frac{1}{\rho} \frac{1}{c_2^2 \Omega^2 + s^2} \bar{f}_z$$

where $c_2 = \sqrt{T/\rho}$ is the wave velocity as can be seen if we assume the loading f_z is a point load at $x = 0$ but then the Laplace transform of the solution for the string becomes

$$\tilde{u}_z(x,s) = -\frac{c_2}{2s} e^{-\frac{|x|s}{c_2}} \frac{\tilde{f}_z(s)}{T}.$$

We observe that viewed from the point of loading the response of the string is that of a pure damper. This is a consequence of the string having no transverse or bending stiffness, and hence all the power injected into the system is transferred away from the source (loading point) and appears lost. The exponential term indicates that the response away from the origin is a time-delayed copy of that at the loading point, but delayed by $T_d = |x|/c_2$ which is according to to the well known result of d'Alembert [61], namely that the solution is a wave traveling in both directions with velocity c_2 away from the origin.

For the membrane, we obtain for a time-varying point-load at the origin that

$$\tilde{u}_z(r,s) = \frac{2\pi \tilde{f}_{z0}(s)}{T} K_0\left(\frac{rs}{c_2}\right)$$

where $K_0(\cdot)$ is a modified Bessel function of the second kind. Using asymptotic expansions for the Bessel function we obtain that the steady-state response to a sinusoidal excitation at the origin for points that are far away from the origin is

$$u_z(r,t) \approx \frac{2\pi F_{z0}}{T} \sqrt{\frac{2c_2}{\pi r \omega}} e^{-J\left(\frac{r\omega}{c_2} - \pi/4\right)} \sin(\omega t),$$

where F_{z0} is the total load and ω is the excitation frequency. This corresponds to a traveling wave, with a phase delay of $\pi/4$ and with amplitude that decreases as $\lambda^{-1/2}$ where λ is the distance from the origin measured in wavelengths $\lambda_2 = \pi c_2/\omega$.

33

4.3 String or Membrane on a Winkler Foundation

If the string or the membrane is supported by a Winkler foundation the transfer function solution becomes

$$\bar{u}_z = \frac{1}{\rho} \frac{1}{c_2^2 \omega_x^2 + \omega_0^2 + s^2} \bar{f}_z$$

for the string and

$$\bar{u}_z = \frac{1}{\rho} \frac{1}{c_2^2 \Omega^2 + \omega_0^2 + s^2} \bar{f}_z$$

for the membrane. For input frequencies less than the resonance frequency of the Winkler foundation, ($|s| < \omega_0$) the response is that of a pure spring but for higher frequencies it behaves in part like a string and some of the power of those frequencies gets radiated away.

Neglecting Inertial Effects: It seems reasonable that for slow motion, the effects of inertia could be neglected as they would be overwhelmed by the static and viscous effects. By inspecting the solution we see that the effects of inertia can be ignored if:

$$\omega_0 \gg \omega \qquad \text{and} \qquad \frac{c_2}{L} \gg \omega$$

where ω is the (maximum) input frequency and L is a (maximum) characteristic length, i.e. scale, of the structure of interest. The first condition indicates that the input frequency should not excite the resonance frequency of the Winkler foundation and the second condition indicates that the wavelength of the wave excited by the highest input frequency of the input should be large compared to the scale of the structure.

Beams and Plates: Solutions for dynamic loading of beams and plates can be obtained using the same method as above. No analysis of their behavior will be given here.

4.4 Infinite Half-space

In this section we will study the dynamic behavior of the infinite halfspace. First we will analyze the mechanics of the different types of plane waves, then how the same types of waves appear from a point source. We will finally analyze the dynamic response of the elastic halfspace subjected to a dynamic line-load, and based on that give conditions under which we can neglect the effects of inertia.

Wave Mechanics of Plane Waves

At a sufficient distance from their source, all waves can be considered plane waves and it is informative to consider the propagation of plane waves. A plane harmonic displacement wave can be represented as

$$u = A\hat{d}\exp\left(jk(r \cdot \hat{p} - ct)\right) \tag{2.35}$$

where u is the displacement vector, $\hat{d}$ is a unit vector defining the direction of motion of the particle, $\hat{p}$ is a unit vector defining the direction of propagation, c is the wave velocity, k is the wave number and A is independent of the position vector r and time t. When Eq. (2.35) is substituted into Navier's Eq. (2.2) we find that two types of plane waves are possible, when either

$$\text{(i)} \quad \hat{d} = \pm\hat{p} \quad \text{and} \quad c = c_p = \left[\frac{\lambda + 2\mu}{\rho}\right]^{1/2} \quad \text{or (ii)} \quad \hat{d}\cdot\hat{p} = 0 \quad \text{and} \quad c = c_{sh} = \left[\frac{\mu}{\rho}\right]^{1/2}. \tag{2.36}$$

In case (i) the motion of the particles is parallel to the direction of propagation and the wave is a longitudinal wave. It can be shown to involve only volume dilation and no shear or rotation. In case (ii), on the other hand, the motion of the particles is perpendicular to the direction of propagation, involving only shear, hence called a shear wave.

A third type of waves occurs close to the surface of the solid as a consequence of an interaction of both the dilational and the shear wave with the free surface. They are called Rayleigh waves and a solution for them can be found by substituting

$$u = A\hat{d}_P e^{k[j(r\,\hat{p} - c_R t) - \alpha_P z]} + \hat{d}_{sh} e^{k[j(r\cdot\hat{p} - c_R t) - \alpha_{sh} z]} \tag{2.37}$$

into Eq. (2.2) and also use the condition that the surface is stress-free, i.e. $\sigma_{zz} = \sigma_{xz} = 0$ when $z = 0$. It can be shown that these conditions lead to an equation for the ratio α_R/α_{sh}

$$\left((c_R/c_{sh})^2 - 1/2\right)^2 - (c_R/c_{sh})^2\sqrt{(c_R/c_{sh})^2 - \beta^{-2}}\sqrt{(c_R/c_{sh})^2 - 1} \tag{2.38}$$

that can be shown to give exactly one solution that can be interpreted as a wave [81]. It turns out that $\dfrac{c_R}{c_{sh}} \in [0.8740, 0.9553]$ for $\nu \in [0, 0.5]$ and we further get that $\alpha_P = \left[1 - c_R^2/c_P^2\right]^{1/2}$, $\alpha_{sh} = \left[1 - c_R^2/c_{sh}^2\right]^{1/2}$. The nature of Rayleigh waves is that they propagate essentially only on the surface, as they attenuate exponentially with depth. Their geometric attenuation is therefore lower than that of the dilational and shear waves and they will die out slower with distance from the load source.

Geometric attenuation: When a sinusoidal point load is applied at the origin $P = P_0\cos(\omega t)$

35

the radial and transverse displacements can be written [36]

$$u_R = \frac{P_0}{2\pi\mu R}\Theta_R(\theta,\beta)\cos(\omega t - k_p R)$$

$$u_\theta = \frac{P_0}{2\pi\mu R}\Theta_\theta(\theta,\beta)\sin(\omega t - k_{sh} R)$$

where $k_p = \omega/c_p$ and $k_{sh} = \omega/c_{sh}$, but $\Theta_R(\cdot)$ and $\Theta_\theta(\cdot)$ depend on the directional angle $\theta = \cos^{-1}(z/R)$ and $\beta = \sqrt{c_p/c_{sh}}$. These equations are valid everywhere, except at the surface $\theta = \pi/2$. We observe that the radial displacement u_R is due to the dilational wave only, and similarly the tangential displacement is due to the shear wave only. At the surface the displacements are due to the Rayleigh wave and are given by

$$u_r = \frac{P_0}{\mu}\left(\frac{k_R}{2\pi r}\right)^{1/2} F_r(\nu)\sin(\omega t - k_R R - \pi/4)$$

$$u_z = \frac{P_0}{\mu}\left(\frac{k_R}{2\pi r}\right)^{1/2} F_z(\nu)\cos(\omega t - k_R R - \pi/4)$$

where $k_R = \omega/c_R$ and $F_r(\cdot)$ and $F_z(\cdot)$ depend on Poisson's ratio [51]. Similar expressions can be obtained in the case of a line-load. The asymptotic behavior of this solution is determined by the geometric attenuation, which is the result of the increasing area of the wavefront with distance from the source. The geometric attenuation depends on how many dimensions the wave propagates in, and we therefore have different attenuation for Rayleigh waves than for dilational and shear waves. The attenuation also depends on the source being a line- or a point-load. We have that the amplitude A behaves with distance from the source λ (measured in wavelengths) as follows [36, 51]:

Line-load
Dilational and shear waves: $A \propto \dfrac{1}{\lambda^{1/2}}$
Rayleigh waves: $A \propto 1$.

Point-load
Dilational and shear waves: $A \propto \dfrac{1}{\lambda}$
Rayleigh waves: $A \propto \dfrac{1}{\lambda^{1/2}}$.

Hence, Rayleigh waves in the halfspace behave like shear waves in a string for a line-load source, and as shear waves in a membrane for a point-load source.

Transfer Function Solution

The dynamic response of the semi-infinite halfspace is considerably more complicated than that of the structures in the previous examples, mainly because displacements are now allowed to vary also in the z-dimension. The solution procedure is however the same as used for the static problems, detailed in section 3.4, and as above, the effects of inertia are included by adding d'Alemberts force $f_{A_i} = \rho \ddot{u}_i \; i = x, y, z$ to the right hand side of the equilibrium equations. For the example in section (3.4) this leads to the modified system of equations

$$
\begin{bmatrix}
D_z^2 - (\omega_x^2 + \frac{\rho}{\mu}s^2) & j(\beta^2 - 1)D_z\omega_x \\[2mm]
j(\beta^2 - 1)D_z\omega_x & \beta^2 D_z^2 - (\omega_x^2 + \frac{\rho}{\mu}s^2)
\end{bmatrix}
\begin{bmatrix}
u_x \\[2mm]
u_x
\end{bmatrix}
=
\begin{bmatrix}
0 \\[2mm]
0
\end{bmatrix},
\tag{2.39}
$$

which has the determinant $\Delta = \beta^2(D_z^2 - n_1^2)(D_z^2 - n_2^2)$, where $n_1 = (\omega_x^2 + \frac{\rho}{\lambda+2\mu}s^2)^{1/2}$ and $n_2 = (\omega_x^2 + \frac{\rho}{\mu}s^2)^{1/2}$. A non-trivial solution will therefore be of the form

$$
\begin{aligned}
u_x &= A_x e^{-n_1 z} + B_x e^{-n_2 z} \\[2mm]
u_z &= A_z e^{-n_1 z} + B_z e^{-n_2 z}
\end{aligned}
\tag{2.40}
$$

A complete solution of both u_x and u_z displacements resulting from a combined tangential. f_x. and normal load, f_z can be obtained using the same method as in section 3.4 as well as the general 3D-solution including u_y and f_y. These can then be used to derive the stress and strain relations as needed. We will leave out the details and only look at the normal displacement response for a distributed line-load and also for a general distributed load, since an analysis of their dynamical behavior will directly carry over to the other displacements, stresses and strains.

The solution for the normal displacement u_z resulting from a line-load is in transfer function form,

$$
\bar{u}_z(\omega_x, s) = \frac{n_1\left[(\omega_x^2 + \frac{\rho}{2\mu}s^2)e^{-n_1 z} - \omega_x^2 e^{-n_2 z}\right]}{2\mu\left[(\omega_x^2 + \frac{\rho}{2\mu}s^2)^2 - \omega_x^2 n_1 n_2\right]}\bar{f}_z(\omega_x, s).
\tag{2.41}
$$

The point-load solution is almost identical, one only has to replace ω_x^2 with $\Omega^2 = \omega_x^2 + \omega_y^2$ in the transfer function and change the arguments in $\bar{u}_z$ and $\bar{f}_z$ to (ω_x, ω_y, s).

Comparing Eqs. (2.35) and (2.36) to the transfer function in Eq. (2.41) we see that the exponents n_1 and n_2 correspond to the dilational and shear waves respectively. The Rayleigh wave on the other hand, corresponds to the pole of the denominator [51]. The exponential terms $e^{-n_1 z}$ and $e^{-n_2 z}$ correspond to the interaction of a traveling wave with the effects of increasing low-pass filtering with depth. For temporal frequencies that are high enough compared to the

spatial frequency, i.e. on coarse spatial scale, the exponent becomes imaginary and therefore corresponds to a time-delay caused by the wavefront traveling at a finite speed, (c_p or c_{sh}). For finer spatial details, the exponent serves the same purpose as in the static case, i.e. the increased spatial low-pass filtering (blurring) of signals with depth.

Neglecting inertia: For further analysis of the transfer function, it is helpful to renormalize and measure distances and displacements in units of shear-wave wavelengths. Let $s = jw$, $\lambda_{sh} = c_{sh}/\omega$ and hence $z = \hat{z}\lambda_{sh}$, $\omega_x = \hat{\omega}_x/\lambda_{sh}$. The ω can then be canceled out from the transfer function which then becomes

$$\hat{u}_z = \frac{n_1 \left[(\hat{\omega}_x^2 - 1/2)e^{-z\hat{n}_1} - \hat{\omega}_x^2 e^{-\hat{n}_2 z}\right]}{2\mu \left[(\hat{\omega}_x^2 - 1/2)^2 - \hat{\omega}_x^2 \hat{n}_1 \hat{n}_2\right]}$$

with $\hat{n}_1 = (\hat{\omega}_x^2 - \beta^{-2})^{1/2}$, and $\hat{n}_2 = (\hat{\omega}_x^2 - 1)^{1/2}$. We observe that there are no singularities and all the terms are real in the transfer function for $\hat{\omega}_x > 1$. This can be interpreted as spatial frequencies with $\hat{\omega}_x > 1$ are not involved in energy transfer away from the source and that the halfspace behaves simply as a spring for those frequencies. The denominator however vanishes for $\hat{\omega}_x = c_R/c_{sh}$, since it is identical to Eq. (2.38) used to obtain c_R/c_{sh}. That the halfspace behaves as a spring for some frequency range becomes important when one considers the conditions under which inertia can be neglected, especially in cases where the solution in Eq. (2.41) is applied to finite domains as will eventually happen in our case. Let $x \in [-L/2, L/2]$. then only a discrete set of spatial frequencies will give valid solutions as discussed in section 2.4. The lowest nonzero frequency is of particular interest to us and the modeshapes (assuming simple boundary conditions at $x = \pm L/2$) corresponding to that have been plotted in Fig. 2-6. We see that the longest possible wavelength is $\lambda_{\max} = 2L$ which is equivalent to $\min(\omega_x) = \pi/L$. We therefore have that $\hat{\omega}_x < c_R/c_{sh}$ is satisfied if

$$\omega < \frac{\pi c_R}{L}$$

giving us a condition as to when we can ignore the effects of inertia for the semi-infinite halfspace.

4.5   Viscoelasticity

Theory of viscoelasticity extends the theory of elasticity to include cases where the stress-strain relation behavior is rate dependent. It all boils down to the choice of timescale, and for shorter intervals of interest, it may be necessary to account the rate dependent behavior of materials. The description linear viscoelastic material applies to materials for which the rate dependent behavior can be adequately described by expressing the stress-strain relation in the viscoelastic
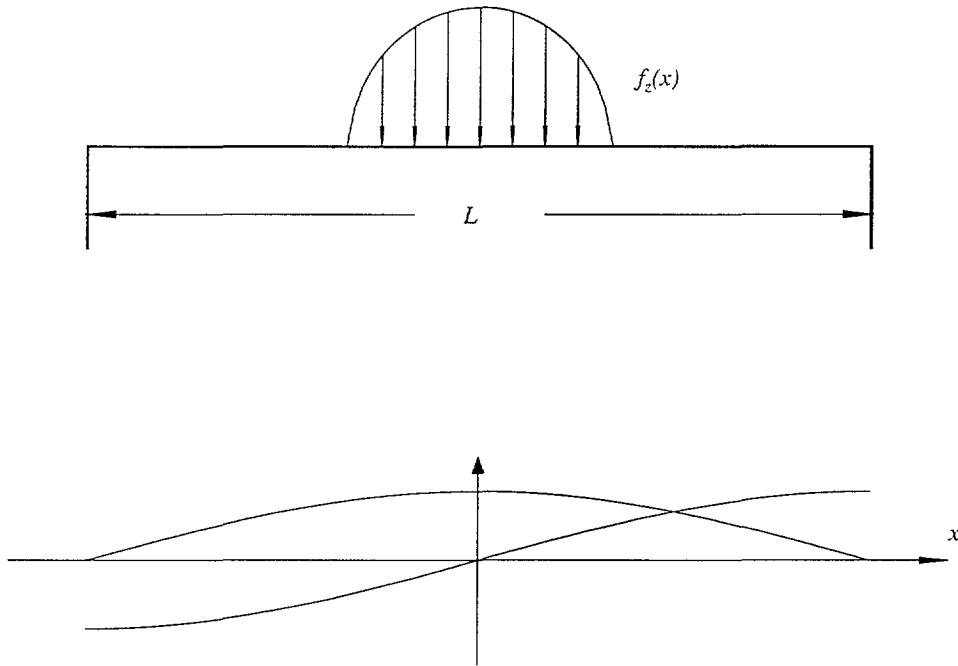
Figure 2-6: Shows the modeshape for the lowest eigenfrequencies of a domain of length L. The maximum wavelength is $\lambda_{\max} = 2L$ and hence the lowest non-zero spatial eigenfrequency is $\min(\omega_x) = \pi/L$.

form of Hooke's law,

$$\bar{\sigma}(s) = Q(s)\bar{\varepsilon}(s).$$

Where $\bar{\sigma}(s)$ and $\bar{\varepsilon}(s)$ are the Laplace transforms of the stress and the strain, respectively. $Q(s)$ is called the *Operational relaxance* and alternatively $Q(s)/s$ is called the *Operational impedance*. The main advantage in using the viscoelastic form of Hooke's law is that we can then apply the *correspondence principle*. According to the principle, if an elastic solution to a stress analysis problem is known, substitution of the appropriate Laplace transforms for the material constants employed in the elastic solution furnishes the viscoelastic solutions [83].

Hence, the effects of viscoelasticity can be incorporated into the elastodynamic solution in (2.41) simply by allowing the material constants to be frequency dependent, i.e. μ and β become $\mu(s)$ and $\beta(s)$. Similarly the effects of viscoelasticity can included in the static solution in Eq. (2.30) or in Eqs. (2.32) and (2.33).

The material constants are in general both independently rate independent, μ describing shear motion and β the dilational behavior. It is however often assumed that only μ is rate dependent. This assumption is reasonable for materials that are near being incompressible, ($\nu > 0.4$) which is the case for polymers and other materials we intent to apply this theory to. The simplest model that captures the behavior of a linearly viscoelastic solid is the 3-parameter
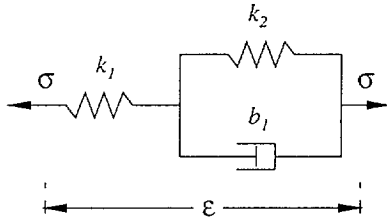
(a) 3–Parameter Standard Linear Solid   (b) Response of stress to a step in strain
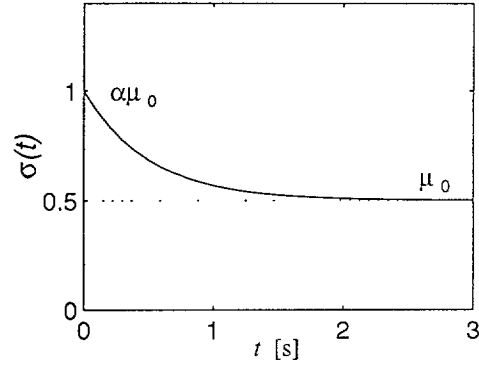
Figure 2-7: (a) Shows a diagram of the 3-parameter linear standard solid model using spring and damper elements. (b) Shows the response in stress to a step change in strain for the 3-parameter linear solid defined in Fig. 2-7. The relation between the parameters is that $\mu_0 = k_1 k_2/(k_1 + k_2)$, $\alpha = (k_1 + k_2)/k_2$. and $t_r = b_1/(k_1 + k_2)$.

standard linear solid.[9] For this model the transfer function for μ is,

$$\mu(s) = \mu_0 \frac{1 + t_r s}{1 + \frac{1}{\alpha} t_r s}$$

where μ_0 is the steady state response, t_r the retardation time and α is the overshoot of a step response. A schematic representation of the model as dampers and springs is shown in Fig. 2-7a. and the step response in Fig. 2-7b. i.e. the response in stress to a step in strain.

This model can be generalized to model materials with more than one time constant. The transfer function for the generalized model is

$$\mu(s) = \mu_0 \prod_{i=1}^{n} \frac{1 + t_{r_i} s}{1 + \frac{1}{\alpha_i} t_{r_i} s}.$$

The transfer function approach to viscoelasticity provides a powerful tool for the modeling of the viscoelastic properties of different materials. One still needs, however, to estimate the parameters in the transfer function for each material and under conditions that are as close as possible to the conditions under which the model is to be applied.

---

[9]Also called Kelvin model.

40

5. Conclusions

In this chapter we have given the basic theory of integral transforms and shown how they can be applied to problems in contact mechanics. We have shown how the solutions to contact problems involving various structures can be presented as transfer functions. The transfer function takes as inputs the boundary conditions but gives the desired solution as output. Analysis of the transfer function has also been shown to give us the qualitative properties and behavior of the solution, irrespective of the exact from of the input. The transfer function approach has further been shown to be equally applicable to problems involving static, dynamic and viscoelastic effects, and further analysis of the solutions has given us conditions under which inertial effects can be ignored and the quasi-static solutions are valid.

Chapter 3

Static Identification

1. Introduction

Manual exploration and manipulation of objects in an environment is important to both humans and robots. Human performance of these tasks is enabled by the haptic system consisting of tactile and kinesthetic sensory systems together with a motor control system. Similar classification is applicable to the sensory and motor systems of robots. A detailed and quantitative understanding of the underlying dynamics, information flow, and control strategies will benefit investigations of both human haptics and the development of machine haptics. It is especially valuable in the development of haptic interfaces through which humans can interact manually with teleoperated systems or computer generated virtual environments [74]. Although the principles of operation of man-made devices are quite different from those of humans, the constraints on the performance of these haptic tasks, such as the laws of physics governing the mechanics of contact and the presence of friction and gravity are the same for both. In addition, the type of tactual sensory information, their processing and the computation of the required control action are sufficiently similar for the two systems that the common aspects of information processing can be functionally separated from the hardware implementations. Therefore a computational theory of haptics that investigates what kind of information is necessary, and how it has to be processed in order to successfully complete a desired haptic task can be common to humans and robotic systems.

It has been recognized for some time that robots with dextrous hands need 'tactile sense' in order to successfully explore and manipulate objects in their environment. Reviews of the various tactile sensors designs have been given by several authors, (see for example [59, 68, 32].)

43

Because of the natural constraints imposed by this mode of sensing, the engineering designs have had to follow nature in overall configuration. By definition, tactile sensing is achieved through direct contact with objects, and therefore a 'skin' is necessary to protect the sensors from physical damage. The requirements that the skin should be soft comes from the need to have (1) regions of contact within which skin surface conforms to the object surface (instead of point or line contact that occurs between two rigid objects) (2) significant deformation within the medium so that the sensors are activated and have enough resolution. If the substrate material on which the sensors and the skin rest is also soft, then, in addition to the above, better prehension stability can be achieved. The fact that a point contact has no torsional resistance and that its stability is highly sensitive to local aberrations implies that compliant skin gives better prehension. Thus, although robotic tactile sensors themselves might differ in their operation, depending upon whether they respond to changes in conductance, capacitance, contact area, light intensity, etc., within each sensing cell caused be local mechanical distortions, the overall configuration of all the designs is that of mechano-sensitive transducers embedded in a deformable medium.

Two stages in tactual information processing, *encoding* and *decoding* make up the *identification problem*, which is so called because it involves the determination of the state of the object and its relationship to the tactual sensory system. The system discussed here differs in some ways from traditional dynamic systems. The most prominent difference is that it has both spatial and temporal variables, whereas traditional lumped parameter systems only have temporal ones. In both natural and man-made tactile systems the *encoding* process is the transduction of the mechanical stimulus into electrical signals that contain, in a coded form, information about the stimulus features. The inverse problem, i.e. the *decoding* process or the calculation of the surface shape or surface tractions from the transduced signals is in many respects significantly more difficult. The encoding is essentially a low-pass filtering process which indicates that the decoding will be ill-posed in the sense that the higher frequency components of the signals will be prone to noise contamination and special methods have to be applied for successful decoding.

Several papers can be found in the robotics literature on the mechanistic modeling, encoding and decoding of surface conditions from subsurface measurements using tactile sensors. The earlier papers dealt primarily with the mechanistic model and only the encoding. In [35] the problem is approached from a physiological point of view and in [20] from robotic point of view. Both papers use the plane strain assumption and give solutions to the 2-dimensional (2D) encoding problem. The decoding problem is first addressed in [73, 63], both of which solve only the 2D plane strain case. [73] uses a frequency domain approach whereas a neural network approach is used in [63]. The plane strain assumption is dropped in [9] but the analysis is limited to the properties of a specific photoelastic sensor. In [18] again plane stress or plane strain is assumed, the effects of finite thickness and the stability of the grasp are investigated.

44

The mathematics of the decoding problem are investigated using matrix regularizing operators in [65], where the loading is assumed to be axisymmetric. The combined results of the above papers are detailed in [19] which is the most thorough treatment so far on the infinite half-space and analytical solutions of the encoding and the decoding problem. [19] further gives the 3-dimensional (3D) half-space solution only to a normal point load in appendix. Additionally, finite element analysis is used in [72], where the effects of shear loads on sub-surface strain and stress are demonstrated graphically, and also in [17] which investigates the differentiation of shapes and the inherent difficulties that arise because of the blurring effect of the skin. In [28] the encoding and decoding of a stress rate sensor are investigated and a scalar Wiener inverse is suggested for the decoding. Finally, in [60] the 2D plane strain solution for a cylindrical finger is given.

In summary, none of the papers above treats either the encoding or the decoding problem fully. All the results published until now on the reconstruction of general surface loads and profiles from subsurface tactile signals do not solve the full 3D problem. The effects and interaction of shear loads and the selection of appropriate sensor signals has not been investigated before. In addition, neither the decoding problem has been fully addressed nor has the multivariate Wiener inverse been applied. In this chapter we will address mainly the mechanistic modeling, encoding, and the decoding problems. The contributions of this chapter can be itemized as follows:

1. A complete solution to the 3D half-space problem is given for arbitrary 3D static loading conditions and any linearly elastic material, instead of the 2D solutions used before. The solution also applies to pseudo dynamic problems which can be described as a sequence of elasto-static problems (such as the estimation of the onset of slip).

2. The solution is formulated using transfer function matrices in the domain of spatial frequency which allows us to look at the qualitative properties and general behavior of the solution, irrespective of particular cases of the loading or object shape. It also enables efficient numerical implementation based on the theory of linear signal processing.

3. Symmetry and signal bandwidth arguments are invoked to select the optimal transducing signals or types of sensors. For decoding, we can then apply the signal processing and regularization theory in a manner similar to what has been done in the development of computational theory of vision.

4. Numerically stable multivariate regularizing solution methods for the decoding problem are delineated. The ill-posedness of the decoding process is analyzed and it is shown as to how the extensively developed methods of image restoration can be applied to avoid the problems associated with the ill-posedness.

45

In Section 2, we formulate and solve the 3D half-space elastic model, which serves as a description of the encoding process. For the sake of clarity, the mathematical expressions are detailed in Appendix A. In Section 3, we analyze the decoding problem, first as an ideal problem without any real world effects such as noise, following which we incorporate the effects of sampling and random additive noise into the solution. This constitutes an algorithm for the decoding process. In Section 4, we give example numerical simulations of the methods proposed in Section 3. Conclusions are given in section 5.

2. The Encoding Problem

From a theoretical viewpoint, tactile sensor response to any given stimulus can be predicted if we have the following:

1. A mechanistic model of the deformable medium which can be used to calculate reliably the stresses and strains at each point in the medium for a given mechanical stimulus.

2. A model of the sensor that provides the relationship between the relevant stimulus. i.e., a particular combination of stresses and strains in the local neighborhood of a sensor that it is responsive to and the sensor response.

For example. an appropriate mechanistic model of the human skin and the soft tissues underneath enables us to investigate one of the important questions in cutaneous neurophysiology. that of identifying the relevant stimulus that causes each receptor type to respond [35, 75]

2.1 Mechanistic Analysis

In the robotic tactile sensing literature, contact analysis problems are frequently simplified by posing them as 2D plane strain problems in the elastic half-space [70, 23, 36]. The surface load or profile is then assumed not to change along one dimension on the planar surface, for example. as in the case of a line load. Almost all the results in the literature on the analysis of tactile sensing have made this assumption. Clearly, this is a serious limitation. In this section we will give the more general solution when 3D loads are arbitrarily distributed over the contact region.

The assumption that the problem can be posed as a contact problem in the semi-infinite half-space still remains, mainly for the sake of analytical tractability. We can, however, partially

justify that assumption based on numerical solutions obtained for finite models [13, 75] which show that the effects of finite extent are minimal when the contact region is small relative to the surface area of the medium. The semi-infinite half-space solution is a good approximation in such cases because the stress/strain response to a load decreases exponentially with distance from the load.

The problem is set up so that the boundary surface coincides with the xy-plane and the positive z-axis points into the medium (See Fig. 3-1). The material is assumed to be lin-
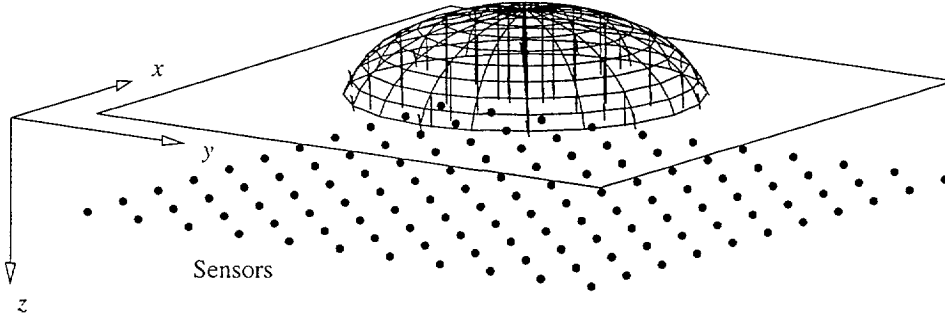
Figure 3-1: Shows the semi-infinite halfspace with surface tractions and subsurface sensors. The x- and y-dimensions extend to infinity in both negative and positive directions. The z-dimension extends from 0 to positive infinity. The tractions are distributed over the contact area, each point being subjected to 3-dimensional loading $f(x,y) = [f_x, \ f_y, \ f_z]^T$.

early elastic and homogeneous. It is also assumed to extend to infinity in both negative and positive x, y directions and in the positive z direction. The surface load is described by the traction vector field $f(x,y) = [f_x(x,y), \ f_y(x,y), \ f_z(x,y)]^T$ and the surface displacement field as $u_0(x,y) = [u_x(x,y,0), \ u_y(x,y.0), \ u_z(x,y,0)]^T$. In our formulation, the boundary conditions can be forces, displacements or mixed, i.e. when any 3 elements from both f and u_0 are given. We intend to present the solution in the space of spatial frequencies and use transfer functions to simplify solutions and gain further insight.

2.2   Transfer Function Matrices (TFM)

Many equivalent routes to the solution of the encoding problem exist, but the simplest and most direct way for our purposes is to transform the fundamental differential equations of equilibrium and the stress-strain relationship equations (Generalized Hooke's law) using the Fourier transform over (x, y) space. Examples of this approach can be seen in [16] and [71]. The derivation of the transfer function matrix form of the solution is given in Appendix A.

Similar to what is done in control theory, we employ here the concept of a transfer function

47

matrix (TFM). The transfer function matrices we give here have the Fourier transform of the components of either $f(x,y)$ or $u_0(x,y)$ as the inputs and any displacements, strains or stresses in the medium as the outputs. Each entry of the TFM would then correspond to the contribution of a particular input component to the corresponding output component. For example the entry in the TFM for the z-displacement resulting from the x-load, or $u_z^x(x,y,z)$ we would write

$$\bar{u}_z^x(\omega_x,\omega_y,z) = T_{u_z^x f}(\omega_x,\omega_y,z)\bar{f}_x(\omega_x,\omega_y)$$

to obtain the Fourier transform $\bar{u}_z^x(\omega_x,\omega_y,z)$ of $u_z^x(x,y,z)$ from the transfer function $T_{u_z^x f}(\omega_x,\omega_y,z)$ and the Fourier transform $\bar{f}_x(\omega_x,\omega_y)$ of the surface shear load $f_x(x,y)$. Here, ω_x and ω_y correspond to spatial frequencies in the x and y directions respectively. Then we can write

$$\bar{u} = T_{uf}\bar{f} \qquad \bar{\varepsilon} = T_{\varepsilon f}\bar{f} \qquad \bar{\sigma} = T_{\sigma f}\bar{f} \qquad \bar{p}_n = T_{p_n f}\bar{f}$$

$$\bar{u} = T_{uu_0}\bar{u}_0 \qquad \bar{\varepsilon} = T_{\varepsilon u_0}\bar{u}_0 \qquad \bar{\sigma} = T_{\sigma u_0}\bar{u}_0 \qquad \bar{p}_n = T_{p_n u_0}\bar{u}_0$$

$$(3.1)$$

where the subscript f indicates that surface tractions are inputs and the subscript u_0 indicates that surface displacements are inputs. As an example, we give here $T_{\varepsilon u_0}$, i.e. the case when the surface displacements (u_0) are the inputs and the subsurface strains (ε) are outputs. The other TFMs are given in Appendix A.

$$T_{\varepsilon u_0} = \frac{e^{-z\Omega}}{(3-4\nu)\Omega}$$

$$\times \begin{bmatrix}
j\omega_x\left((3-4\nu)\Omega - \omega_x^2 z\right) & -j\omega_x^2\omega_y z & \Omega\omega_x^2 z \\
-j\omega_x\omega_y^2 z & j\omega_y\left((3-4\nu)\Omega - \omega_y^2 z\right) & \Omega\omega_y^2 z \\
-j\Omega\omega_x(1-\Omega z) & -j\Omega\omega_y(1-\Omega z) & -\Omega^2\left(2(1-2\nu)+\Omega z\right) \\
\frac{1}{2}\omega_y\left((3-4\nu)\Omega - 2\omega_x^2 z\right) & \frac{1}{2}\omega_x\left((3-4\nu)\Omega - 2\omega_y^2 z\right) & \Omega\omega_x\omega_y z \\
-\frac{1}{2}\left((3-4\nu)\Omega^2 + \omega_x^2(1-2\Omega z)\right) & -\frac{1}{2}\omega_x\omega_y(1-2z\Omega) & j\Omega\omega_x(1-2\nu)+\Omega z) \\
-\frac{1}{2}\omega_x\omega_y(1-2z\Omega) & -\frac{1}{2}\left((3-4\nu)\Omega^2 + \omega_y^2(1-2\Omega z)\right) & j\Omega\omega_x(1-2\nu)+\Omega z)
\end{bmatrix}$$

$$(3.2)$$

where $\Omega = \left(\omega_x^2 + \omega_y^2\right)^{1/2}$, μ is the shear modulus, and ν is the Poisson ratio. TFMs for mixed cases can also be easily constructed by choosing appropriate elements from the TFMs above.

The equations in (3.1) represent the solution for the encoding problem, because given $f(x,y)$, $u_0(x,y)$ or a combination of 3 elements from the two, we can predict $u(x,y,z)$, $\varepsilon(x,y,z)$, $\sigma(x,y,z)$ and $p_n(x,y,z)$. If the relevant stimulus, i.e. a particular combination of stresses and strains in the local neighborhood of the sensor that it is responsive to, is known, we can predict the sensor response. For example, if the sensor response is linearly related to the strain ε_{zz}, then it is the relevant stimulus for that sensor. On the other hand, if the relevant stimulus

48

needs to be identified, we can use Eq. (3.1) to generate hypotheses that can be tested against the empirically measured sensor response, as is done in [35, 75].

3. The Decoding Problem

Tactile information is obtained with mechanosensors embedded in a deformable medium that is in contact with a shaped object. Mechanosensors, embedded within the medium can, at best, provide information on skin surface shape and surface traction distribution. From this information, contact region, shape of the object and the contact state need to be inferred. The problem at hand is therefore the decoding, i.e. reconstruction of the surface shape of the medium, the tractions on the surface as well as the region of contact from sub-surface mechanosensory information.

The approach we have chosen is to represent the solution in the spatial frequency domain, in terms of transfer functions as in Eq. (3.1). Equivalently, using superposition of the point load solution, the solutions can also be presented as convolution integrals. The transfer function approach gives, however, solutions whose properties are more transparent and some important statements can be made regarding their qualitative properties (such as the symmetry and bandwidth properties of subsurface stress or strain components), irrespective of the exact form of the loading. This approach also enables the use of efficient tools of linear signal processing, such as the Fast Fourier Transform.

This section is organized as follows. In section 3.1 we discuss the constraints that the task of tactile identification puts on the selection and the number of necessary sensor signals, and furthermore identify possible candidates of sensor signal combinations. In section 3.2 we use symmetry arguments to analyze the TFMs of the previously identified candidates in order to find an optimal combination. Finally, in section 3.3 we show how an optimal multivariate Wiener inverse can be used to reconstruct the surface signals from measurements of the sensor signal in the presence of noise and sampling errors.

.

3.1 Sensory Information Necessary for Reconstruction

The most obvious signals to reconstruct are the deformed shape of the surface of the medium and the spatial distribution of surface tractions. The extents of the contact area need to be assessed but the surface displacements are necessarily continuous at the edge of the contact area, so they provide limited information. Discontinuities in slope or curvature of surface shape however, do not reliably indicate contact borders as an object surface within the contact region could have similar discontinuities and therefore be mistakenly identified as borders of the contact region. Each of the regions where the surface tractions (e.g. normal pressure) are non-zero indicates the region of contact with the object. Within these regions the object shape is the same as the shape of the deformed medium surface. In addition, the surface traction distribution can directly give valuable information on the stability of grasp and the type of contact, be it static or vibrating.

Some interesting properties of the TFM can be obtained when dynamic systems theory is applied to them. In what follows we assume that the sensors pick up a strain component or mean normal stress and further that the components of the strain are expressed in the global coordinate system (x, y, z). If the medium is incompressible, uniform normal pressure on its surface does not cause any strains within. Therefore, measurements of strains only are not sufficient to fully reconstruct surface force distributions, as the mean normal stress component will not be detectable in the strains for incompressible materials. This is the main reason for the use of the mean normal stress as a variable that needs to be sensed.

If no shear loads are present, or if the relationship between normal and shear loads is known, only one component of strain needs to be sensed. However, if shear independent of the normal load is present, the more general TFM formulation must be employed, as the surface tractions must be obtained by the inversion of some of the equations in Eq. (A.7) and (A.9) in Appendix A. What and how many components of the strain tensor are needed depend on the assumptions we make on the loading conditions. This can be detailed in the following cases.

1. **No shear loading:** In this case the normal pressure distribution and surface displacements need to be reconstructed. Sensing of any strain or the mean normal pressure is generally sufficient, but the need for rotational symmetry about the z-axis makes either of p_n or ε_{zz} the natural choice. Using p_n will enable the calculation of the uniform pressure component of the total load which no combination of strains can provide if $\nu = 0.5$ (i.e. incompressible material). However, the combination of p_n and ε_{zz} can also be used to obtain increased spatial frequency bandwidth (see section 3.2), in addition to obtaining

the full load distribution.

2. **Relationship between normal loads and shear loads is fully or partially known:** This is the case for example, if the object is sliding over in an unknown direction over the surface under Coulomb friction conditions, or if the relationship between normal and shear loads is unknown but the direction of the shear load is known. Then any two subsurface stress and strain components need to be sensed to fully reconstruct all three surface traction or displacement components, and a natural choice would again be p_n and ε_{zz} as above.

3. **All tractions unknown:** All 3 traction components and surface displacements need to be reconstructed. Considering only combinations symmetric in (x, y) the following combinations become candidates: (a) $(\varepsilon_{xy}, \varepsilon_{xx}, \varepsilon_{yy})$, (b) $(\varepsilon_{xx}, \varepsilon_{yy}, \varepsilon_{zz})$, (c) $(\varepsilon_{zz}, \varepsilon_{xz}, \varepsilon_{yz})$, (d) $(\varepsilon_{xy}, \varepsilon_{xz}, \varepsilon_{yz})$, (e) $(p_n, \varepsilon_{zz}, \varepsilon_{xy})$, (f) $p_n, \varepsilon_{xx}, \varepsilon_{yy}$, and (g) $(p_n, \varepsilon_{xz}, \varepsilon_{yz})$.

We will shortly show how we can make an optimal choice among these component sets.

Case 3 is the most general one and it indicates that any sensor population that is suitable for reconstructing arbitrary loading conditions must measure at least three independent stress/strain components (out of a total of six). More components could be used to get redundant measurements, and hence more reliable estimates, but here we will only look at the minimal set.

3.2 Analysis of TFM Properties

We now try to use the properties of the TFM to identify the sensor combination that is most suitable for tactile sensing. Particulary we will a look at the rank of the TFM and its bandwidth.

Rank of the TFM

Since we intend to invert the TFM, we need to consider its rank, which is a key property and has to be full for an inversion to be possible. If the TFM loses rank, information is lost as the output will span fewer dimensions than the input. The conditions under which the TFM looses rank are closely related to zero-properties of dynamic systems, just as the conditions under

which the TFM becomes infinite are related to the poles. The TFMs in our case are however always finite and therefore do not possess any pole-like properties, which is to be expected from a linear mechanical system in stable equilibrium.

The TFM looses rank when its determinant becomes zero. When the traction vector f is the input, the determinants of the TFM candidates detailed in section 3.1 are

$$\det(T_{\varepsilon_{xy},\varepsilon_{xx},\varepsilon_{yy}}) = 0 \tag{a}$$

$$\det(T_{\varepsilon_{xx},\varepsilon_{yy},\varepsilon_{zz}}) = -(1-2\nu)\frac{\omega_x\omega_y}{\Omega^2}e^{-z\Omega} \tag{b}$$

$$\det(T_{\varepsilon_{zz},\varepsilon_{xx},\varepsilon_{yz}}) = -(1-2\nu)e^{-z\Omega} \tag{c}$$

$$\det(T_{\varepsilon_{xy},\varepsilon_{xz},\varepsilon_{yz}}) = -(1-2\nu)\frac{\omega_x\omega_y}{\Omega^2}e^{-z\Omega} \tag{d}$$

$$\det(T_{p_n,\varepsilon_{zz},\varepsilon_{xy}}) = \frac{2(1+\nu)}{3}\frac{\omega_x^2 - \omega_y^2}{\Omega^2}e^{-z\Omega} \tag{e}$$

$$\det(T_{p_n,\varepsilon_{xx},\varepsilon_{yy}}) = \frac{2(1+\nu)}{3}\frac{2\omega_x\omega_y}{\Omega^2}e^{-z\Omega} \tag{f}$$

$$\det(T_{p_n,\varepsilon_{xz},\varepsilon_{yz}}) = \frac{2(1+\nu)}{3}e^{-z\Omega} \tag{g}$$

We see that the first one is always rank deficient. If the medium is incompressible, i.e. if $1 - 2\nu = 0$, then the next three TFMs loose rank. As discussed in section 3.1 the mean normal stress, p_n, must be among the sensor signals in the case of an incompressible material. Otherwise the component of the surface load that contributes to the mean normal stress cannot be reconstructed. A special case is a solid subjected to uniform pressure. No strains will be detected inside the solid, although the pressure can be arbitrary.

We also note that the TFM looses rank for candidate (e) when $\omega_x = \pm\omega_y$ and for candidate (f) when $\omega_x = 0$ or $\omega_y = 0$. That the TFM looses rank for certain directions in the (ω_x, ω_y) plane, means that the inputs cannot be reconstructed along those same lines. In the case of candidate (f) this means that the cumulative load distribution in either x or y direction cannot be reconstructed. For example, if $\omega_y = 0$, in frequency space we have $\bar{f}(\omega_x, 0) = \bar{g}(\omega_x)$ and $g(x) = \int_{-\infty}^{+\infty} f(x,y)dy$, which is the cumulative load distribution along x. Therefore, since the TFM for candidate (f), $T_{(f)}$, is rank deficient for $\omega_y = 0$, the component containing information on the cumulative distribution of the input along x will be lost in the encoding. The same arguments apply to candidate (e), with the coordinate system rotated by $\pm45°$ around the z-axis. Candidate (g) is the only one that does not loose rank and therefore has the desirable combination of p_n and strains that the sensors need to transduce for decoding.

Remark: The comments above are also valid when the displacement vector u_0 or any combination of tractions and displacements are the inputs, since $T_{uu_0} = T_{uf}T_{fu_0}$ and the TFM that relates u_0 and f (Eq. (A.10) in the Appendix) has the determinant,

$$\det T_{u_0 f} = \frac{2(1 + \nu)^3}{3 - 4\nu} E^3 \frac{1}{\Omega^3} \tag{3.3}$$

which does not alter the rank properties of each of the TFMs of candidates (a)-(g) above.

Bandwidth of Spatial Frequency

A frequently used property of dynamic systems is the bandwidth of the components of the TFM which measures how the attenuation of each signal in the medium depends on frequency. High bandwidth would mean that reconstruction is possible with finer details and is therefore desirable. However, since the frequency is 2D, the bandwidth will also depend on orientation in the (x, y) plane, which in turn can be used to exclude sensor combinations which lack rotational symmetry about the z-axis.

To compare the bandwidth of the various combinations (a)-(g) listed above, we look at the power spectrum of the TFMs, a line at a time. That is, the power spectrum of each sensor signal is the norm of the corresponding line vector in the TFM. For example

$$\mathcal{P}_{\varepsilon_{xz}} = \| \left[T_{\varepsilon_{xz}^x} \; T_{\varepsilon_{xz}^y} \; T_{\varepsilon_{xz}^z} \right] \|^2,$$

but this implicitly assumes that the all the traction imputs are weighted equally. Weighing the normal traction differently than the shear traction does not alter the result of the following arguments, as long as the shear tractions are weighted equally. The power spectrum for the possible sensory signals can be seen in Figs. 3-2-3-7. The figures show the power spectrum as density plots with darker and lighter areas indicating frequencies where attenuation is low and high, respectively. Also shown along the border of the density plot, are projected profiles of the power spectrum along the lines $\omega_x = 0$, $\omega_y = 0$, and $\omega_x = \omega_y$. Figures 3-2-3-7 show the power spectrum respectively for p_n, $\varepsilon_{xx}, \varepsilon_{zz}, \varepsilon_{xy}, \varepsilon_{xz}$ and candidate (g) ($\mathcal{P}_{p_n} + \mathcal{P}_{\varepsilon_{xz}} + \mathcal{P}_{\varepsilon_{yz}}$). We note that the power spectrums for ε_{yy} or ε_{yz} are obtained from that of ε_{xx} or ε_{xz} rotated by 90°.

Two most important features of the spectrums are their frequency bandwidth and rotational symmetry. If the sensor responses cannot be combined to form a rotationally symmetric spectrum, the sensor response would depend on stimulus orientation in the xy-plane, which is undesirable, because of different proportions of signal to noise, (i.e. assuming that the noise is

at least partially independent of the signal amplitude).

We note that $\mathcal{P}_{\varepsilon_{zz}}$ has similar shape as $\mathcal{P}_{p_n}$ but higher bandwidth, while the other strains have orientation dependent bandwidth. This excludes candidate (e) since for $\mathcal{P}_{\varepsilon_{xy}}$ (Fig. 3-5), frequencies along $\pm 45°$ are attenuated. Candidate (f) is also excluded because both ε_{xx} and ε_{yy} attenuate frequencies along 0 and 90° and using both will therefore not produce rotational symmetry. It is worth noting that the directions of attenuation coincide with the conditions under which the TFM looses rank (see section 3.2). Candidate (g) is therefore the only one remaining and it can provide rotational symmetry as seen in Fig. 3-7. The importance of having full rank and bandwidth in all directions becomes apparent when one considers that loss of rank means that infinitely many load combinations produce identical sensor responses and hence make inversion impossible for those cases, and lower bandwidth in any one direction means that less information on the spatial features characterizing that dimension of the object is observable by the sensors. The conclusion is therefore that given the assumption that we are using Cartesian strain sensors, the only combination that works for incompressible materials and possesses symmetry is $(p_n, \varepsilon_{xz}, \varepsilon_{yz})$ and the TFM for that selection is (ref. Appendix A):

$$
T_{sf} = \frac{(1+\nu)e^{-z\Omega}}{E\Omega}
\begin{bmatrix}
-j\omega_x & -j\omega_y & \Omega \\
-(\Omega - \omega_x^2 z) & \omega_x \omega_y z & j\Omega\omega_x z \\
\omega_x \omega_y z & -(\Omega - \omega_y^2 z) & j\Omega\omega_y z
\end{bmatrix}
\tag{3.4}
$$

where s stands for a normalized sensor signal $s = \left[\frac{3}{2E}p_n, \varepsilon_{xz}, \varepsilon_{yz}\right]^T$.

Remark: The sensor combination $(\sigma_{zz}, \sigma_{xz}, \sigma_{yz})$ is equivalent to $(p_n, \varepsilon_{xz}, \varepsilon_{yz})$, but the latter combination can be considered to be unique and optimal because in almost all sensors, it is the strains that are directly measured and stresses are then inferred from the strains. The mean normal stress, p_n, is however needed for incompressible materials and therefore included. As long as we are sensing stresses or strains, the range of spatial frequency sensed through each component is of the same order. But only some of the components and combinations are rotationally symmetric about the z-axis.

The Structure of the Sensor TFM

Analyzing the structure of the TFM in Eq. (3.4) we observe that the $e^{-\Omega z}$ factor, which is common to all the terms, expresses how the signals get increasingly lowpass filtered or blurred
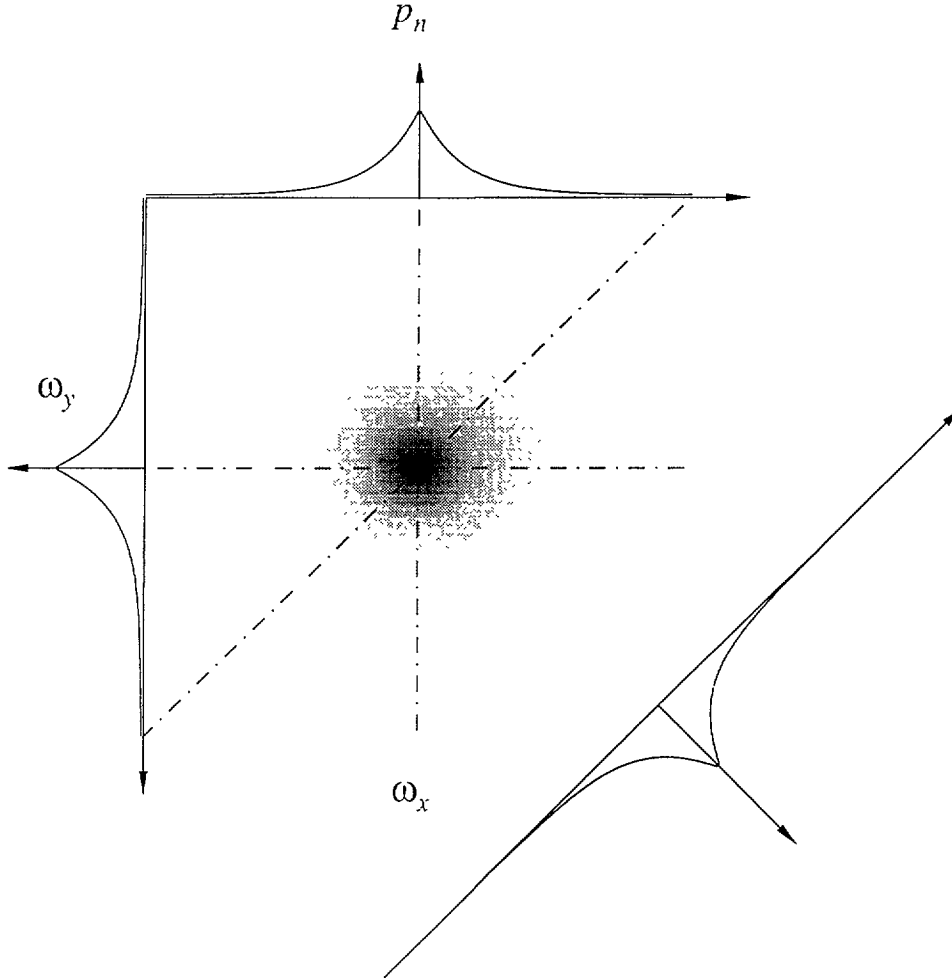
Figure 3-2: The power spectrum of the mean normal stress $\mathcal{P}_{p_n}$. We observe that it is rotationally symmetric with a smaller bandwidth than $\mathcal{P}_{\varepsilon_{zz}}$ (Fig. 3-4).

with depth. It is a consequence of the model including the resistance of the medium to shear and is therefore necessary if the sensors are to have a subsurface location. We further observe that there are two basic variants of transfer functions in the sensor transfer function matrix, which we will call T1 and T2. T1 is characterized by its norm behaving like $e^{-\Omega z}$, for example $T_{p_n f_z} = e^{-\Omega z}$. T2, on the other hand, is characterized by its norm behaving like $|\omega_i| z e^{-\Omega z}$, $i = x, y$, e.g. $|T_{\varepsilon_{xz} f_z}| = |\omega_x| z e^{-\Omega z}$. They differ in that the T1 transfer function has lowpass characteristics but the T2 transfer function has bandpass characteristics. In the spatial domain this means that the response of the T1 terms is spread over larger area since a predominantly low frequency content indicates slow variations in the spatial domain. The response of the T2 terms on the other hand, is more localized and they respond better to sudden changes in the loading since they have higher bandwidth.
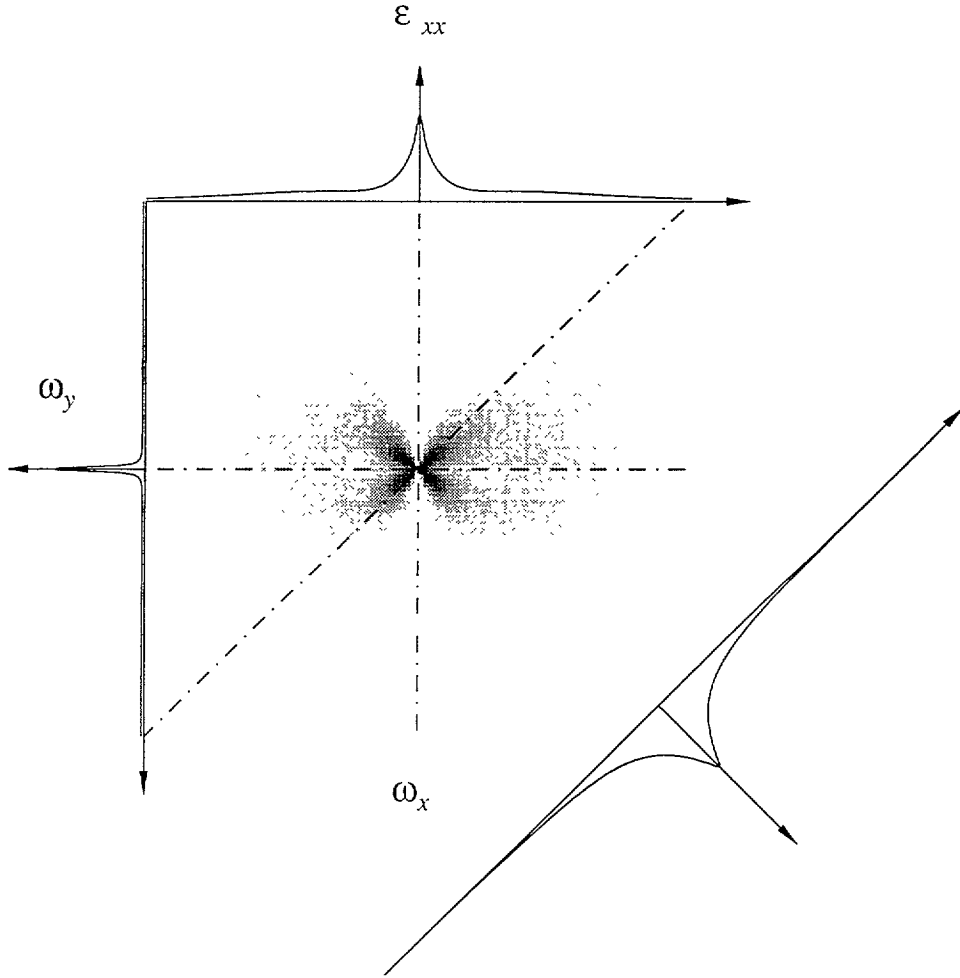
Figure 3-3: The power spectrum of the x normal strain $\mathcal{P}_{\varepsilon_{xx}}$. This power spectrum is not rotationally symmetric as it behaves like $\mathcal{P}_{p_n}$ in the $\omega_x = \pm\omega_y$ directions but as $\mathcal{P}_{\varepsilon_{zz}}$ in the ω_x-direction (along $\omega_y = 0$.)

Terms like $j\frac{\omega_i}{\Omega}e^{-\Omega_z}$, $i = x, y$, have the same bandwidth as the T1 and but terms like $\frac{\omega_i\omega_k z}{\Omega}e^{-\Omega_z}$, $i, k = x, y$ on the other hand are of type T2.

The TFM is symmetric with respect to x and y, since the halfspace model is identical for x and y. Looking at the TFM linewise, we see that line 1, ($\hat{p}_n$ terms) contains only T1 terms, but lines 2 and 3 (ε_{xz} and ε_{yz} terms) contain mostly T2 terms. T1 terms appear in the subdiagonal, in $T_{\varepsilon_{xz}f_x}$ and $T_{\varepsilon_{yz}f_y}$. These T1 terms serve their purpose as they are are the reason that the matrix is non-singular for $\Omega = 0$.

Looking at the TFM columnwise, and column 3 first, we see that $\hat{p}_n$ term in line 1 is type T1 and the ε_{xz} and ε_{yz} terms are type T2, and we observe that they are proportional to the
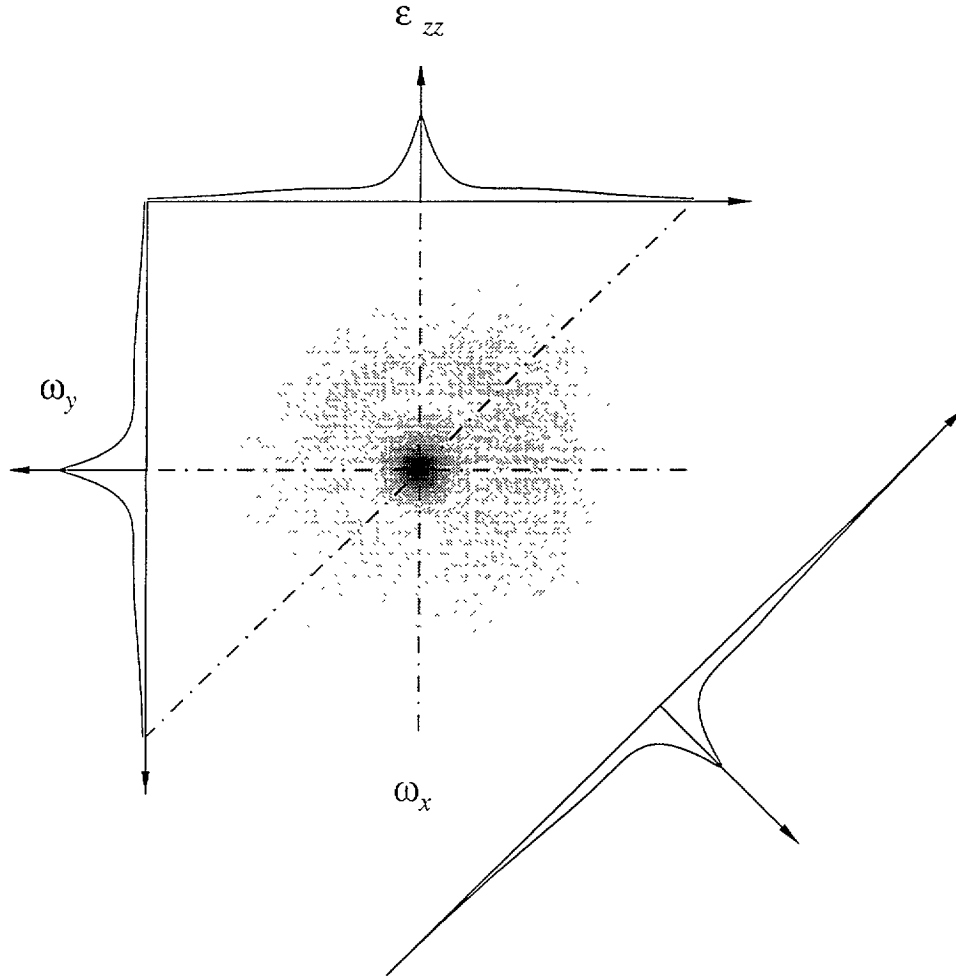
Figure 3-4: The power spectrum of the z normal strain $\mathcal{P}_{\varepsilon_{zz}}$. This one is also rotationally symmetric as $\mathcal{P}_{p_n}$ (Fig 3-2) but it has higher bandwidth.

x and y partial derivatives of the p_n term (in addition also multiplied by z). The same is true for the other two columns, except for the previously mentioned additional T1 terms on the subdiagonal.

In summary, the TFM can be interpreted as the $\hat{p}_n$ terms measuring the surface force as directly as possible within the constraints posed by the subsurface location while the other two sensor signals complement the $\hat{p}_n$ signal by measuring its x and y spatial derivatives.
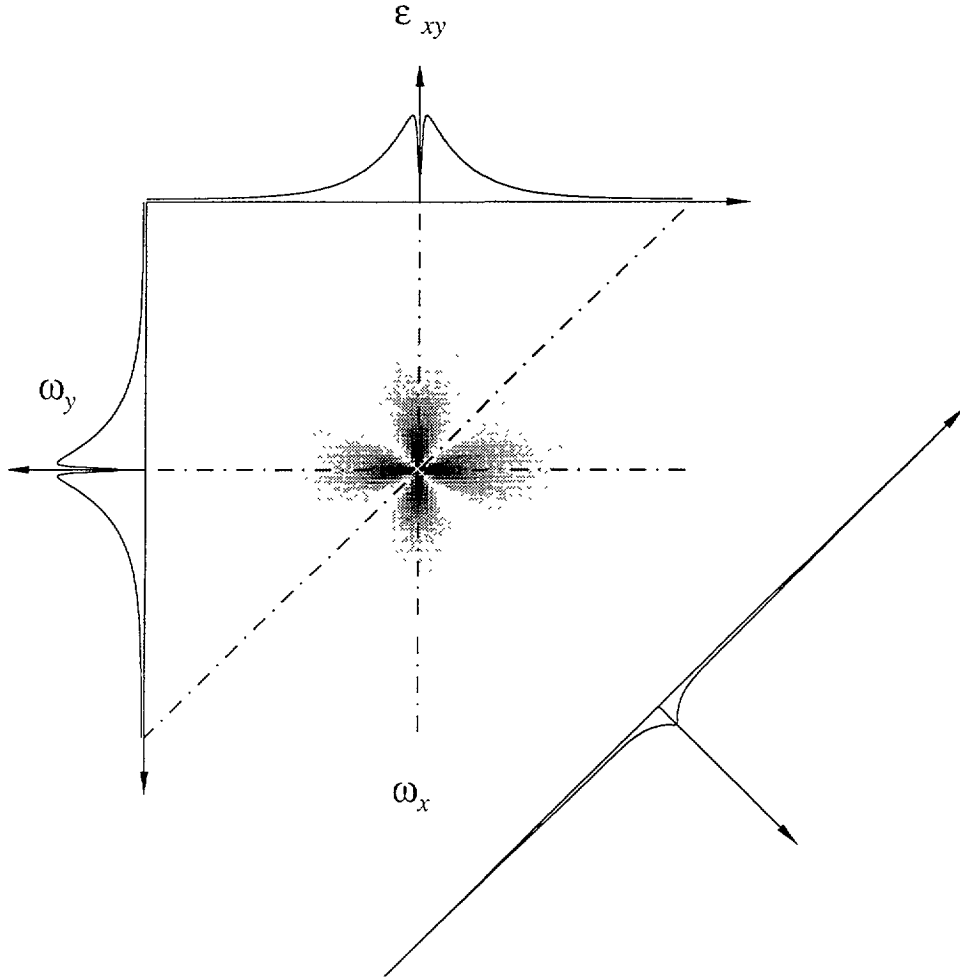
Figure 3-5: The power spectrum of the xy shear strain $\mathcal{P}_{\varepsilon_{xy}}$. It is not rotationally symmetric and it differs from the other spectrums in that it has a sharp minimum at the origin.

3.3 The Decoding Solution

The Ideal Case

Ideally the solution to the problem would be obtained by simply dividing the sensor output by the transfer function in the frequency domain, i.e.

$$\phi_0(\omega_x, \omega_y, 0) \quad = \quad T^{-1}(\omega_x, \omega_y, z)s(\omega_x, \omega_y, z)$$

where ϕ_0 is the desired surface signal that needs to be calculated during the decoding process (can be either tractions, displacements or a combination), $T(\omega_x, \omega_y, z)$ is the transfer function
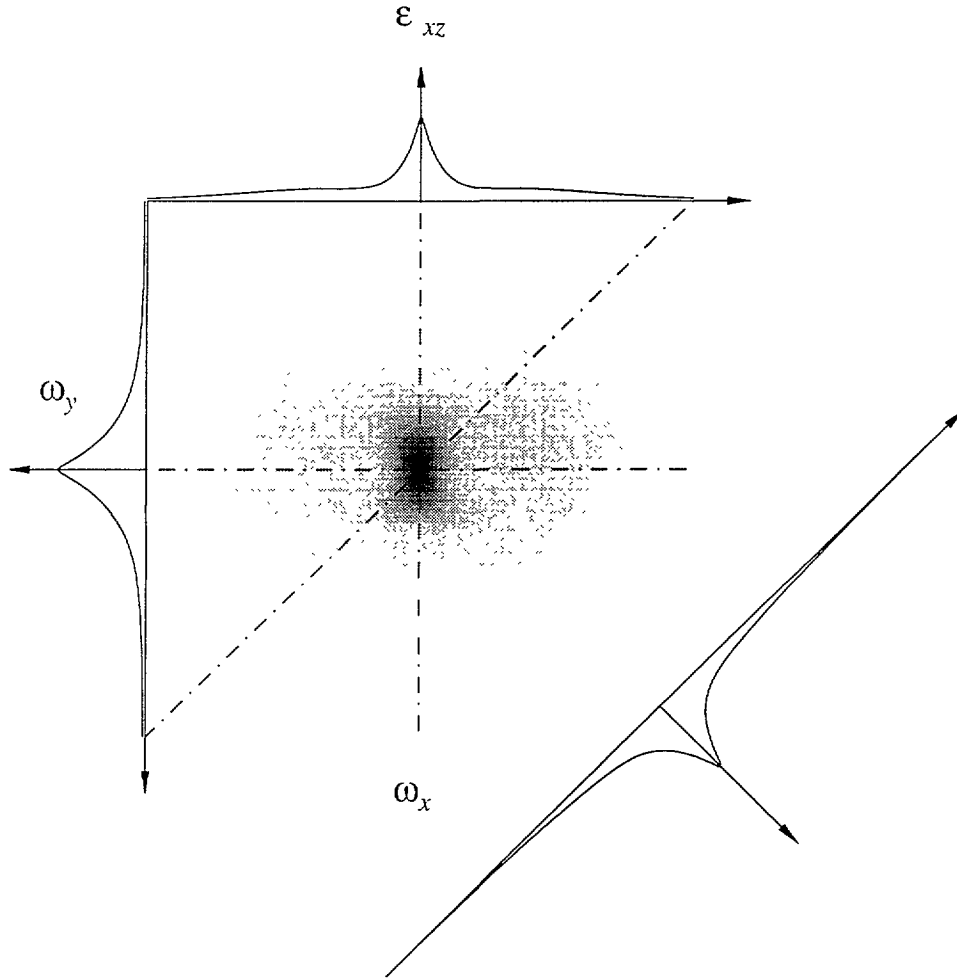
Figure 3-6: The power spectrum of the xz shear strain $\mathcal{P}_{\varepsilon_{xz}}$. This power spectrum behaves like $\mathcal{P}_{\varepsilon_{zz}}$ in the ω_x-direction, but as $\mathcal{P}_{p_n}$ in the ω_y-direction, and it is therefore not rotationally symmetric. The $\mathcal{P}_{\varepsilon_{yz}}$ power spectrum can be obtained from this one by a permuationa of x, y or a rotation of the axis by $\pm 90_o$.

and s is the measured signal. As can be seen from the TFM expressions, the transfer function is a low-pass filter where the high-frequency response goes exponentially to zero as Ω tends to ∞. Therefore the inverted transfer function will become arbitrarily large for high frequencies. This is very impractical and will lead to serious errors in real circumstances. To avoid this problem we will instead use regularized solutions, which is a common practice in treating ill-posed problems such as this one. Most regularization problems are formulated as scalar problems, here however we will need to use multivariate regularization which happens to be used in specialized problems such as the digital restoration of multichannel images [21, 22].
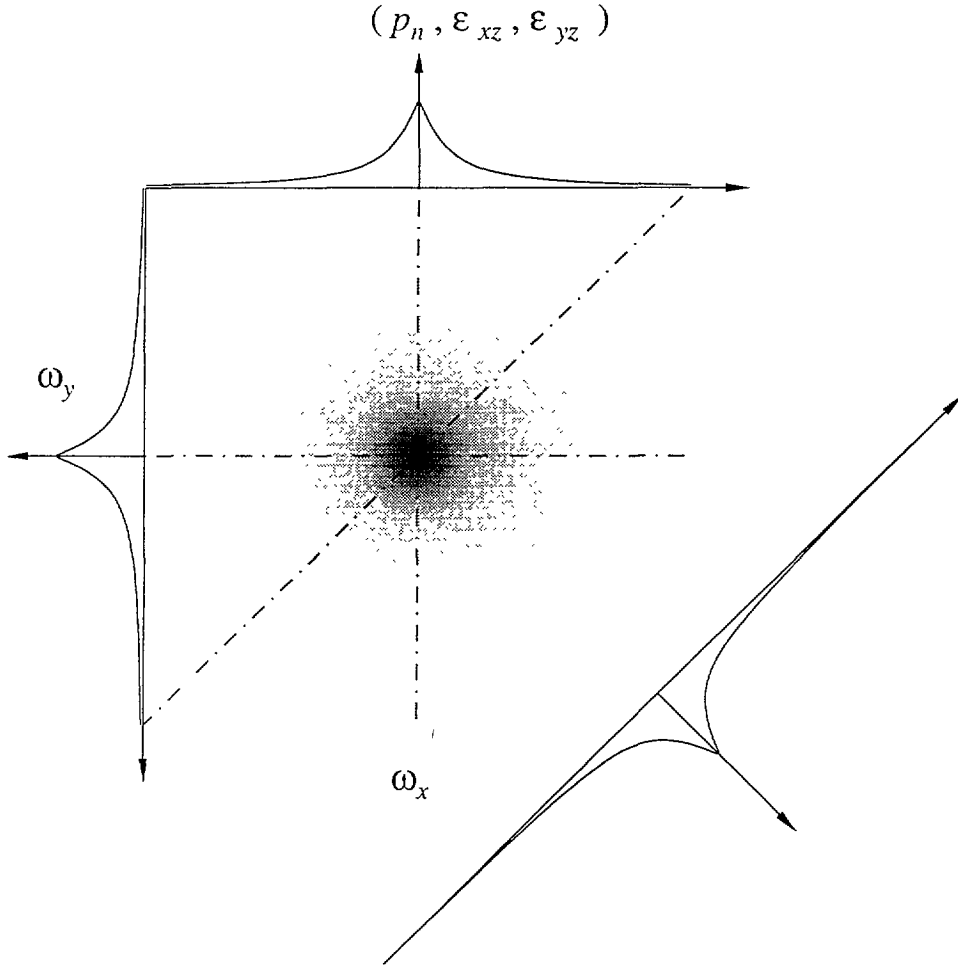
Figure 3-7: The power spectrum of the sensor signals in candidate (g), i.e. $\mathcal{P}_{(p_n, \varepsilon_{xz}, \varepsilon_{yz})} = \mathcal{P}_{p_n} + \mathcal{P}_{\varepsilon_{xz}} + \mathcal{P}_{\varepsilon_{yz}}$. We observe that it is rotationally symmetric and as the ε_{xz} and ε_{yz} components complement each other.

The Real Case

In addition to the features of the ideal problem, the real problem involves the unfavorable effects of noise and spatial sampling. Both these effects can be effectively minimized using regularizing agents in the solution as shown in [80]. One possible way of solving the resulting integral equations is to discretize the integral and put it in the form of a system of linear equations [65, 63]. A more intuitive way is to construct a regularizing operator in the frequency domain using transfer functions as follows. The solution is obtained as in the ideal case except for the multiplication factor $\psi(\omega_x, \omega_y, z, \sigma)$ where σ is a regularizing parameter, i.e.

$$\hat{\phi}_0(\omega_x, \omega_y) = \psi(\omega_x, \omega_y, z, \sigma) T^{-1}(\omega_x, \omega_y, z) \bar{s}(\omega_x, \omega_y, z).$$

where $\hat{\phi}_0$ is an estimate of the surface signal vector (inputs) and $\bar{s}$ is stimuli (output) vector.

One possible family of regularizing operators that can be constructed are weighted norm filters [80, 38] which are of the form

$$\psi_{H,\alpha}(\omega_x, \omega_y, z, \alpha) = [T^*T + \alpha H]^{-1} T^*T$$

where $H(\omega_x, \omega_y, z)$ is weighting function to be determined and will depend on the problem at hand, the sampling interval and the noise characteristics. The solution is then

$$\hat{\phi}_0 = [T^*T + \alpha H]^{-1} T^* \bar{s}$$

It is shown in [80] and in further detail in [38], that in the case of scalar signals this regularizing agent corresponds to the minimization of a functional. This generalizes readily in the vector case to the functional

$$M_\alpha[\phi_0, s, \alpha] = \int_{-\infty}^{\infty} \int_{-\infty}^{\infty} [T\phi_0 - s]^T [T\phi_0 - s] \, d\omega_x d\omega_y +$$
$$\alpha \int_{-\infty}^{\infty} \int_{-\infty}^{\infty} \bar{\phi}_0^*(\omega_x, \omega_y) H(\omega_x, \omega_y, z) \bar{\phi}_0(\omega_x, \omega_y) d\omega_x d\omega_y.$$

This means that in the solution the frequencies of the solution are weighted by the matrix H.

It is also shown in [80, 38] how the selection of the parameter α and the matrix H can be optimized further. If we assume additive sensor noise which is uncorrelated with the solution, x, y and load, i.e. $s = s_T + s_N$ then H and α can be specified such the expected value of the squared difference is minimized, i.e.

$$E\left[\|\tilde{\phi}_0^H\|^2\right] \quad \text{where} \quad \tilde{\phi}_0^H \triangleq \hat{\phi}_0^H - \phi_0^s.$$

where ϕ_0^s is the uncontaminated signal. The solution to this problem is the *multivariate Wiener inverse* used in problems which appear in digital restoration of multichannel images. It is shown in [21, 22] that in the multivariate case it is

$$H(\omega_x, \omega_y, z) = \frac{1}{\alpha} P_s^{-1}(\omega_x, \omega_y) P_n(\omega_x, \omega_y, z)$$

where $P_s(\omega_x, \omega_y, z)$ is the power spectrum matrix of the solution and $P_n(\omega_x, \omega_y)$ is the power spectrum matrix of the sensor noise. The multivariate Wiener inverse then finally becomes

$$\hat{\phi}_0^w = [P_s T^*T + P_n]^{-1} P_s T^* s. \tag{3.5}$$

The need for the power spectrum of the solution indicates that the solution is not in a closed

form. This problem can be circumvented in several ways. First, the power spectrum can be put equal to qI where I is the identity matrix and q is a constant, indicating that nothing is known about the solution *a priori* and the solution is therefore assumed to be white noise. Second, the solution can be iterated. Third, all prior information about the solution that can be included in a power spectrum can be used there. For example, suppose Coulomb's law of friction applies at all points at the contact inferface and the coefficient of friction is known. The solution can then be constrained to satisfy Coulomb's law by explicitly expressing the correlation between the normal and the tangential tractions in the components of the P_s matrix. Let us further assume that it is known that the object is sliding over the surface but the direction of motion in the (x, y)-plane is unknown, then the power spectrum matrix would be of the form

$$ P_s = \begin{bmatrix} \mu_f^2 & 0 & \mu_f \\ 0 & \mu_f^2 & \mu_f \\ \mu_f & \mu_f & 1 \end{bmatrix} P_{f_z}, $$

where P_{f_z} is the power spectrum of f_z and μ_f is the friction coefficient between the object and the surface. Using this P_s in Eq. (3.5) will constrain the solution to satisfy Coulomb's law, i.e. $f_x = \mu_f f_z$ and $f_y = \mu_f f_z$.

Remark: The linear filter presented here is based on the assumption that the noise properties are shift-invariant and uncorrelated with the input signal. Also, its optimality is achieved with respect to a Euclidian norm functional. The shift-invariance assumption comes naturally with with our formulation of the encoding problem as a contact problem on the homogeneous semi-infinite half-space. However, if needed, the Wiener filter can be extended to correctly treat cases when the input and the noise are correlated [6]. Finally, different cost functionals can be prescribed, such as absolute value, p-norm and maximum entropy [10]. These filters should be considered when the Wiener filter has proven inadequate. The details of their construction is hence considered to be a matter of implementation and beyond the scope of this thesis.

4. Identification of Shape and the Onset of Slip

In this section we present an example that implements the theory discussed above which brings together contact mechanics and tactile sensing. The simulations have two main objectives i) shape identifaction and ii) the detection of the onset of slip. In both cases we will (a) show the necessity and usefulness of the full 3D formulation presented here, especially in the context of

a pseudo-dynamic problem, and (b) show the necessity of the multivariate regularizing inverse in the solution of the decoding problem.

The example problem chosen is that of the incipient relative sliding of two elastic bodies in contact. This problem is particularily interesting in the context of haptics, as the identification of object shape and the prediction of the onset of and the prevention of slip is a fundamental problem for both human and robotic exploration and manipulation. It has also been observed by [66, 67] that objects of general shape will have qualitatively similar behavior as spherical objects, so the results presented here will extend to general objects.

The problem demonstrated here is the indentation of an infinite half space by an object shaped as a paraboloid, with simultaneous tangential (F_{x0}, F_{y0}) and normal (F_{z0}) load. Assuming Coulomb friction with friction coefficient μ_f, the condition for local slip can be expressed as

$$\mu_f f_z(x, y) \begin{cases} \leq & \sqrt{f_x^2(x,y) + f_y^2(x,y)} \quad \Rightarrow \quad \text{no slip} \\ \\ > & \sqrt{f_x^2(x,y) + f_y^2(x,y)} \quad \Rightarrow \quad \text{slip occurs} \end{cases} \tag{3.6}$$

It is shown in [36] that the unique solution to this problem is that local slip occurs on the outer edge of the contact area where $c \leq r \leq a$, $(r = \sqrt{x^2 + y^2})$ where

$$\frac{c}{a} = \left[1 - \frac{\sqrt{F_{x0}^2 + F_{y0}^2}}{\mu_f F_{z0}} \right]^{1/3} \tag{3.7}$$

is the relative size of the non-slip region and no slip occurs for $r < c$, (see Fig 3-13). The resulting surface tractions are

$$f_z(x, y) = \frac{F_{z0}}{\pi a^2} \sqrt{1 - \frac{r^2}{a^2}} \quad \text{for } 0 \leq r \leq a$$

$$f_t(x, y) = \begin{cases} \dfrac{\mu F_{z0}}{\pi a^2} \sqrt{1 - \dfrac{r^2}{a^2}} & \text{where } c \leq r \leq a \\ \\ \dfrac{\mu F_{z0}}{\pi a^2} \sqrt{1 - \dfrac{r^2}{a^2}} - \dfrac{c}{a} \dfrac{F_{z0}}{\pi a^2} \sqrt{1 - \dfrac{r^2}{c^2}} & \text{where } r < c \end{cases}$$

where $f_t = f_z = 0$ for $r > a$, and $f_t(x, y)$ is directed along $[F_{x0}, F_{y0}]^T$ with $f_t(x, y) = \sqrt{f_x^2(x,y) + f_y^2(x,y)}$.

4.1 Identification of shape

We use here the optimal sensor combination obtained in section 3.2 and hence the *encoding* part consists of predicting the sensor signal set $(\frac{3}{2E}p_n, \varepsilon_{xz}, \varepsilon_{yz})$ by using the traction vector f above with the TFM, T_{sf} given in Eq. (3.4). The form of these sensor signals is shown in Fig. 3-8(a)-(c). The *decoding* part consists of reconstructing the traction and the displacement vectors, from noise contaminated sensor signals. The displacements will give us the shape of the object where it is in contact with the surface, but that is by definition where the traction is non-zero, and hence both displacements and tractions are needed for object shape identification.

We will now illustrate the necessity of regularization in the decoding algorithm by adding noise to the sensor signals. In this example we use a high-pass filtered Gaussian noise, and in Figs. 3-8(d)-(e) we show the resulting noise contaminated sensor signals. Profiles of an unregularized solution obtained by inverting T_{sf} in Eq. (3.4) is shown in Fig. 3-10 and profiles of a regularized solution obtained using the Wiener inverse given in Eq. (3.5) is shown in Fig. 3-9. Surface plots of the same solutions are shown in Figs. 3-11 and 3-12. The displacements are shown in Fig. 3-11 and the surface tractions in Fig. 3-12. We observe that the regularized inverse is quite close to the uncontaminated solution but the unregularized one is not recognizable.

4.2 Onset of Slip

As the total tangential load, $F_{t_0} = \sqrt{F_{x_0}^2 + F_{y_0}^2}$, takes increasing values, the size of the non-slip region decreases and when $F_{t_0} = \mu_f F_{z_0}$ global slip will occur. Therefore, knowing the relative size of the non-slip region will enable us to estimate how close a particular loading situation is to slipping. The size of the non-slip region can be inferred from the tangential traction distribution as there will a sharp edge along $r = c$ in that distribution. This edge can be seen as two peaks on the 2D profile plot of $f_t(x, y)$ in Fig. 3-9 and as an edge in the f_t-surface plot in Fig. 3-12. We can measure a and c from the reconstructed $f_t(x, y)$ with the help of standard edge detecting techniques. That information along with the total tangential and normal loads, F_{t_0}, F_{z_0}, can either be used in Eq. 3.7 to solve for μ_f or compared to the line plot in Fig. 3-13 to estimate how close the contact is to global slip. For example we see from Fig. 3-13, that if $c = 0.5a$ then the tangential load has reached 87.5% of its maximum value ($F_{t_0} = 0.875\mu_f F_{z_0}$).

(a) Noise free sensor signal p_n (b) Noise free sensor signal ε_{xz} (c) Noise free sensor signal ε_{yz}

(d) Real sensor signal p_n (e) Real sensor signal ε_{xz} (f) Real sensor signal ε_{yz}
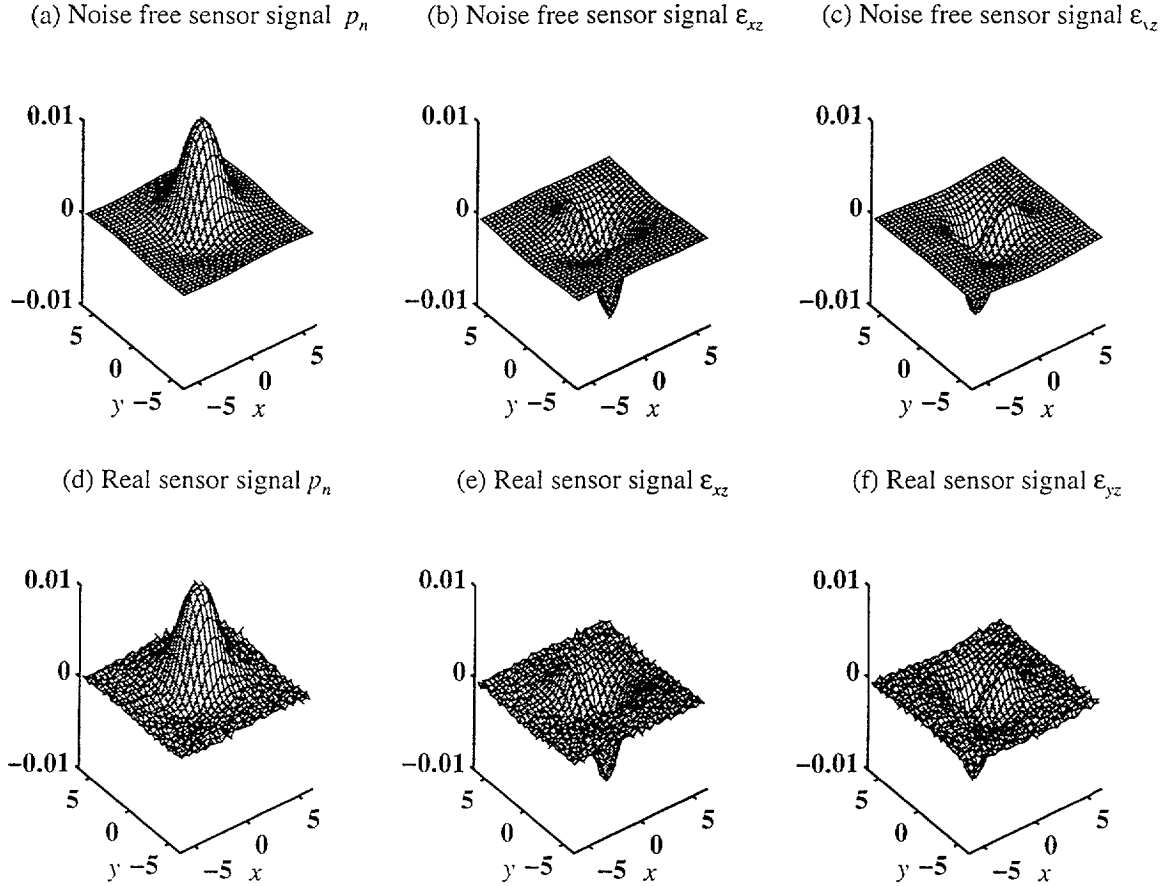
Figure 3-8: Sensors signals without (a) - (c) and with (d) - (f) noise.

5. Conclusions

In this chapter we have delineated a basic computational theory of haptics that is common to humans and robots. The tactile identification problem is separated into the encoding and decoding problems and solutions for both are given. Analysis of the results is shown to lead to a unique and optimal combination of sensors suitable for tactile sensing. An optimized multivariate regularizing algorithm for the solution of the decoding problem is also presented. Using simulations, it is shown how the formulation used here can be applied to predict the onset of slip using tactile sensors.

The conclusions of this chapter can thus be summarized as follows:

1. To sucessfully decode a general tactile 3D signal from a tactile sensor array, a minimum of three independent sensors are needed; $(p_n, \varepsilon_{xz}, \varepsilon_{yz})$ is a unique combination of

65
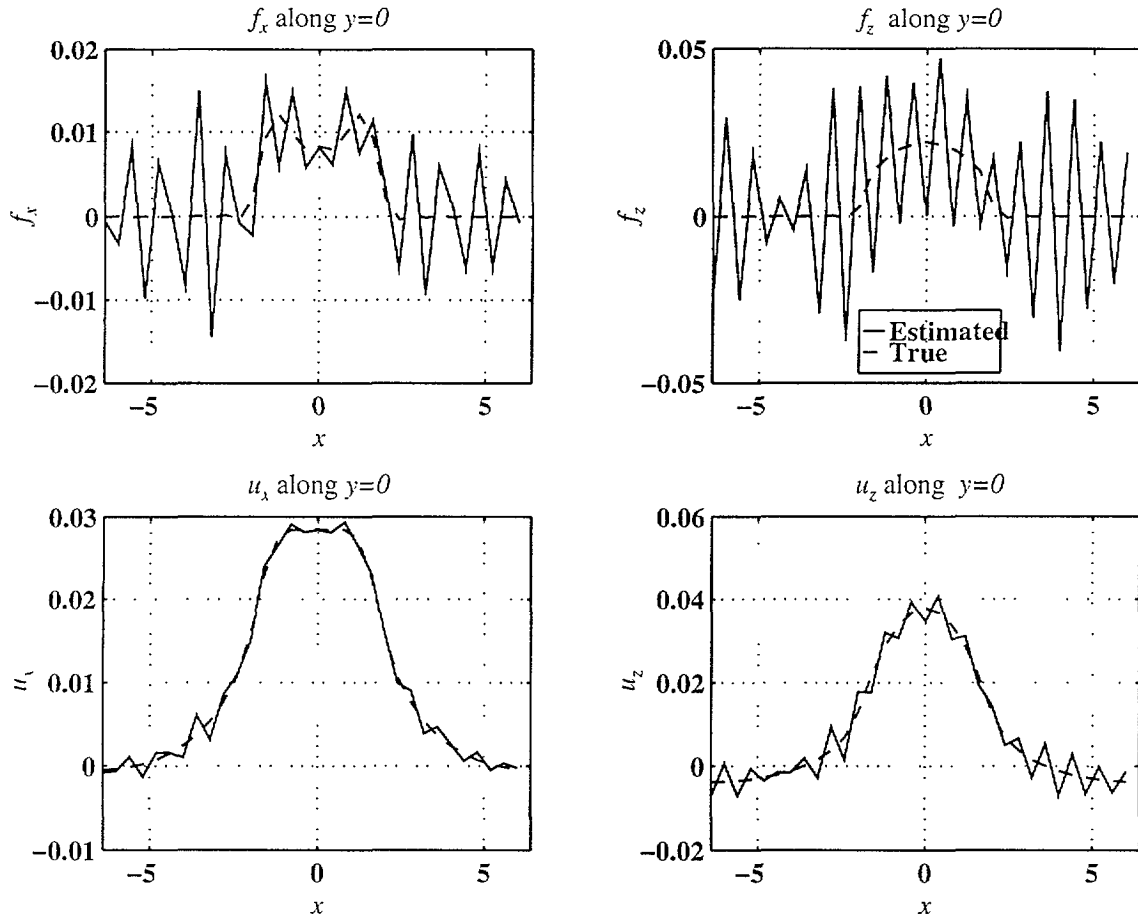
Figure 3-9: Shows profiles of solutions f_x, f_z, u_x, u_z along $y = 0$ to the decoding problem obtained using an unregularized inverse. We observe that the tractions are hardly recognizable although the solutions for the displacements, u_x, u_z are closer to the true solution f_x, f_z.

stress/strain sensory signals which do not have a directional bias.

2. The transfer function approach developed here allows us to look at the qualitative properties and behavior of the solution, irrespective of the exact form of the load or object shape.

3. The two items above lead to the transfer function matrix (TFM) formulation, a convenient and compact formulation that is well known in control theory. The decoding problem is then reduced, essentially, to the inversion of the (TFM).

4. Since the inversion is ill-posed in the presence of noise and discrete sampling, regularization is needed, for which the multivariate Wiener inverse exists as a standard tool.

5. Simulations presented in section 4 show that the above can be used to calculate surface shape, load distribution, contact area, and further has a possible application in estimating the onset of slip.
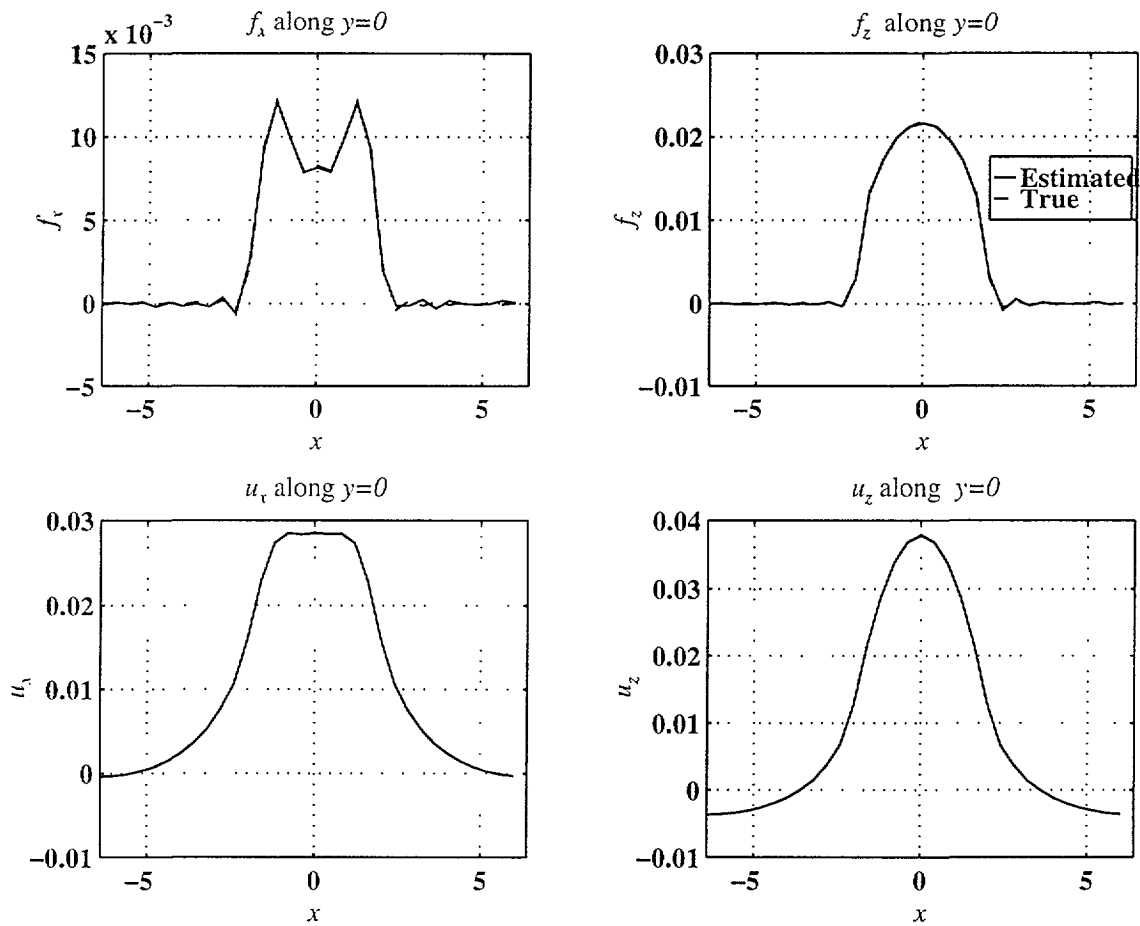
Figure 3-10: Shows profiles of solutions to the decoding problem obtained using the regularized Wiener inverse. We observe that it coincides almost everywhere with the true solution and that the error is therefore small.

(a) True u_x displacement　　(b) Estimated u_x (Wiener)　　(c) Estimated u_x (unregularized)

(d) True u_z displacement　　(e) Estimated u_z (Wiener)　　(f) Estimated u_z (unregularized)
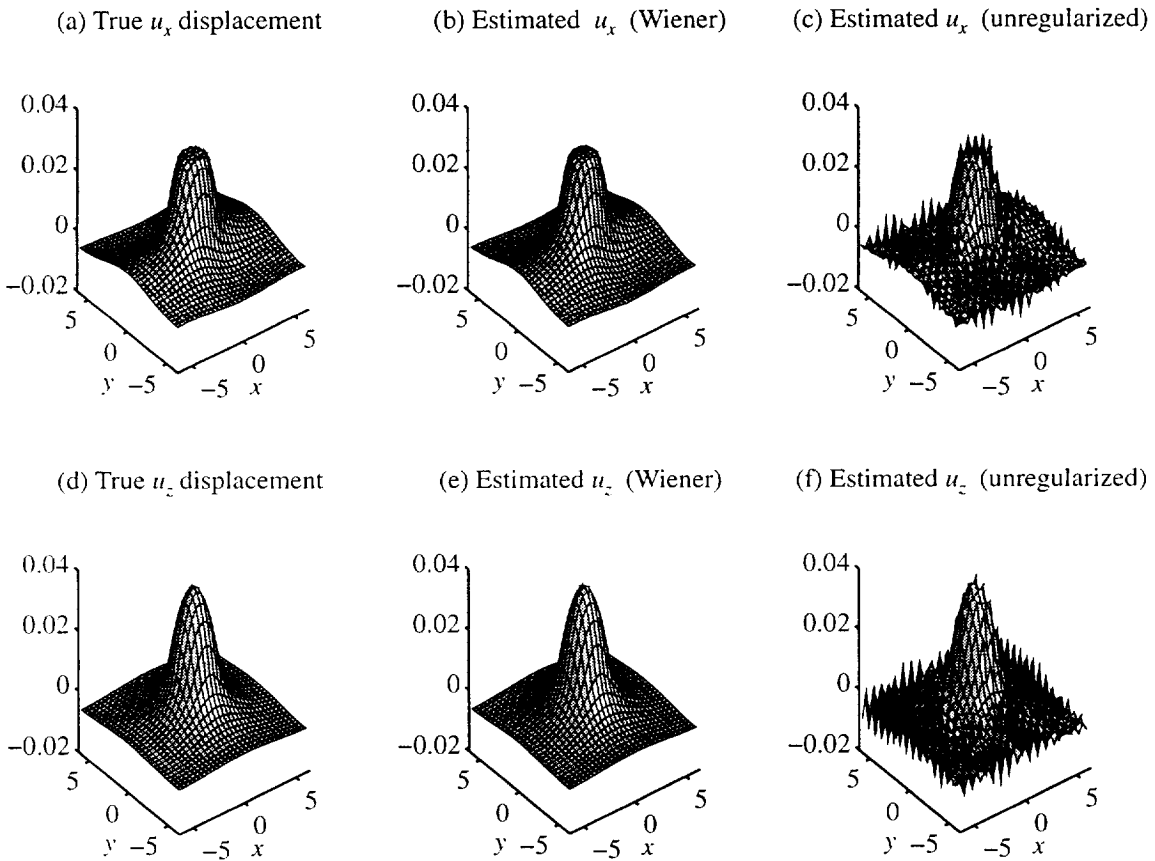
Figure 3-11: Shows surface plots of decoded surface displacements u_x in (a)-(c), and u_z in (d)-(f). As in Figs. 3-10 and 3-9 we observe that the true solution and the solution obtained using the Wiener inverse look very similar but the solution obtained using an unregularized inverse is considerably worse.

(a) True f_x loading   (b) Estimated f_x (Wiener)   (c) Estimated f_x (unregularized)

(d) True f_z loading   (e) Estimated f_z (Wiener)   (f) Estimated f_z (unregularized)
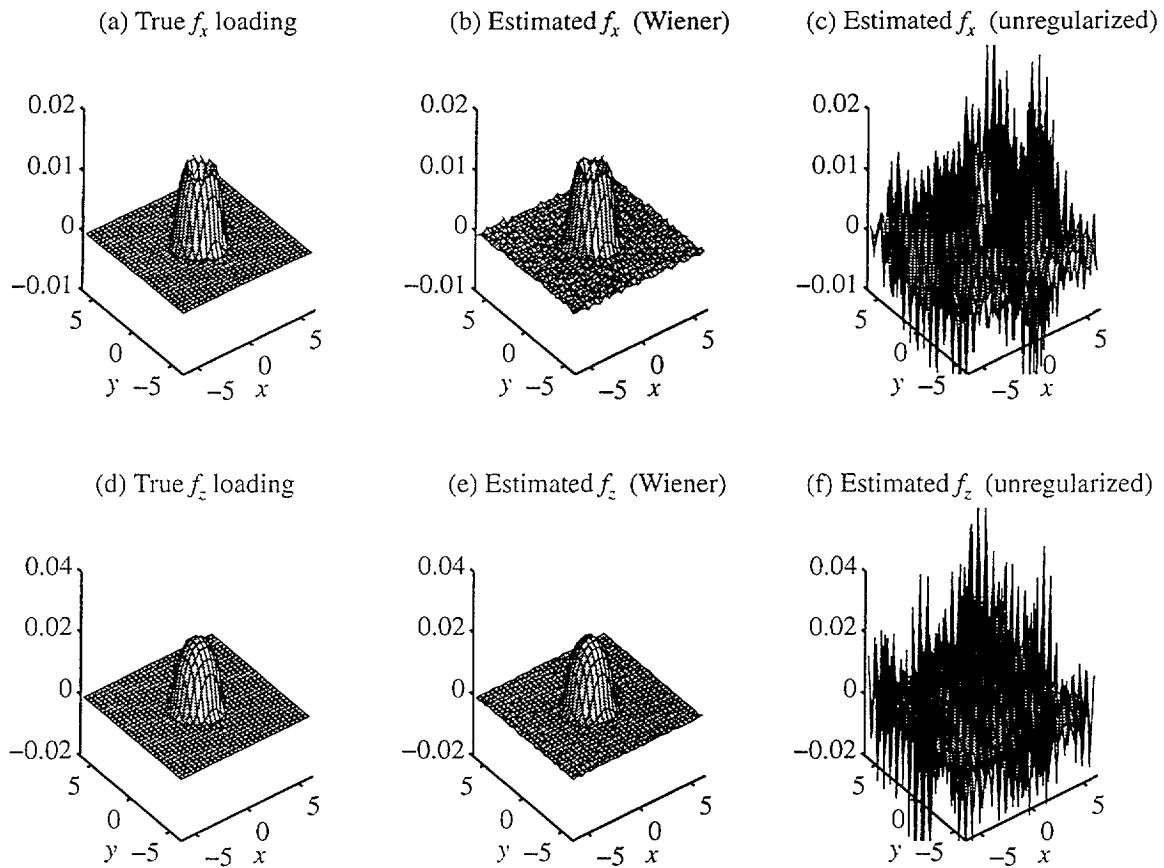
Figure 3-12: Shows surface plots of decoded surface load distributions f_x in (a)-(c), and f_z in (d)-(f). Again observe that the true solution and the solution obtained using the Wiener inverse look very similar but the solution obtained using an unregularized inverse is mostly noise.
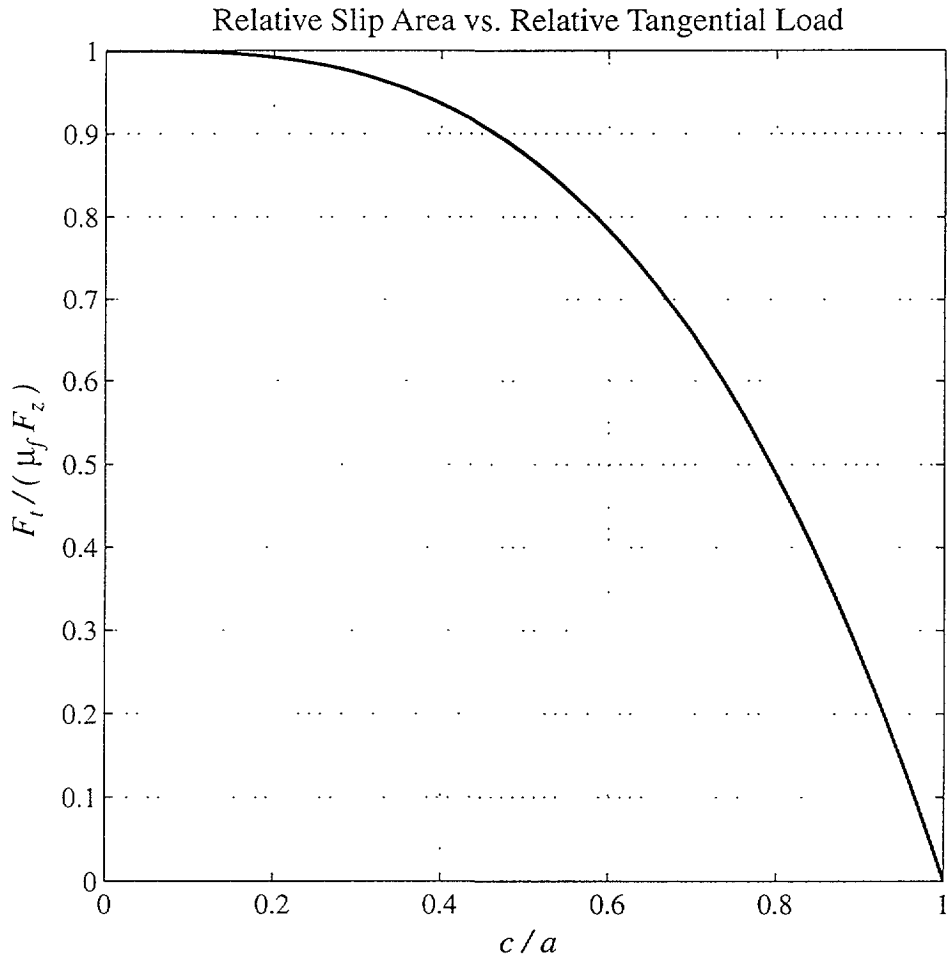
Figure 3-13: The relation between the relative tangential load $F_{t_0}/(\mu_f F_{z_0})$, where $F_{t_0} = (F_x^2 + F_y^2)^{1/2}$, and the relative no-slip radius $c/a = 1 - F_{t_0}^3/(\mu_f F_{z_0})^3$. As an example, this relation indicates that when the no-slip radius is equal to half the contact radius ($c/a = 1/2$) then $F_{t_0} = 0.875\mu_f F_{z_0}$ or that the tangential load is 87.5% of the maximum tangential load.

Chapter 4

Dynamic Identification

1. Introduction

An understanding on the nature of touch, especially the mechanics and the information transfer involved, is important for both physiological and robotics research. The workings of human touch are presently not fully known and a computational model providing theoretical basis would be useful when interpreting experimental results as a tool to generate and validate consistent hypothesis. In robotics, a theoretical model would be of use in the design and development of sensor arrays, addition to providing data processing algorithms and paradigms for their implementation. Finally, in the emerging fields of virtual environments and telerobotics depend considerably on detailed knowledge on the nature of the interaction of humans and machines through touch. The above leads us to conclude that a computational theory which would cover the common aspects of humans and robotic touch could be of considerable and far reaching value and we will in this chapter discuss the details of such a theory which relates to tactile sensing under dynamic contact conditions.

In chapter 3, we have treated a related problem, where we assumed that the loading is static or quasi-static. The dynamic effects become important when the loading varies significantly on a timescale measured in units of time constants characteristic of the medium in the fingerpad. In this chapter we will include the dynamic effects of inertia and viscoelasticity in our analysis of the tactile sensing problem. We will then delineate the cases in, and conditions under which

these effects become significant and when the can be neglected – giving examples where the static solution given in chapter 3 is no longer valid and this dynamic formulation becomes necessary.

We use the same framework and definition of terms as in chapter 3, which we state here again for review: Two stages in tactual information processing, *encoding* and *decoding* make up the *identification problem*, which is so called because it involves the determination of the state of the object and its relationship to the tactual sensory system. The system discussed here differs in some ways from traditional dynamic systems. The most prominent difference is that it has both spatial and temporal variables, whereas traditional lumped parameter systems only have temporal ones. In both natural and man-made tactile systems the *encoding* process is the transduction of the mechanical stimulus into electric signals that contain, in a coded form, information about the stimulus features. The inverse problem, i.e. the *decoding* process or the calculation of the surface shape or surface tractions from the transduced signals is in many respects significantly more difficult. The encoding is essentially a spatial low-pass filtering process which indicates that the decoding will be ill-posed in the sense that the higher frequency components of the signals will be prone to noise contamination and special methods have to be applied for successful decoding. This applies equally to the static formulation given in chapter 3. but several features are added to this problem with the dynamic formulation. Temporal properties such as inertia and viscosity now play a role in the dynamic encoding solution. and the decoding problem also involves the causality constraint on the temporal dimension that needs to treated accordingly.

Several papers can be found in the robotics literature on the mechanistic modeling, encoding and decoding of surface conditions from subsurface measurements using tactile sensors under static conditions and the reader is refered to chapter 3 for an overview. Papers where dynamic effects are included are much more scarce, but in [28] the encoding and decoding of a stress rate sensor are investigated and a scalar Wiener inverse is suggested for the decoding. In [84] the response of a 2D plane strain model to vibrating sinusoidal gratings is analyzed and it compared to the sensitivity of the human fingerpad at different vibration and grating frequencies.

All previously published results on the reconstruction of general time-varying surface loads and profiles from subsurface tactile signals do not solve the full 3D problem including the effects of inertia and viscoelasticity and the effects and interaction of shear loads. In this chapter we will address those aspects of the mechanistic modeling, encoding, and the decoding problems, and the contributions of this chapter can be itemized as follows:

1. A complete solution to the 3D half-space problem is given for arbitrary 3D dynamic loading conditions and any linearly elastic material. The solution is formulated using transfer function matrices in the domains of spatial and temporal frequencies which allows us to look at the qualitative properties and behavior of the solution, irrespective of the exact form of the load or object shape.

2. The effects of inertia and viscoelasticity are analyzed and it is shown that inertial effects can be neglected whereas the visocelastic effects are dominant for low temporal frequencies. The use of linear viscoelastic models further leads to solutions that can be expressed using Transfer Function Matrices that are rational in the temporal frequency.

3. For decoding, we can then apply the extensively developed and numerically efficient Kalman filter to estimate the inputs which at the same time avoids the problems associated with the ill-posedness caused by the spatial low-pass filtering.

In Section 2, we formulate and solve the 3D half-space elastic model, which serves as a description of the encoding process. For the sake of clarity, the mathematical expressions are detailed in Appendix C. We analyze the solutions in order to assess if and when the effects of inertia can be neglected and further show how viscoelastic effects are included. In Section 3. we solve and analyze the decoding problem. and in Section 4, we give example numerical simulations of the methods proposed in Section 3. Conclusions are given in section 5.

2. The Encoding Problem

From theoretical viewpoint, tactile sensor response to any given stimulus can be predicted if we have the following:

1. A mechanistic model of the deformable medium which can be used to calculate reliably the stresses and strains at each instant and at each point in the medium for a given time history of the mechanical stimulus.

2. A model of the sensor that provides the relationship between the relevant stimulus, i.e., a particular combination of stresses and strains in the local neighborhood of a sensor that it is responsive to and the temporal characteristics of the sensor response.
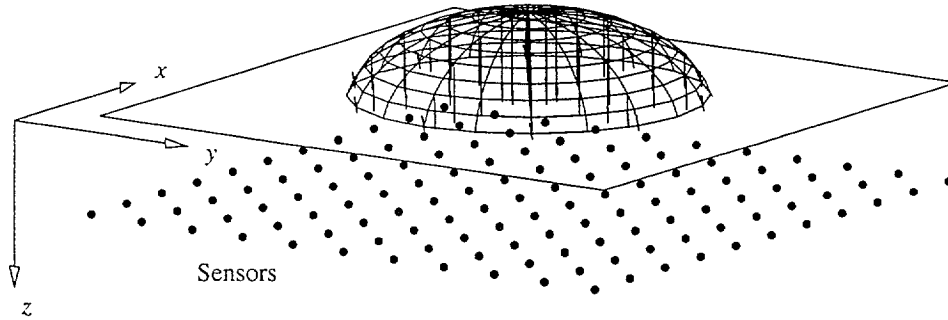
Figure 4-1: Shows the semi-infinite halfspace with surface tractions and subsurface sensors. The x- and y-dimensions extend to infinity in both negative and positive directions. The z-dimension extends from 0 to positive infinity. The tractions are distributed over the contact area, each point being subjected to 3-dimensional loading $f(x, y, t) = [f_x, f_y, f_z]^T$.

For example, an appropriate mechanistic model of the human skin and the soft tissues underneath enables us to investigate one of the important questions in cutaneous neurophysiology, that of identifying the relevant stimulus that causes each receptor type to respond [35, 75], where only the temporal characteristics are known but the particular combination of strains is not agreed upon.

In this section we will find and analyze the dynamic response of the elastic halfspace subjected to a time-varying load distribution, and based on that give conditions under which we can neglect the effects of inertia and how viscoelasticity can be included in the solution.

The problem is set up so that the boundary surface coincides with the xy-plane and the positive z-axis points into the medium (See Fig. 4-1). The material is assumed to be linearly elastic and homogeneous. It is also assumed to extend to infinity in both negative and positive x, y directions and in the positive z direction. The surface load is described by the time-varying traction vector field $f(x, y, t) = [f_x(x, y, t), f_y(x, y, t), f_z(x, y, t)]^T$ and the surface displacement field as $u_0(x, y, t) = [u_x(x, y, 0, t), u_y(x, y, 0, t), u_z(x, y, 0, t)]^T$. In our formulation, the boundary conditions can be forces, displacements or mixed, i.e. when any 3 elements from both f and u_0 are given. As in chapter 3 we intend to present the solution in the space of spatial frequencies and use transfer functions to simplify solutions and gain further insight.

2.1 Transfer Function Matrices (TFM)

We solve the encoding problem by transforming the fundamental differential equations of equilibrium and the stress-strain relationship equations (Generalized Hooke's law) using the Fourier-Laplace transform over (x, y, t) space. This is analogous to what was done to solve the static problem in chapter 3 and examples of this approach can also be seen in [16] and [71].

The differential equations of equilibrium[1] are given by

$$\sigma_{ij,j} = \rho \ddot{u}_i \quad i, j = x, y, z \tag{4.1}$$

and the linear stress strain relations according to Hooke's law are

$$\sigma_{ij} = \lambda \varepsilon_{ij} \delta_{ij} + 2\mu \varepsilon_{ij} \quad i, j = x, y, z \tag{4.2}$$

where

$$\varepsilon_{ij} = \frac{1}{2} \left(u_{i,j} + u_{j,i} \right) \quad i, j = x, y, z \tag{4.3}$$

and $\delta_{ij} = 1$ if and only if $i = j$, and is zero otherwise. Further, rho is density and the Lamè constants λ and μ (shear modulus) are in terms of Young's modulus and Poisson ratio:

$$\lambda = \frac{\nu E}{(1 + \nu)(1 - 2\nu)}, \quad \mu = \frac{E}{2(1 + \nu)}.$$

The details of the derivation are given in Appendix C for the purely elastic case. The complete solution when viscoelastic effects are also present is treated in section 2.3.

As is done in chapter 3, we employ here the concept of a transfer function matrix (TFM). The transfer function matrices we give here have the Fourier-Laplace transform of the components of either $f(x, y, t)$ or $u_0(x, y, t)$ as the inputs and any displacements, strains or stresses in the medium as the outputs. Each entry of the TFM would then correspond to the contribution of a particular input component to the corresponding output component. For example the entry in the TFM for the z-displacement resulting from the x-load, or $u_z^x(x, y, z, t)$ we would write

$$\overline{u}_z^x(\omega_x, \omega_y, z, s) = T_{u_z^x f}(\omega_x, \omega_y, z, s) \overline{f}_x(\omega_x, \omega_y, s)$$

---

[1]Here we use tensor notation for compactness, where a ",j" in subscript means a partial derivative with respect to the independent variable represented by j and repeated symbols in subscript stand for summation over all indices.

to obtain the Fourier-Laplace transform $\overline{u}_z^x(\omega_x, \omega_y, z, s)$ of $u_z^x(x, y, z, t)$ from the transfer function $T_{u_z^x f}(\omega_x, \omega_y, z, s)$ and the Fourier-Laplace transform $\overline{f}_x(\omega_x, \omega_y, s)$ of the surface shear load $f_x(x, y, t)$. Here, ω_x and ω_y correspond to spatial frequencies in the x and y directions respectively, and s is the Laplace variable (related to the temporal frequency by $s = j\omega$). Then we can write

$$\overline{u} = T_{uf}\overline{f} \quad \overline{\varepsilon} = T_{\varepsilon f}\overline{f} \quad \overline{\sigma} = T_{\sigma f}\overline{f} \quad \overline{p}_n = T_{p_n f}\overline{f}$$

$$\overline{u} = T_{uu_0}\overline{u}_0 \quad \overline{\varepsilon} = T_{\varepsilon u_0}\overline{u}_0 \quad \overline{\sigma} = T_{\sigma u_0}\overline{u}_0 \quad \overline{p}_n = T_{p_n u_0}\overline{u}_0$$

(4.4)

where the subscript f indicates that surface tractions are inputs and the subscript u_0 indicates that surface displacements are inputs.

The equations in (4.4) represent the solution for the encoding problem, because given $f(x, y, t)$, $u_0(x, y, t)$ or a combination of 3 elements from the two, we can predict $u(x, y, z, t)$, $\varepsilon(x, y, z, t)$, $\sigma(x, y, z, t)$ and $p_n(x, y, z, t)$. If the relevant stimulus, i.e. a particular combination of stresses and strains in the local neighborhood of the sensor that it is responsive to, is known, we can predict the sensor response. For example, if the sensor response is linearly related to the strain ε_{zz}, then it is the relevant stimulus for that sensor. On the other hand, if the relevant stimulus needs to be identified, we can use Eq. (4.4) to generate hypotheses that can be tested against the empirically determined sensor response, as is done in [35, 75].

2.2 Analysis of the Encoding Solution

The above solution to the decoding problem gives us every component of both the strain and stress tensors but since the input is a 3-dimensional vector we only need to select three signals, or three independent combinations of signal, which the sensors should transduce. In chapter 3 the selection of suitable sensors was discussed and there we showed using symmetry arguments that the sensors should optimally transduce three signals: the mean normal pressure, p_n and two z shear strains ε_{xz} and ε_{yz}. The arguments made in chapter 3 will also hold for the dynamic encoding solution as introduction of time as a variable does not destroy spatial symmetry[2]. We therefore use transfer functions for the signals above as examples in our analysis of the encoding solution. We however note that the same analysis could be applied to all the other strain and stress signals and the conclusions would be the same. Hence, we will analyze two transfer functions, one between the mean normal stress p_n and the normal load f_z, and the

---

[2]The Laplace variable s only appears in the sensor signals as some constant times s^2 being added to Ω^2 and will therefore not introduce any spatial asymmetry

other between the xz-shear strain, ε_{xz} and f_z.

Transfer Functions: In the dynamic solution the transfer functions for those two variables become

$$
\begin{aligned}
T_{p_n f_z} &= \frac{3\beta^2 - 4}{6\beta^2} \frac{s^2}{c_{sh}^2} \frac{(\Omega^2 + \frac{1}{2}c_{sh}^{-2}s^2)e^{-n_1 z}}{F_3} \\
T_{\varepsilon_{xz} f_z} &= \frac{1}{2\mu} \frac{j\omega_x n_1(\Omega^2 + \frac{1}{2}c_{sh}^{-2}s^2)\left(e^{-n_2 z} - e^{-n_1 z}\right)}{F_3}
\end{aligned}
\tag{4.5}
$$

where

$$
F_3 = (\Omega^2 + \frac{1}{2}c_{sh}^{-2}s^2)^2 - \Omega^2 n_1 n_2, \qquad n_1 = \sqrt{\Omega^2 + c_p^{-2}s^2}, \qquad n_2 = \sqrt{\Omega^2 + c_{sh}^{-2}s^2},
$$

and $c_p = \sqrt{(\lambda + 2\mu)/\rho}$ and $c_{sh} = \sqrt{\mu/\rho}$ are the dilational- and shear-wave wavespeeds (see [81]), with λ and μ as bulk and shear modulus respectively, ρ is the density, and $\beta = c_p/c_{sh}$. As before ω_x and ω_y are the spatial frequencies, $\Omega = \sqrt{\omega_x^2 + \omega_y^2}$, and s is the Laplace transform variable. related to the temporal frequency by $s = j\omega$. The solution obtained here should therefore approach the static solution when $s \to 0$, and we show that does so in Appendix D.

Analysis: For analysis of the transfer function, it is helpful to normalize and measure distances and displacements in units of shear-wave wavelengths. Let $s = j\omega$, $\lambda_{sh} = c_{sh}/\omega$ and hence

$$
\begin{aligned}
z &= \hat{z}\lambda_{sh} &&= \hat{z}c_{sh}/\omega \\
\Omega &= \hat{\Omega}/\lambda_{sh} &&= \hat{\Omega}\omega/c_{sh} \\
\omega_x &= \hat{\omega}_x/\lambda_{sh} &&= \hat{\omega}_x\omega/c_{sh}
\end{aligned}
$$

The temporal frequency. ω, can now be canceled out from the transfer functions, which then become

$$
\begin{aligned}
T_{p_n f_z} &= \frac{3\beta^2 - 4}{6\beta^2} \frac{(\hat{\Omega}^2 - \frac{1}{2})e^{-\hat{n}_1 z}}{\left[(\hat{\Omega}^2 - 1/2)^2 - \hat{\Omega}^2\hat{n}_1\hat{n}_2\right]} \\
T_{\varepsilon_{xz} f_z} &= \frac{1}{2\mu} \frac{j\hat{\omega}_x\hat{n}_1(\hat{\Omega}^2 - \frac{1}{2})\left(e^{-\hat{n}_2 z} - e^{-\hat{n}_1 z}\right)}{\left[(\hat{\Omega}^2 - 1/2)^2 - \hat{\Omega}^2\hat{n}_1\hat{n}_2\right]}
\end{aligned}
$$

with $\hat{n}_1 = (\hat{\Omega}^2 - \beta^{-2})^{1/2}$, and $\hat{n}_2 = (\hat{\Omega}^2 - 1)^{1/2}$.

We observe that all the terms in the transfer function are real for $\hat{\Omega} \geq 1$. This can be interpreted as those spatial frequencies which satisfy $\hat{\Omega}c_{sh} \geq \omega$ that are not involved in the transfer of energy away from the source and that the halfspace behaves as an elastic spring for

77
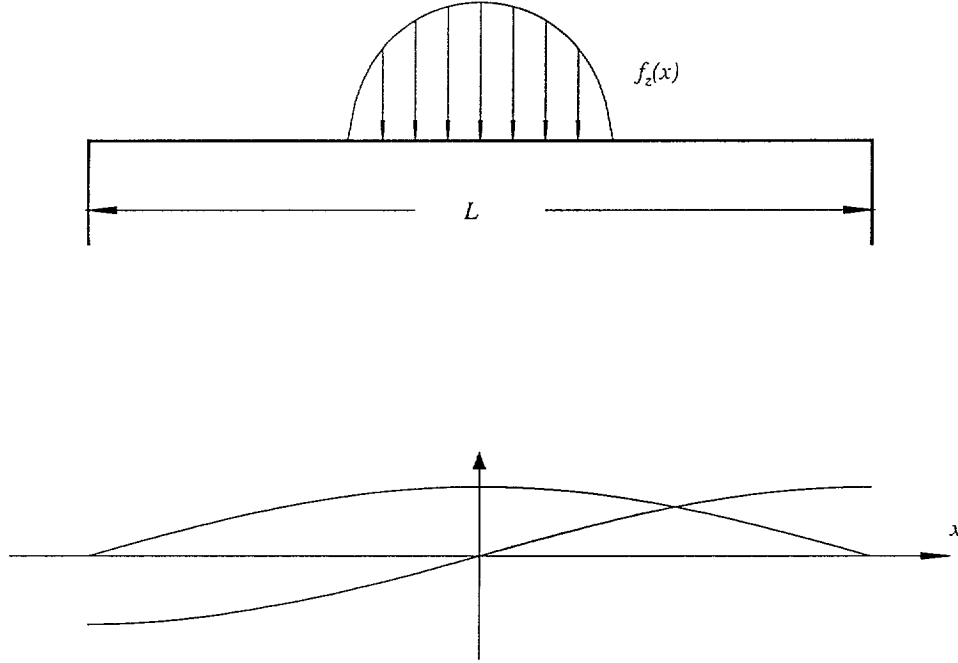
Figure 4-2: Shows the modeshape for the lowest eigenfrequencies of a domain with length L, assuming either fixed or free boundary conditions at $x = \pm L/2$. The maximum wavelength is $\lambda_{\mathrm{max}} = 2L$ and hence the lowest non-zero spatial eigenfrequency is $\Omega_{\mathrm{min}} = \pi/L$.

those frequencies.

The denominator of the transfer functions, however vanishes for $\hat{\Omega} \overset{\triangle}{=} \hat{\Omega}_R$, something we know because the denominator is the characteristic equation for the Rayleigh wavespeed (see [81]). The transfer functions therefore become singular and a resonance phenomena occurs when $\hat{\Omega} = c_R/c_{sh}$, where c_R is the Rayleigh[3] wavespeed.

Inertia and Finite Domains: The above can be used to establish conditions under which one can neglect inertia, especially in cases where the solution in Eq. (4.5) is applied to finite domains. As an example, for a rectangular domain, i.e. $(x, y) \in [-L/2, L/2] \times [-L/2, L/2]$, only a discrete set of spatial frequencies will give valid solutions. The lowest nonzero spatial frequency is of particular interest to us, and we have plotted corresponding the modeshapes assuming either free or fixed boundary conditions at $x, y = \pm L/2$ in Fig. 4-2.

We see that the longest possible[4] wavelength is $\lambda_{\mathrm{max}} = 2L$ which is equivalent to $\Omega_{\mathrm{min}} =$

---

[3]The value of c_R depends on $\beta = c_P/c_{sh}$. For materials that are nearly incompressible ($\beta \to \infty$) we have that $c_R \approx 0.95 c_{sh}$.

[4]This is assuming fixed or free boundary conditions. A third kind of boundary conditions, elastic boundary condition is also possible, and the lowest eigenfrequency will then depend on the stiffness of the boundary

π/L. We therefore have that $\hat{\Omega} < c_R/c_{sh}$ is satisfied if

$$\omega < \omega_{cr} = \frac{\pi c_R}{L} \tag{4.6}$$

giving us a condition as to when we can ignore the effects of inertia for the semi-infinite halfspace.

Figures 4-3 and 4-4 show how the condition above appears in a Bode plot of the transfer functions in Eq. (4.5). The numerical values were chosen so that the system resembled the human fingerpad in size and material properties, i.e. $L = 12.8$ [mm], $\mu = 2.8 \cdot 10^4$ Pa, $\nu = 4.995$, and density $\rho = 1000$ [kg/m^3], which substituted into the condition in Eq. (4.6) gives that $\omega_{cr} = 1095$ rads^{-1} or that inertia can be ignored and the quasi-static solution used if the bandwidth of the loading is less than 174 Hz. We observe in Figs. 4-3 and 4-4 that the static and the dynamic solution are identical below the temporal frequency predicted, but that there are complex pole-zero pairs (i.e. $(s^2 + z^2)/(s^2 + p^2)$) which are very close to each other at the critical frequency. Viscoelastic behavior for frequencies lower than that critical frequency can now be modeled by letting the elastic constants in the static solution, given in chapter 3, be rate dependent, which will give some shape to the transfer functions in that range, characterizing the particular material being modeled. We will see in section 3 that this will simplify the decoding part significantly and in fact make it numerically feasible.

2.3 Viscoelasticity

Theory of viscoelasticity extends the theory of elasticity to include cases where the stress-strain relation behavior is not time independent. It all boils down to the choice of timescale, and for shorter intervals of interest, it may be necessary to include the rate dependent behavior of materials. The description linear viscoelastic material applies to materials for which the rate dependent behavior can be adequately described explained by expressing the stress-strain relation in the viscoelastic form of Hooke's law,

$$\bar{\sigma}(s) = Q(s)\bar{\varepsilon}(s).$$

Where $\bar{\sigma}(s)$ and $\bar{\varepsilon}(s)$ are the Laplace transforms of the stress and the strain, respectively. $Q(s)$ is called the *Operational relaxance* and alternatively $Q(s)/s$ is called the *Operational impedance*. The main advantage in using the viscoelastic form of Hooke's law is that we then can apply the

---

condition. There will be a minimum eigenvalue similar to the other boundary conditions, with the exception of the singular case when the stiffness of the boundary condition matches that of the material.
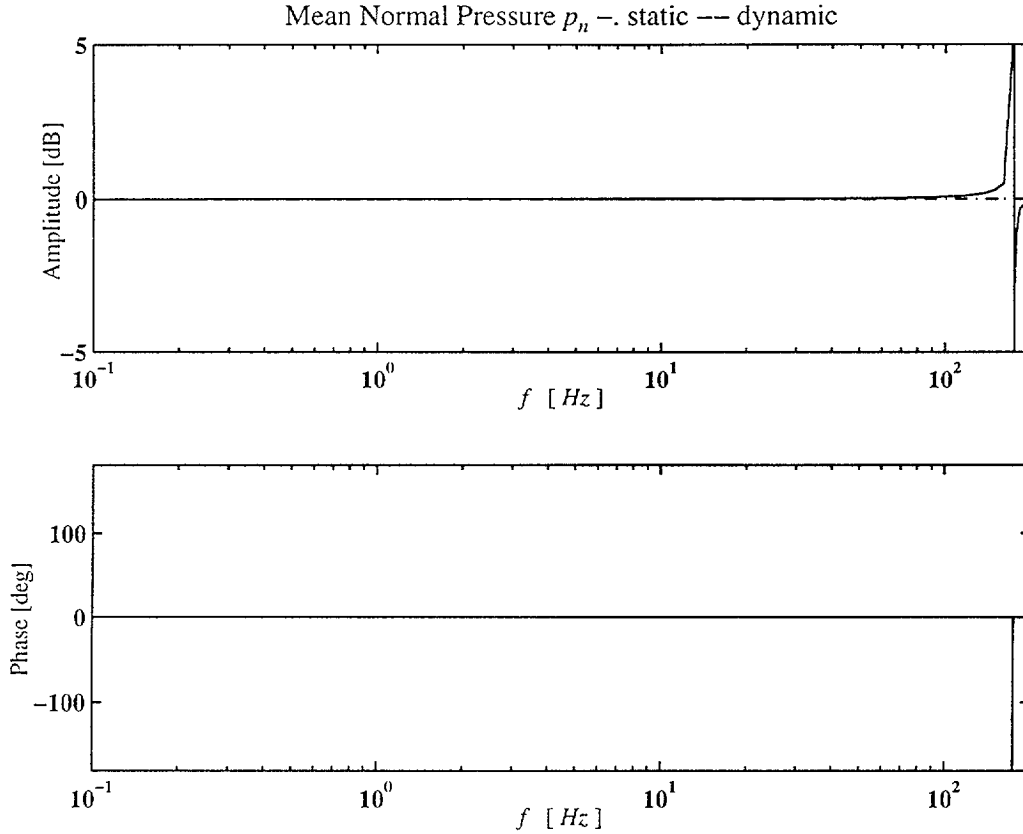
Figure 4-3: Shows a Bode plot of the mean normal pressure, p_n for both the static and dynamic solution at $z = 1$ mm below the loading point. The amplitude is normalized with the static response. We observe that the solutions are identical up to a critical frequency, given by $\omega_{cr} = \pi c_R/L$. ($f < 174$ Hz when estimates of the material parameters for the human fingerpad are used.

correspondence principle. According to the principle, if an elastic solution to a stress analysis problem is known, substitution of the appropriate Laplace transforms for the material constants employed in the elastic solution furnishes the viscoelastic solutions [83].

Hence, the effects of viscoelasticity can be incorporated into the elastodynamic solution in Appendix C, simply by allowing the material constants to be frequency dependent, i.e. μ and β become $\mu(s)$ and $\beta(s)$. Similarly the effects of viscoelasticity can included in the static solution given in chapter 3.

The material constants are in general both independently rate independent, μ describing shear motion and β the dilational behavior. It is however often assumed that only μ is rate dependent. This assumption is reasonable for materials that are near being incompressible, ($\nu > 0.4$) which is the case for polymers and other materials we intent to apply this theory to. The simplest model that captures the behavior of a linearly viscoelastic solid is the 3-parameter
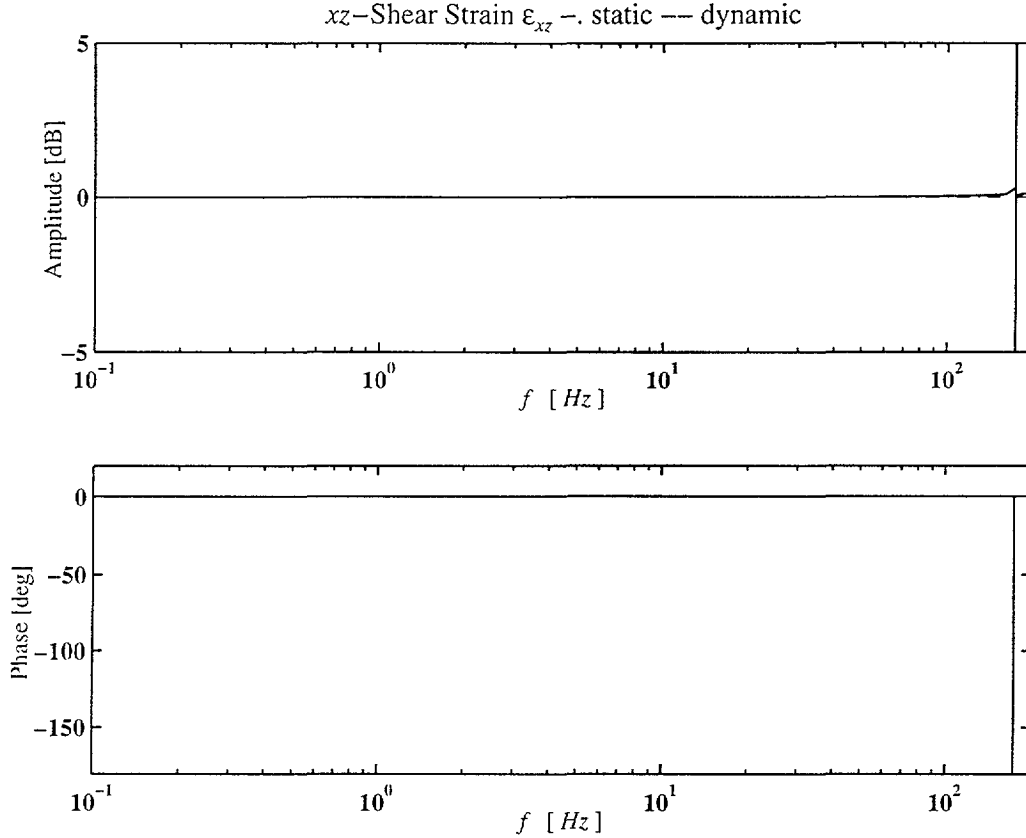
Figure 4-4: Shows a Bode plot for the xz-shear strain, ε_{xz} for both the dynamic and static solutions. The location is at depth $z = 1$ [mm] below where the static solution has a maximum (see Fig. 3). As in the case of the mean normal pressure, we observe that the solutions are identical up to a critical frequency, given by $\omega_{cr} = \pi c_R / L$ or while $f < 174Hz$.

standard linear solid.[5] The transfer function for μ is for this model,

$$\mu(s) = \mu_0 \frac{1 + t_r s}{1 + \frac{1}{\alpha} t_r s}$$

where μ_0 is the steady state response, t_r the retardation time and α is the overshoot of a step response. A schematic representation of the model as dampers and springs is shown in Fig. 4-5a, and the step response in Fig. 4-5b, i.e. the response in stress to a step in strain.

This model can be generalized to model materials with more than one time constant. The transfer function for the generalized model is

$$\mu(s) = \mu_0 \prod_{i=1}^{n} \frac{1 + t_{r_i} s}{1 + \frac{1}{\alpha_i} t_{r_i} s}.$$

---

[5]Also called Kelvin model.

81
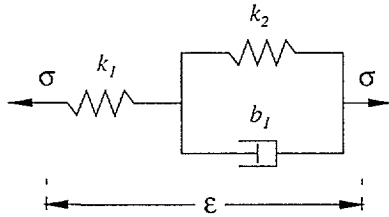
(a) 3-Parameter Standard Linear Solid   (b) Response of stress to a step in strain
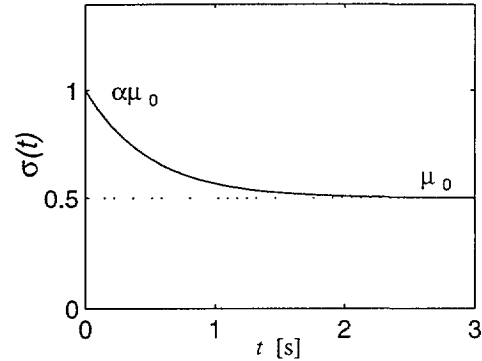
Figure 4-5: (a) Shows a diagram of the 3-parameter linear standard solid model using spring and damper elements. (b) Shows the response in stress to a step change in strain for the 3-parameter linear solid defined in Fig. 4-5. The relation between the parameters is that $\mu_0 = k_1 k_2 / (k_1 + k_2)$, $\alpha = (k_1 + k_2)/k_2$, and $t_r = b_1 / (k_1 + k_2)$.

The transfer function approach to viscoelasticity provides a powerful tool for the modeling of the viscoelastic properties of different materials. One still needs, however, to estimate the parameters in the transfer function for each material and under conditions that are as close as possible to the conditions under which the model is to be applied.

This model captures the general behavior of an viscoelastic solid, in that the net effect is a phase delay between the loading and the displacement occuring because energy is absorbed by the medium. This phase delay is one of the factors that makes a dynamic formulation necessary, even when only viscoelastic effects are dominant and the encoding solution is identical, in form, to the static solution. This we will discuss in the section 3.

3. The Decoding Problem

Tactile information is obtained with mechano-sensors embedded in a deformable medium that is in contact with a shaped object. Mechanosensors, embedded within the medium can, at best, provide information on skin surface shape and surface traction distribution. From this information, contact region, shape of the object and the contact state need to be inferred. The problem at hand is therefore the decoding, i.e. reconstruction of the surface shape of the medium, the tractions on the surface as well as the region of contact using sub-surface mechanosensory information.

An important part of the decoding solution is the selection of the sensor signals, i.e. the particular strains or stresses the sensors should pick up. As the introduction of the dynamics does not alter the symmetry properties of the halfspace we will refer to the treatment of the static solution in chapter 3 and not need repeat it here.

In Eq. (4.4), we have chosen to represent the solution for the encoding problem in terms of transfer functions in both the spatial and temporal frequency domains. We will show in this section that for the solution to the decoding problem, it is more efficient to use state-space representation for the temporal dimension when possible.

3.1 The Decoding Solution

The solution to the decoding problem essentially gives us an estimate of the conditions on the surface given a time history of the sensor signals. This estimate must be such that it minimizes some error measure. One such measure is the expected total square error defined as

$$
\begin{aligned}
\mathcal{E} &= E\left[\iint_{-\infty}^{+\infty} \|\xi(x,y,t) - \hat{\xi}(x,y,t)\|^2 dx dy\right] \\
&= E\left[\iint_{-\infty}^{+\infty} \|\bar{\xi}(\omega_x,\omega_y,t) - \hat{\bar{\xi}}(\omega_x,\omega_y,t)\|^2 d\omega_x d\omega_y\right]
\end{aligned}
\tag{4.7}
$$

where ξ and $\hat{\xi}$ are, respectively, the true and estimated signals describing the conditions at the surface. The latter relation follows from Parceval's theorem, and it shows us that we can with identical results minimize the error in the domain of spatial frequency.

When the effects of inertia is included in the encoding solution, the resulting TFMs are irrational in the frequency variable s. This indicates that the system being described does not have a finite number of states and hence cannot be represented using the state-space approach. We have shown in section 2.2 that the effects of inertia are only of importance for higher temporal frequencies which are in most cases out of the range of interest in most applications. Hence, we will concentrate on the solution when viscoelastic effects dominate.

The decoding problem as posed here is in most aspects identical to optimal linear filtering problems encountered in signal processing and control theory. In those fields, extensive research has lead to the now accepted conclusion that for this problem effective solutions can only be obtained for signals that can be described using rational power spectral functions [86, 37, 52]. The system can then be represented in a state-space and the resulting filter is the wellknown

Kalman filter.

Translating the shear modulus $\mu(s)$ from transfer function to state space representation can be done using any of the standard control theory methods, cf. [62]. In order to represent the surface load to sensor TFM,(T_{sf} in Eq. (3.4)), in state space, we need to use as many state variable as the order of $\mu(s)$ dictates for each of ε_{xz}, ε_{yz}. However, since p_n is a stress variable and the input is load, μ does not appear in the corresponding TFs. Therefore for p_n, there are no viscoelastice effects that need to expressed as state variables. Effectively, we assume that the response, of the mean stress sensors to surface load, is instantaneous. Denoting the states for ε_{xz} and ε_{yz} as $\xi_{\varepsilon_{xz}}$, $\xi_{\varepsilon_{yz}} \in \mathbb{R}^n$, respectively, where n is the order of $\mu(s)$, we get, using control canonical form for each sensor variable, that the TFM can be represented in state space as

$$
\begin{bmatrix} \dot{\bar{\xi}}_{\varepsilon_{xz}} \\ \dot{\bar{\xi}}_{\varepsilon_{yz}} \end{bmatrix}
\begin{bmatrix} A_\mu & 0_{n\times n} \\ 0_{n\times n} & A_\mu \end{bmatrix}
\begin{bmatrix} \bar{\xi}_{\varepsilon_{xz}} \\ \bar{\xi}_{\varepsilon_{yz}} \end{bmatrix}
+
\begin{bmatrix} b_{\varepsilon_{xz}}^T \\ 0_{n-1\times 3} \\ b_{\varepsilon_{yz}}^T \\ 0_{n-1\times 3} \end{bmatrix}
\begin{bmatrix} \bar{f}_x \\ \bar{f}_y \\ \bar{f}_z \end{bmatrix}
$$

$$
\begin{bmatrix} \bar{p}_n \\ \bar{\varepsilon}_{xz} \\ \bar{\varepsilon}_{yz} \end{bmatrix}
=
\begin{bmatrix} 0_{1\times n} & 0_{1\times n} \\ c_\mu^T & 0_{1\times n} \\ 0_{1\times n} & c_\mu^T \end{bmatrix}
\begin{bmatrix} \bar{\xi}_{\varepsilon_{xz}} \\ \bar{\xi}_{\varepsilon_{yz}} \end{bmatrix}
+ [T_{sf}]
\begin{bmatrix} \bar{f}_x \\ \bar{f}_y \\ \bar{f}_z \end{bmatrix}
\tag{4.8}
$$

where $A_\mu \in \mathbb{R}^{n\times n}$ and $c_\mu \in \mathbb{R}^n$ are obtained from $\mu(s)$, and the input matrix is made of the static encoding solution TFs from T_{sf} in Eq. (3.4) as follows

$$
b_{\varepsilon_{xz}} = \begin{bmatrix} T_{\varepsilon_{xz}f_x} \\ T_{\varepsilon_{xz}f_y} \\ T_{\varepsilon_{xz}f_z} \end{bmatrix}
\quad
b_{\varepsilon_{yz}} = \begin{bmatrix} T_{\varepsilon_{yz}f_x} \\ T_{\varepsilon_{yz}f_y} \\ T_{\varepsilon_{yz}f_z} \end{bmatrix} .
$$

The Kalman Filter

In order to formulate the decoding problem as a filtering problem we assume that known properties of the surface signal can be modeled using a colored noise signal, i.e. a signal filtered through a known linear system that characterizes the expected spatial and temporal properties

of the signal, primarily bandwidth. The form and the parameters of that system need to be assessed for each model or implementation, but this paradigm provides a tool to incorporate and utilize known properties of the input in the decoding. For example, if we assume that the temporal and spatial characteristics are separable and write

$$E[\overline{f}(\omega_x, \omega_y, s)\overline{f}^T(\omega_x, \omega_y, s)] = P_s(\omega_x, \omega_y)\Phi(s),$$

where P_s is the spatial power spectrum matrix of the solution discussed in chapter 3 section 3.3 but Φ is the temporal power spectrum matrix that can be used as a shaping filter to model the temporal characteristics of the load signals. Φ can be any valid rational power spectrum, but a simple example of such a model is the Markov process model, where the power spectrum and the corresponding shaping filter is given by

$$\Phi(s) = \frac{2\beta}{-s^2 + \beta^2} qquad H_\Phi = \frac{\sqrt{2\beta}}{s + \beta}$$

where β represents the temporal bandwidth of the load signal. Using the above example, the spatial and temporal spectrum characteristics can then be combined, e.g. for the normal load $\overline{f}_z$

$$\dot{\overline{f}}_z = -\beta\overline{f}_z + \sqrt{2\beta P_s^{zz}(\omega_x, \omega_y)}w(t)$$

where w is a white noise signals, P_s^{zz} is the spatial power spectrum of f_z, and we have made the simplifying assumption that P_s is diagonal.

Having expressed both the encoding solution and the known spectral properties as state variables, we combine those and obtain the system in form that we can directly apply the Kalman filter to

$$\begin{aligned}\dot{\overline{\xi}} &= A\overline{\xi} + B\overline{w} \\ \overline{\zeta} &= C\overline{\xi} + \overline{v}.\end{aligned} \tag{4.9}$$

A, B and C are obtained by augmenting the system Eq. (4.8) with the states used to model the temporal spectral properties of the surface loads or or displacements as discussed above. The resulting state is ξ and we have used ζ for the measurement vector, i.e. $\zeta = [p_n,\ \varepsilon_{xz},\ \varepsilon_{yz}]^T$ The input w and the sensor noise v are assumed to be white noise processes with the following properties:

$$\begin{aligned}E\left[\overline{w}(t)\overline{w}(\tau)^*\right] &= Q\delta(t - \tau) \\ E\left[\overline{v}(t)\overline{v}(\tau)^*\right] &= R\delta(t - \tau) \\ E\left[\overline{w}(t)\overline{v}(\tau)^*\right] &= 0.\end{aligned} \tag{4.10}$$

where $R = P_n$ the same as delineated in section 3.3, chapter 3 and $Q = P_s$, if temporal and spatial properties are separable, as discussed above. We further note that the Kalman filter

allows A, B, C, Q and R functions of spatial frequency and time, i.e. $A = A(\omega_x, \omega_y, t)$, hence the separability assumption above is not necessary but we only present it to show the relation of this solution to the static solution (see also Appendix E).

For linear systems in state space it is known that a filter that minimizes the expected covariance of the estimation error $P = E\left[tr\left((\bar{\xi} - \hat{\bar{\xi}})(\bar{\xi} - \hat{\bar{\xi}})^*\right)\right]$ and hence, minimizes the error in Eq. (4.7), is the Kalman filter given by the following equations:

$$
\begin{aligned}
\dot{\hat{\bar{\xi}}} &= A\hat{\bar{\xi}} + K(\hat{\zeta} - C\hat{\bar{\xi}}) \\
K &= PC^*R^{-1} \\
\dot{P} &= AP + PA^* - PC^*R^{-1}CP + BQB^* \qquad P(0) = P_0
\end{aligned}
\tag{4.11}
$$

and we get our solution to the decoding problem from the state estimate since the inputs are contained in that part state vector that models the input characteristics. (For examples see simulations in section 4..

This state representation in the spatial frequency domain is a straightforward and a powerful extension to the static decoding solution. It retains the numerical efficiency of the Fourier transform (i.e. with the use of FFT) and at the same time provides a well developed modeling tool. The Kalman filter further has many guaranteed properties and an important one is that if the signals involved (w and v) can be assumed to be Gaussian the the Kalman filter is the best possible filter for a large class of criterion [6], i.e. it can be shown that it minimizes the expectation of nondecreasing functions of the magnitude of the error.

Remark: Many of the assumptions made above (e.g. that $E\left[w(t)v^T(\tau)\right] = 0$) can be dropped or weakened but we believe that more detailed discussion on the properties of the Kalman filter is beyond the scope of this thesis and the reader is refered to the rich literature that exist on the kalman filtering and its many applications, (e.g. [6, 37].)

Remark: Even though this formulation of a solution to the decoding problem appears quite different than the one obtained in the case of static loading in chapter 3 it is in fact equivalent in the sense that the Kalman filter solution can be shown to converge to the Wiener filter under static conditions. This we show in appendix E.

4. Simulations

The simulations presented here are designed to clearly draw out the specific aspects of the encoding and decoding problems treated in this chapter, i.e. the dynamic effects of viscoelasticity on these problems. In order not to clutter the results, we chose the examples to be as simple as possible while still being able to reach the main objective of this simulation section, which is to confer the following: 1) Viscoelastic effects need be accounted for if one wants to correctly solve the encoding and decoding problems under dynamic conditions. 2) State space representation and the Kalman filter can be successfully applied to solve the above problems.

The example presented here will be a model of a smooth rigid body, shaped in the form of a paraboloid, indenting a viscoelastic halfspace. The normal load is assumed to be a time-varying Hertzian distribution, which is one of the few available analytical solutions to viscoelastic contact problems. The time varying Hertz distribution can be shown to correctly model the indentation of an object of this shape into a viscoelastic halfspace during the indentation phase, i.e. while the contact area is nondecreasing [44, 30].

The contact area is time-varying but the contact radius is obtained by integrating the relation

$$\left[a^3\right](s) = \frac{3R}{8}\frac{F_z(s)}{\mu(s)} \tag{4.12}$$

where the parameter R is the curvature of the object, as $u_z^* = (x^2 + y^2)/2R$ and we have assumed that the material is incompressible ($\nu = 0.5$). We use here the simple Kelvin model, discussed in section 2.3 for the shear modulus, or

$$\mu(s) = \frac{1+s}{1+s/3}$$

i.e. $t_r = 1\ s$ and $a_r = 3$. We further choose the total normal load trajectory to be a low-pass filtered step (see Fig. 4-6a) The resulting time history for the contact radius $a(t)$ is shown in Fig. 4-6b and corresponding surface load and displacement distributions are shown in Figs. 4-6c and 4-6d for the time points $t = 0.02, 0.1, 1,$ and $4\ s$. The surface normal load and the displacement distributions shown in Fig. 4-6 are calculated using the known Hertzian solution
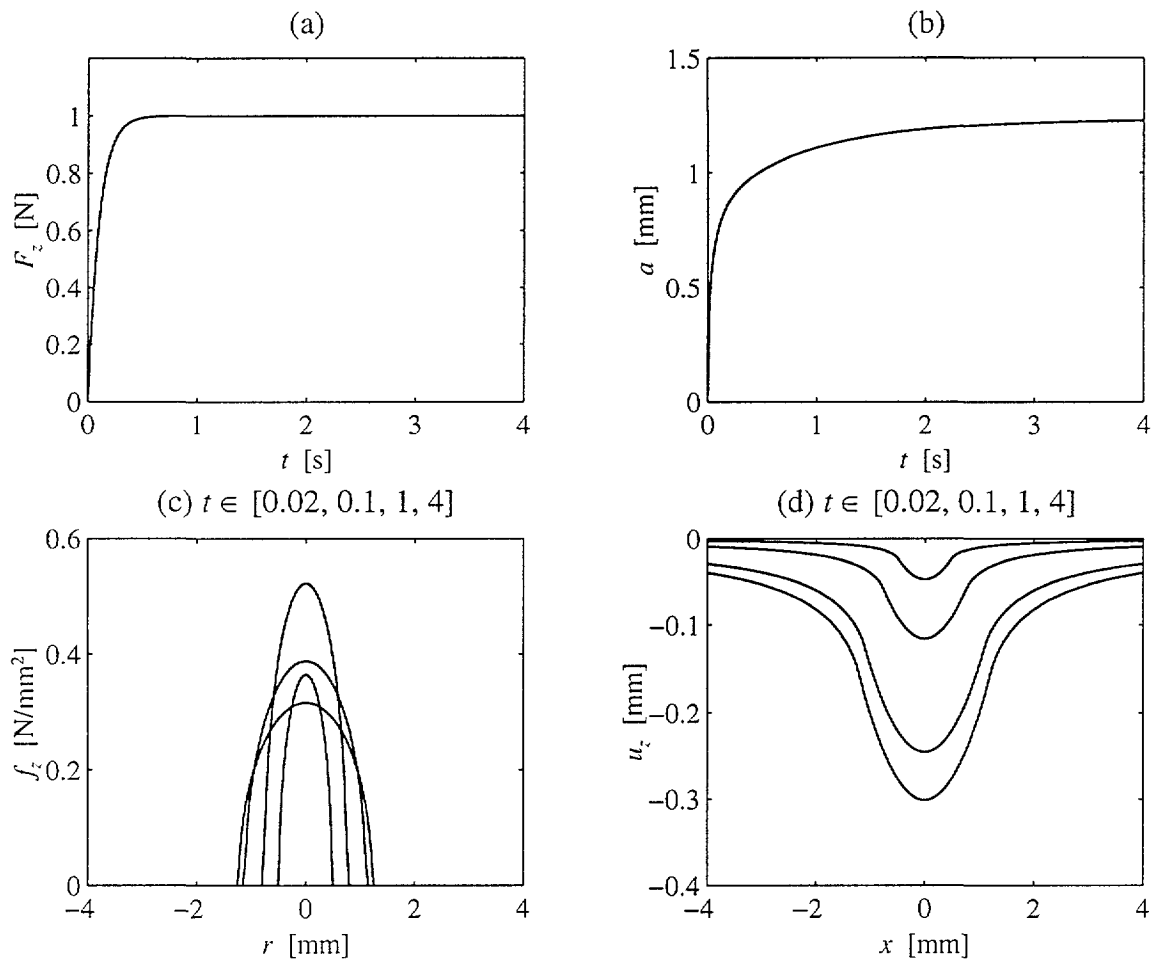
Figure 4-6: (a) Shows the time history of the total normal load $F_z(t)$ which is a low-pass filtered step. (b) Shows the corresponding contact radius time history obtained from Eq. (4.12). (c) Shows sections of the resulting surface normal load distribution, f_z,obtained using Eq. (4.13) at for different times, ($t = [0.02, 0.1, 1, 4]$). We note that the maximum load, is not monotonic in time as the total load but reaches a maximum in $t \in [0.1, 1]$ (see also Fig. 4-7. (d) Shows sections of the resulting surface normal displacement for the same time points as (c).

[36]:

$$f_z(r,t) = \frac{3}{2\pi} \frac{F_z(t)}{a^2(t)} \sqrt{1 - \frac{r^2}{a^2(t)}}$$

$$u_z(r,t) = \begin{cases} \dfrac{1}{2R} \left(2a^2(t) - r^2 \right) & \text{if } r \leq a \quad (4.13) \\[2ex] -\dfrac{2}{\pi} \dfrac{1}{R} \left[\left(2a^2(t) - r^2 \right) \sin^{-1} \left(\dfrac{a(t)}{r} \right) + ra(t)\sqrt{1 - \dfrac{r^2}{a^2(t)}} \right] & \text{if } r > a \end{cases}$$

Although the solution presented in section 3. is valid for a general 3D loading we only include the normal load since we are concentrating on the dynamic and viscoelastic effects in this chapter and they are independent of the effects of the shear loads. Hence, the results and comments on the effects of static shear loading obtained in chapter 3 are equally applicable when dynamics and viscoelasticity are included and we therefore do not repeat them here.

4.1   The Encoding

We pose the encoding problem here, as the prediction or calculaction of the subsurface signals that the sensors transduce, given the surface load or displacement distributions. We have already decided that the sensors are the set $(p_n, \varepsilon_{xz}, \varepsilon_{yz})$ and since we later on intend to apply the Kalman filter, we use the state space representation given in Eq. (4.8). The state space matrices, not already specified, for this system become

$$A_\mu = -\frac{a_r}{t_r} \qquad \text{and} \qquad c_\mu = t_r \left(1 - \frac{1}{a_r} \right)$$

and Fig. 4-7 shows the shape of the resulting signals for the same time points as Fig. 4-6. We note that the shape of mean normal stress, p_n sections (Fig. 4-7a-b) is a low-pass filter version of the surface normal load in Fig. 4-6c and that the response is instantaneous. The shear strain response shown in Fig. 4-7c, on the other hand, is not instantaneous and there the viscoelastic effects become clearly visible. The instantaneous, or static, response is shown as a dotted line and we see that it behaves quite differently, with time, than the viscoelastic response, shown as a solid line. We further note that the sections corresponding to $t = 4\,s$ coincide so the responses converge in the end as expected.
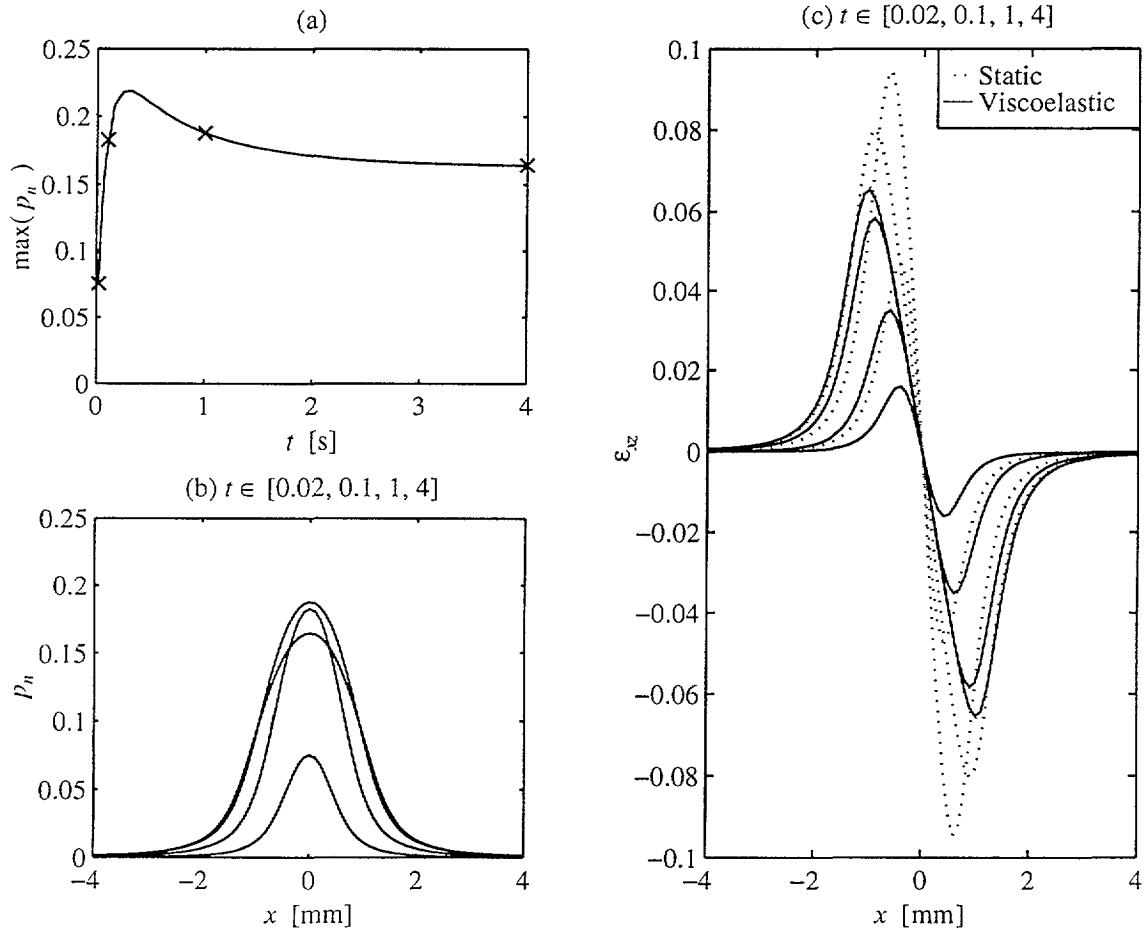
Figure 4-7: (a) Shows the time history of maximum mean normal pressure, $\max(p_n)$. The time points selected to show the distribution profiles are marked with $\times$ on the plot and we note that there is a maximum at $t \approx 0.3s$. (b) Shows sections of the mean normal pressure distribution. (c) Shows sections of the xz-shear strain distribution. The solid lines show the viscoelastic response but the dotted lines what the predicted response would be if viscoelastic effects were ignored. We note that they are quite different for all time points, except for $t = 4\,s$ when the response profiles coincide as then the static assumption becomes valid.

4.2 The Decoding

Here the problem is to reconstruct the surface load and displacement distributions from the sensor signals. We only consider normal loads so the input signal is 1D and we therefore only need one sensor signal for which we choose p_n. We could use the other signals, i.e. ε_{xz} and ε_{yz} instead or as well but that would not have any effects on the dynamic side of this problem, which we want to expose.

Reconstructing the surface load distribution, f_z, from p_n will not involve viscoelastic effects as our assumptions implicitly say that this response is instantaneous. The reconstruction of the displacement distribution, u_z, does however involve dynamics and then we use the above state space model with the transfer function $T_{p_n u_z} = 2\mu\Omega \exp(-\Omega z)$ in both the B and C matrices. We further use the Markov process to model the temporal properties of the surface signals and choose the parameter β to be large enough to match approximately the bandwidth of the surface signals. Finally, we add a spatially high-pass filtered Gaussian sensor noise, so that the rms. error to signal ratio[6] is $\approx 23\%$, see Fig. 4-8.

The results from the Kalman filter are shown in Figs. 4-9a-c and there we note that the filter successfully estimates the surface signals and that the rms. error ratios are $\approx 14\%$ for f_z, the surface normal load and $\approx 3\%$ for u_z, the surface normal displacent.

In this section we have given an example of how the theory presented in this chapter can be applied to solve the encoding and decoding problems under dynamic conditions. The results of the simulations indicate that the state space approach can be used to model viscoelastic properties and, simultaneously include known spatial and temporal properties of the signals. The encoding results indicate that viscoelastic effects can have significant effects on the predicted sensor response and that viscoelastic effects need to be accounted for under dynamic conditions. The decoding results give us that the Kalman filter is successful in filtering out sensor errors and gives relatively accurate estimates of the surface signals, where the displacement estimates are more accurate than the load distribution estimates.

---

[6]That is, square root of the ratio between the integrated squared error and squared signal, respectively

(a)   (b)
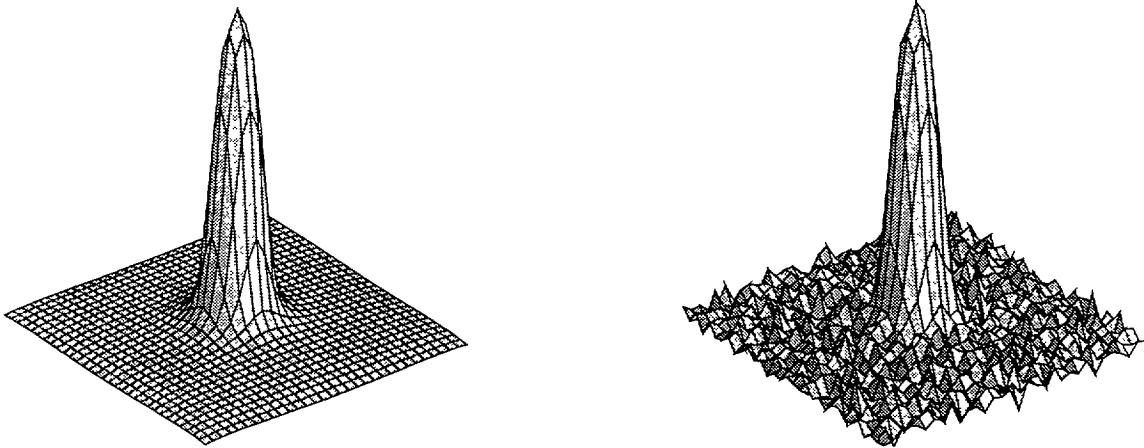
Figure 4-8: (a) Shows the distribution of the mean normal stress, p_n, at sensor depth. (b) Shows the same distribution with spatially high-pass filtered measurment noise added. The rms. error level is $\approx 23\%$.
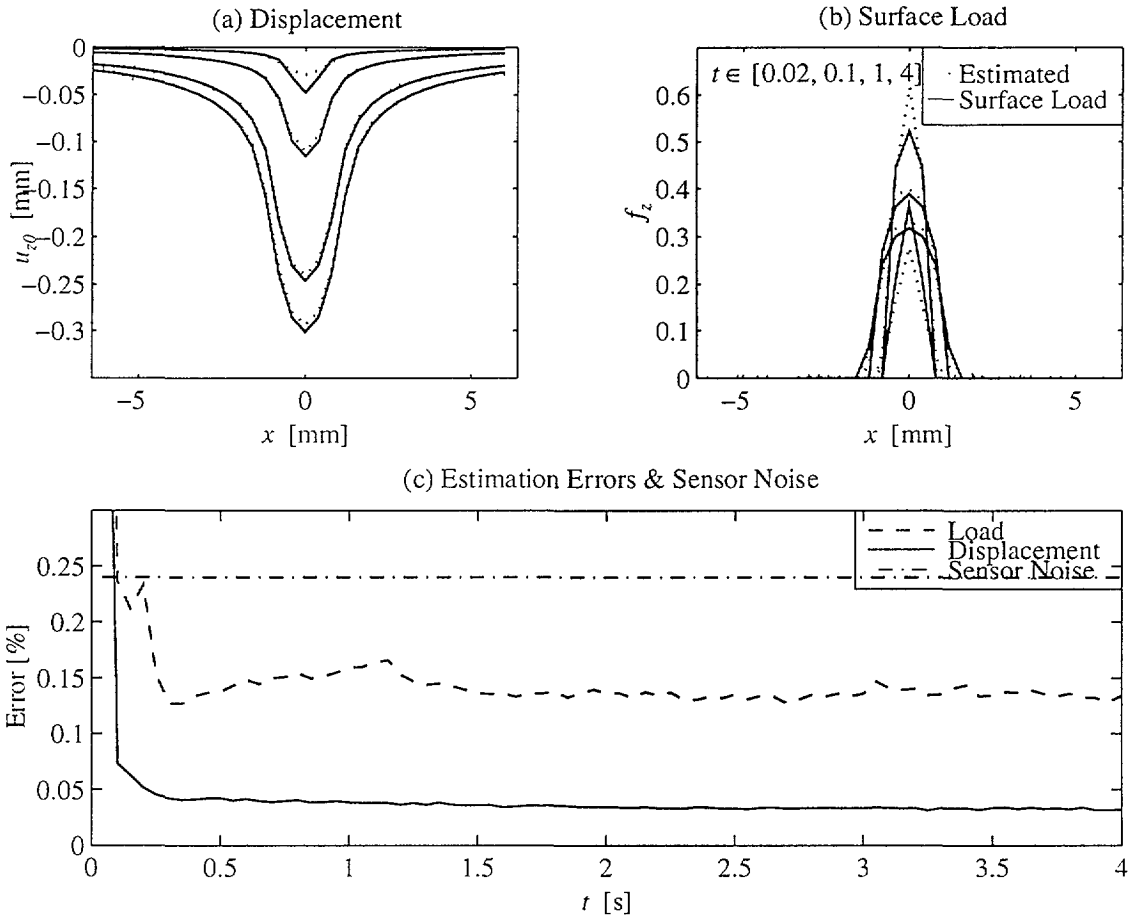
Figure 4-9: The results of decoding simulations. (a) Shows the actual and decoded estimates of surface normal displacement distribution u_z. The estimates are shown using dotted lines but the actual displacements using solid lines. (b) Shows the actual and decoded estimates of surface normal load distribution f_z. The estimates are shown using dotted lines but the actual loads using solid lines. (c) Shows the rms. errors as percentage ratios to the total response of each signal. We note that both the load and displacement errors are less than the sensor noise and that the displacment error ratio are always less than the load error ratio but that is caused by the smoothing nature of continuous materials.

5.   Conclusions

In this chapter we have delineated the aspects of haptic computational theory that relate to dynamic properties of the fingerpad. Separating the problem of shape identification into an encoding and decoding problem we give a solution to the encoding problem using a Transfer function Matrix formulation obtained using a combined 2D-Fourier-Laplace transform. We show how the effects of inertia and viscoelasticity enter the solution and analyze the contribution of each. We further show that the effects of inertia can be neglected for a significant lower range of the temporal (lower bandwidth signals). We give a solution to the decoding problem in the form of a Kalman filter operating on the 2D-Fourier transform of the sensor signals. The Kalman filter is a numerically effective and well developed tool with many desirable properties, and it has proven its validity in numerous applications. Finally we show how the solutions to the encoding and the decoding problems become identical to the solutions to the static problem given in chapter 3 when the surface loads become static or quasi-static.

A computational model of dynamic tactile contact provides an important extension to previous results on the static haptic identification problem. Robots can generally be expected to operate under dynamic conditions where contact loads cannot be assumed to be quasi-static. It is also known that for humans stroking enhances performance when carrying out haptic tasks. We further know that the characteristic time constants of the fingerpad are on the order of a second or more and that viscoelastic effects are significant and cannot be ignored. Finally in virtual environments, it is the dynamic interaction that simultaneously provides most of the illusion and implementation difficulties, making detailed modeling necessary. A related problem is how the information that is obtained using the methods described in this chapter can be used to touch and grasp, and consequently explore environments or manipulate objects , but that will be the subject of next chapter.

Chapter 5

Exploration Strategies and Finger Control

1. Introduction

A comprehension of the nature of contact, grasping and subsequent exploration or manipulation is of significant importance in both physiological and robotics research. In physiological research the objective is to understand the mechanics of hand movements, especially which factors govern the shape of motion trajectories and more importantly why they do so. This knowledge has in addition to its scientific value, uses in such areas as rehabilitation, learning and development of motion skills and ergonomic studies, just to name a few. On the robotics side the goal has been to make a robots perform tasks that demand human level of dexterity. This goal has proven elusive, mainly because of the inherent complexity of the mechanics involved. But the difficulty is easy to underestimate considering the relative ease humans seem to have with performing these tasks. Robots have until now also lagged behind their human counterparts on the sensory side and it is only recently that sensor arrays have been produced that in some ways duplicate the properties of the human sensory organs. The problem of grasping and manipulating an object has been investigated by many researchers (for review see [69]) and in view of that and the above we will in this chapter discuss how this sensory information can be used for the exploration of objects. We will try to make our arguments independent of implementation and therefore equally applicable to robots and humans. By this, we hope to extract a common

thread in a web that could be called a computational theory of haptics.

In chapters 3 and 4 we have discussed the processing of sensor signals resulting in algorithms and guidelines for sensor design that together give optimal estimates of the loading and displacement distributions on the surface of the fingerpad. That is the *Surface Signal Identification Problem*, which details can be found in chapters 3 and 4. Fig. 5-1 shows a diagram which explains the relation of that part to the problems we are going to discuss here. In this chapter we will focus on two blocks of Fig. 5-1, the *Exploration Strategy* and the *Finger Control* blocks. Our main goal is to explore objects, but the Exploration Strategy block refers to the problem of inferring object properties such as shape, texture, and compliance and the state of contact from the estimated surface signals. This involves determining, given a property that is to be explored, what kind of sensor information and also what kind of action is needed for successful exploration. Thus, in addition to actual information processing, a specific action, that brings the desired information to the sensors, is also needed. This is the role of the *Finger Control* block, but it refers to the translation of the desired actions into command trajectories for the fingerpad. We will show that for continued exploration we will need information about the local curvature of the object at the contact location. We further give a method to extract that information from the surface signals estimates in a robust manner. Finally, Fig. 5-1 shows how the command trajectories are fed into a low-level manipulator controller which we assume is capable of producing motor commands that will make the manipulator move accurately enough[1] along the command trajectories, which in turn closes the loop at the fingerpad.

The *Supervisor* figure in Fig. 5-1 provides external information labeled *control strategy* which for example includes the desired direction of stroking. We therefore, assign to the Supervisor the role of providing 'global' information which is not readily accessible through tactile channels. e.g. visual information. One of the implications of this assumption is that we will not dwell on various problems that arise when an object is explored, such as how can we ensure we will cover the whole surface of an object when stroking it. We believe that such questions are more naturally answered using either heuristic or AI techniques and as such are beyond the scope of this thesis.

We are not aware of any reference that treats the problems discussed here as whole and we believe the reason is the fact that it has been addressed from different directions in various disciplines. Exploration strategies have mostly been investigated from the human side. [42, 43]

---

[1]The manipulator we discuss here can be a human arm or finger as well as a robot manipulator. We acknowledge that the human arm has in general inferior position and force accuracy when compared to robot arms. However, we also know that measured in dexterity it is superior so the human accuracy, or lack thereof, must be sufficient in some way and this is what we mean by saying "accurately enough".

investigates exploratory procedures, [48] delineates sensor channels and coding in general, but [76, 77, 48, 12, 33, 29] discuss the same with respect to specific object properties, mainly texture. Most of the definitions in these references are implementation independent and therefore usable for robots as well. It is only the definition of object properties such as texture that is often subjective and often hard to get any consensus on what the term texture means. We will therefore explicitly define the object properties we will discuss so that they can be quantitively identified. For shape sensing we rely mainly on image analysis literature, [1, 31, 3, 50, 78, 27], and for texture measures we borrow concepts from triboloby in work on surface roughness [79, 47, 46, 58, 25]. The robotics literature dominates in the formulation of control laws as can be expected. For contact and grasping stability during manipulation we confer [69, 54, 7], but for stroking and manipulation kinematics we confer [57, 53, 55], and finally for the formulation of control laws we confer [2, 26, 11].

The contributions of this chapter lie mainly in the arrangement in a common framework the different components and processes of haptic exploration. These components and processes have until now been treated treated separately, but we identify them as different facets of a larger structure, ie. the structure illustrated in Fig. 5-1. On the more detailed level, we define and discuss in a consistent manner the constituting parts, i.e. the Exploratory Procedures for each object Property and contact state and also the relevant Sensor Channels and Codes in each case. We finally show how these exploration strategies can be implemented and specifically delineate how stroking can be achieved using robust estimates of local shape information.

This chapter is organized sectionwise as follows: In section 2 we discuss the Exploration Strategies including definitions of the term used, i.e. Exploratory Procedures, Sensor Channels and Sensor Codes. We then apply the tools introduced for the identification of object properties, and the state of contact. In section 3 we discuss translation of the Exploratory Procedures into control laws and we do that separately for directions tangential and normal to the fingerpad. We finally give our conclusions and remarks in section 4.

2. Exploration Strategies

In this section we will discuss exploration strategies suitable for object property or state-of-contact identification. More specifically we will list the types of actions, i.e. *Exploratory Procedures* human and robots have available. We will also list different types of sensors, ie. *Sensor Channels* and further what part of the sensor signal is of interest, i.e. *Sensor Codings.*

Table 5.1: Explicitly lists the available exploratory procedures, sensor channels and codes as well as object properties. For further clarifications of terms used in the table see text.

Exploratory Procedures	Sensor Channels	Sensor Codes
Static Touch	SA1	Intensive
Indenting	Sensor Array	Temporal
Stretch	RA1	Spatial
Stroking	SA2	Spatio-
Tapping	PC	temporal
(Enclosure)	Accelerometer	
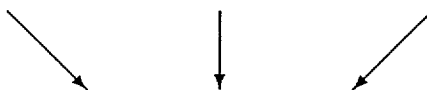
Object Properties	Shape, Texture, μTexture Compliance, State of Contact

Finally, we will list and define the object properties that are identifiable using the previously listed exploratory procedures and sensor channels and codes. For overview, Table 5.1 explicitly lists the available exploratory procedures, sensor channels and codes as well as the object properties that we discuss in more detail below.

Exploratory Procedures

The term *Exploratory Procedure* as defined in [42], refers to a "stereotyped movement pattern having certain characteristics that are invariant and others that are highly typical". Here we will only include simple movements that only require the movement of a single fingerpad and exclude more complicated procedures such as function tests or part motion tests that may require the relative motion of two hands. The "enclosure" procedure actually violates this condition since it would require multiple fingerpads, but we include it since it adds insight when explaining object shape identification (see section 2.1).

1. **Static Touch** is the most basic procedure and it can only give information on the shape of the fingerpad within the contact area, and only spatial information is available.

2. **Indenting** gives also information about the force-displacement relationship of an object and can therefore be used to infer the normal compliance of the object.

3. **Stretch** gives same addition as indenting but in the tangential direction and will therefore give information on the lateral stiffness of an object.

4. **Stroking** adds the temporal dimension and the spatio-temporal information becomes available. One feature of stroking is that if position accuracy is better than sensor resolution then one can increase the effective spatial bandwidth as then the surface is effectively re-sampled. The extents of this bandwidth enhancement are limited by the position accuracy.

5. **Tapping** is a ballistic movement where the finger impacts the object, and provides the same information as indenting.

6. **Enclosure** is the simultaneous contact of multiple fingers and may include other parts of the hands such as the palms.

Physiological experiments involving analysis of videotaped hand movements indicate that humans use these exploratory procedures to a high degree and further that they select different procedure to match the required object property [43]. We therefore believe that this approach is of value and can be used for robotic exploration.

Sensor Channels and Codes

The concept of sensor channels and the coding principle introduced in [34, 40] has its roots in neurophysiology where researchers were interested in how different textures and other stimuli to the fingerpad of monkeys was coded in the measured peripheral neural signals. There this classification has been proven to be useful in generating hypothesis on phenomena such as roughness perception. It can however, also be useful for the identification of other object properties such as shape and compliance.

Sensor Channels

The need to define different sensor channels arises from the fact that there are known at least four different types of mechanoreceptors the human fingerpad. These are frequently classified as: slowly adapting type I (SA1), slowly adapting type II (SA2), rapidly adapting (RA1) and Pacinian (PC). We have in table 5.1 where applicable identified the robot sensor types that are roughly parallel to the human mechanoreceptors. The criteria we used in matching human and

99

Table 5.2: Lists the different sensor channels for humans and robots and matches them according to temporal and spatial bandwidth.

Human Mechanorepectors	Spatial and Temporal bandwidths	Robotic Sensors
SA1	Low temporal, high spatial	Strain gauge array
SA2	Low temporal, low spatial	Force sensor
RA1	Medium temporal, medium spatial	
PC	High temporal, low spatial	Force sensor

robotic are the sensor's differing temporal and spatial bandwidth of the sensors. Table 5.2 lists how this comparison is made.

Sensors with limited spatial and temporal frequency range are easier to make than sensors that cover large ranges of both. It is, however, possible to make several sensors each targeting a different frequency range and combine the information from the different sensor channels to cover the frequency ranges of interest. How this concept is realized in the human fingerpad is shown schematically in Fig. 5-2, where the the temporal and spatial frequencies are on the horizontal and vertical axis, respectively.

An interesting coupling between the temporal and spatial frequency responses occurs during stroking and it does play a role in shape and texture identification. Assuming that under static loading the loading distribution is represented by its Fourier transform, $\bar{f}_z(\omega_x, \omega_y)$, then the same loading distribution traveling along the surface with a constant x-velocity, v_t will result in a loading distribution which has a Fourier transform $\bar{f}_z(\omega_x, \omega_y) \exp(-j\omega_x v_t t)$. (This result is easily obtained directly from the definition of the Fourier transform.) This means that a ω_x-component of the loading distribution will give rise to a temporal variations of frequency

$$\omega_t = \omega_x v_t. \tag{5.1}$$

Details on this phenomenon are to be found in Fig. 5-3, where we superimpose a typical spatial frequency distribution onto the observed temporal sensitivity properties of human receptors. The relation in Eq. (5.1) appears as a line on a loglog (ω_t, ω_x) plot and the line is translated sideways by changing the stroking velocity v_t. A consequence of this result is that the stroking velocity can be selected based on a desired spatial frequency range to match the temporal sensitivity range of the sensor/receptor.

Sensor Codes

Sensor coding refers to how the sensors signals are pre-processed or what part of its content is used for object property identification. Four principal codes, $C_1 - C_4$, have been identified [34, 40] based on the assumption that we have a distributed sensors response signals $r_i(x, y, t)$, that are the response to some stimuli, where i represents different sensor channels.

1. **Intensive** code is when $C = C_1$ =const., i.e. all spatial and all temporal variations has been integrated or averaged out.

2. **Temporal** code is when $C = C_2(t)$, i.e. all spatial variations have been removed.

3. **Spatial** code is when $C = C_2(x, y)$, i.e. all temporal variations have been removed.

4. **Spatio-temporal** code is when $C = C_4(x, y, t)$, i.e. at least one channel preserves information about both spatial and temporal variations.

All sensor channels may not be used to identify every object property and it is mainly for complicated object properties such as texture that we can expect more than one channel to be used. We will now discuss how we match the sensor channels and codes with various object properties, which we will also define along the way.

2.1 Identification of Object Properties

In this section we will give details on how one can go about identifying object properties. We will go through each of the properties listed in Table 5.1, define it and give a modeling method suitable for identification, and further delineate the appropriate exploratory procedures and relevant sensor channels and codes.

Scale Segmentation

Most of object properties that can be identified using touch are a part of the geometry of the object and one can define different object properties by segmenting the spatial scale and

Table 5.3: Lists definitions of geometric object properties and how the different scale segments arise from human sensing abilities.

Name	Scale	Comment
Shape	1000-1 mm	Lower limit set by sensor resolution
Texture	1-0.1 mm	Lower limit set by estimated position accuracy
μTexture	100-0.1 μm	Practical lower limit set by sensor sensitivity

identifying a scale interval with an object property. This is necessary because there will always be an upper and a lower limit on the size of the geometric features of interest, but real objects will continue to have geometric variations right down to atomic scale. We define here three object properties by segmenting the spatial scale and Figure 5-4 shows this schematically, but Table 5.2 in numbers. We name the scales *Shape*, *Texture* and *μTexture*, and where the limits are decided approximately by human sensing abilities.

Having defined shape using scale segmentation we can now simply define shape identification as follows:

Definition 1 *Shape identification: Identification of the geometric boundary of an object to a given resolution.*

Shape Identification

Humans recognize common objects reliable in a matter of few seconds [39, 43] and based on observation made in human experiments the identification procedure has been separated into:

1. **Scanning**, i.e. finding the object.

2. **Positioning**, establishing extents or a point of reckoning.

3. **Enclosure** with one or both hands to get an initial size estimate.

4. **Contour following** where the outlines and contours of the object are traced.

The trend is therefore to begin the identification on a coarse scale and the proceed to the finer scales. This approach appears intuitively feasible and it is natural to assume that the same

approach could work for robots as well. This approach may however, not always be optimal e.g. if the task at hand is to classify objects that only differ in some detail at a fine scale, then the coarse scale identification would only give limited information. In order to compare or recognize an object we must somehow be able to register its features and for that we use object models. The problem we face is to construct a geometrical model of an object from surface measurements. A similar problem occurs in machine vision and there, fortunately for us, considerable research has been done and several approaches to this problem have been developed (for review cf. [1, 31, 3]). There this problem has been divided into five subtasks:

1. Data acquisition.

2. Low-level processing.

3. Object representation.

4. Model Construction.

5. Model matching.

and we note that this subdivision is directly applicable to our problem. We have already in previous chapters discussed subtasks 1 and 2 and we go therefore directly to number 3.

Object representation: Object representation refers to method we use to describe the shape of the object. Many representations have been developed, such as vertex- or edge based, surface based, moment based, or volume based. We believe surface representation is natural, since the sensor data we have available gives information about a patch of the surface, i.e. the contact area, but because of the compliant fingerpad will not give direct information about either vertices or edges.

Model Construction: As an example we will give a short description of a surface based object representation that can be used in shape identification [50, 78]. It is a physics-based approach in the sense that it utilizes a 3D elastically deformable finite element balloon model with both membrane and plate properties. The spatial data then acts as external forces pulling the model surface towards where it has been measured and the internal membrane/plane forces strive to regularize the surface to be smooth and continuous in areas where the surface shape is unknown.

Model Matching: Once we have a shape model of the object we can attempt to match it with a known object. Many schemes designed for this task have been developed in the related fields

of machine vision and artificial intelligence. Examples of those are feature matching, where a distance between feature vectors for the shape model and object is used as a criteria to decide which object the shape model most likely represents [27]. Other more sophisticated methods are constantly being developed and we believe detailed discussion of those is beyond the scope of this thesis.

As a matter of completeness we list in Table 5.4 the relevant exploratory procedures as well as the relevant sensor channels and codes.

Table 5.4: Lists exploratory procedures, sensor channels and sensor codes used for shape identification.

Exploratory Procedure	Sensor Channel	Sensor Code
Static Touch	SA1, RA1	Spatial
Stroking	Strain gauge arrays	Spatio-temporal

Texture Identification

Definition 2 *Texture identification: Identification of the geometric features of an object that are of finer scale than sensor resolution but that can in principle be reconstructed by stroking.*

Texture Measures As defined, texture could be identified the same way as shape (both are in fact geometry of the object) but we propose a different identification method solely based on human experience and abilities. Since knowing the exact shape at such a small scale is of limited interest to humans it is natural to look for a collective measures characterizing the shape variation. We will now discuss different approaches to texture identification and their characteristics.

In the field of neuro-physiology considerable research has gone into identifying how texture is coded in the peripheral nerve signals [76, 77, 48, 12, 33, 29]. There definitions of texture, roughness and measures thereof are widely varying. Usually specimens used in the experiments are regular patterns such as dot patterns, that vary only in their frequency or spacing. The measure applied is usually single scale, smooth to rough or equivalent. The research suffers from inconsistent definitions of texture and non-standard specimens, but still has some interesting results. In [33] are presented results which indicate that the tactual roughness perception for

104

the set of specimens used, is based on spatial variation in the SA1 population response (which in fact is similar to σ_m defined in Eq. (5.3) below). The perceived roughness was further observed to be independent of stroking velocity, but to be proportional to the load which is consistent with our definition of texture above. The problem is however that most natural textured surfaces are not as simple as the specimens used and can rarely be described using a single parameter.

A related problem is encountered in the characterization of surfaces in the field of tribology. The most common engineering measure is roughness, R_a, which is primarily used along with a prescribed machining process to characterize a surface texture for machine parts. Engineering roughness is defined as the mean absolute deviation of a height profile $z(x)$, from its mean:

$$R_a = \frac{1}{L} \int_0^L |z(x) - \bar{z}| \, dx.$$

A plethora of other engineering measures and standards for the measure of surface roughness exist [79] but all suffer to some degree to from the same shortcomings as the measures detailed above, i.e. that there are surfaces are identical in terms of roughness measures but clearly have different surface textures.

The third type of measures are the scientific measures and they are based on a statistical approach, i.e. the surface is modeled as a two-dimensional random process and analyzed as such cf. [47, 46, 58, 25]. If the surface shape is decided by the effects of many random and independent processes, we can apply the Central Limit Theorem which gives us that the result will be a Gaussian surface. Analysis of the joint Gaussian probability distribution for the height, the first and the second spatial derivatives, $p(z, z', z'')$ then gives that such a surface can be characterized by only three parameters:

1. Root mean square height of surface,

$$\sigma = E\left[(z - z_0)^2\right]^{1/2} \approx 0.8 R_z \qquad (5.2)$$

   i.e. the standard deviation of surface height.

2. Root mean square slope of surface,

$$\sigma_m = E\left[(z' - z_0')^2\right]^{1/2} \qquad (5.3)$$

3. Root mean square curvature of z,

$$\sigma_k = E\left[(z'' - z_0'')^2\right]^{1/2} \tag{5.4}$$

.

From these parameters others can be derived, such as peak density

$$D_s = (\sigma_k/\sigma_m)^2 \tag{5.5}$$

and average wavelength

$$\bar{\lambda} = 2\pi\sigma/\sigma_m \tag{5.6}$$

and many more. If the surface is close to being Gaussian these statistical parameters can be used to identify and compare textures, e.g. by constructing a feature vector [27]. Not all surfaces are Gaussian and there certainly will exist surfaces with the same $(\sigma, \sigma_m, \sigma_k)$ but that still cannot be considered to have similar surface textures. This can never be completely avoided as we cannot completely describe an arbitrary surface geometry using a finite number of parameters, hence the question is how many parameters and which do we need to characterize a given class of surfaces. A related issue is that there will always be some part of the geometry that cannot be sensed using tactile sensors, namely sharp and deep minima, which give arise to some asymmetry. Here we will not elaborate further on these question but end with the conclusion that in order to identify texture of surfaces one needs in general more than one parameter, three statistical parameters for a Gaussian random surface but more for a general surface.

Table 5.5: Lists Exploratory procedures, sensor channels and sensor codes used for texture identification.

Exploratory Procedure	Sensor Channel	Sensor Code
Stroking	SA1, RA1 Strain gauge arrays	Temporal Spatio-temporal

μTexture Identification

Definition 3 *μTexture identification: Identification of geometric features of an object that are of a finer scale than stroking resolution but can still be detected as temporal variations.*

Microtexture differs from texture only by scale, but the scale boundary between them is set by the estimated sensor properties of the human hand. The sensor signals will be the results of the interaction of geometric variations that are smaller than spatial resolution and all the information can therefore be contained in a temporal code. Further, the signals will typically be high frequency so suitable sensors channels would be PC for humans and accelerometers for robots. Stroking velocity will effect the temporal frequency content of that temporal code, higher velocity will translate the signal into higher temporal frequency range as illustrated in Fig. 5-3. This in turn has the consequence that if the sensors have some optimal sensitivity in some specific frequency range, one can translate the dominant spatial frequency, if any, into that range. For that purpose Eq. (5.1) can be rewritten as $v_t^* = \bar{\lambda} f^*$ where $\bar{\lambda}$ is the average wavelength of the surface defined in Eq. (5.6), f^* is the optimal temporal frequency of the sensor, and v_t^* is the corresponding optimal stroking velocity.

Table 5.6: Lists Exploratory procedures, sensor channels and sensor codes used for μtexture identification.

Exploratory Procedure	Sensor Channel	Sensor Code
Stroking	PC Accelerometers	Intensive Temporal

Compliance Identification

Definition 4 *Compliance Identification: the estimation of the effective compliance of an object, at the contact location, averaged over the contact area, assuming that the object is smooth and made of homogeneous and linearly elastic material.*

The compliance of an object is a material property that refers to how much the material deforms with increased loading. The identified compliance should ideally not depend on the loading or geometry of the object. That is however not practical as it is generally not possible to distinguish between the effects of geometry and material properties if both are unknown. Here we will therefore neglect the effects of geometry and assume that the object is smooth over the contact area. We are then calculating the effective compliance of that surface averaged over the contact area. When the object is smooth and slowly varying, the contact area will have the shape of an ellipse and the loading distribution will be ellipsoidal, i.e. Hertzian contact conditions [36]. Further, when a compliant material is contacted with compliant fingerpad the compliances of add the same way as springs in series. Assuming that the compliance

107

of the fingerpad is known we can then infer the compliance of an object from the combined compliance. For a linearly elastic material the compliance depends on two constants, E, ν, the Young's modulus and Poisson's ratio. How they combine depends on what exploration procedure is used, indentation or stretch, or equivalently the direction of the load, normal or tangential, but the general form is similar.

Normal Compliance: In [36] it is shown that if the contact area has the form of the circle with radius, a, then the overall normal displacement, δ_z, is related to the total normal load, F_z by

$$\delta_z = \frac{1}{E_n^*} \frac{3F_z}{4a}. \tag{5.7}$$

Where $1/E_n^*$ is the combined normal compliance, given by

$$\frac{1}{E_n^*} = \frac{1 - \nu_f^2}{E_f} + \frac{1 - \nu_o^2}{E_o} \tag{5.8}$$

and where the subscript, f refers to the material properties of the finger, but o to that of the object. This relation is also valid if linear viscous effects are present, [30, 44, 36], but then only while the contact area is increasing[2] $\dot{a} \geq 0$, but then $E_n^* = E^*(s)$ is in the form of a Laplace transfer function describing the rate dependent behavior of the material. In this case one can simply apply system identification techniques from control theory (cf. [45]) to identify the parameters of $E_n^*(s)$.

In the more general case, when the contact area is an ellipse, with axes a and b, the relation in Eq. (5.7) is only slightly modified and becomes

$$\delta_z = \frac{1}{E^*} \frac{3F_z}{4(ab)^{1/2}} \frac{b}{a} K(e). \tag{5.9}$$

where $K(e)$ is a complete elliptic integral, and $e = (1 - (b/a)^2)^{1/2}$, This solution is similarly valid for viscoelastic materials while the contact area is non-decreasing [85].

Compliance by Tapping: It has been observed that humans can quite effectively discriminate between differently compliant materials by tapping it with a stylus. Sound is evidentially an important cue and besides that experiments also indicate that the initial rise time of the loading transmitted to the fingerpad is the most important tactile feature used [41].

---

[2]This solution becomes invalid if $\dot{a}(t)$ at any time becomes negative and then the solution becomes significantly more complicated, which form depends on the loading history [82, 8].

Table 5.7: Lists Exploratory procedures, sensor channels and sensor codes used for normal compliance identification.

Exploratory Procedure	Sensor Channel	Sensor Code
Indenting	SA1, SA2 Strain gauge array Force sensors	Intensive Spatial Spatio-temporal

These results can be explained theoretically by calculating the time to peak force, t_*, for a stylus that impacts a linearly elastic half-space [49, 36]. The time depends on the shape of the end of the stylus but for spherical and flat ends t^* can be calculated to be

$$t^*_{\text{Spherical}} = \left[\frac{1-\nu^2}{E}\right]^{2/5} \qquad t^*_{\text{Flat}} = \left[\frac{1-\nu^2}{E}\right]^{1/2}. \tag{5.10}$$

Figure 5-5 further shows the response force trajectory for three different materials, from which we conclude that this relation between the time to peak force and compliance sufficiently explains experimental results.

Table 5.8: Lists Exploratory procedures, sensor channels and sensor codes used for normal compliance identification using tapping.

Exploratory Procedure	Sensor Channel	Sensor Code
Tapping	RA1, PC Force sensors Accelerometers	Temporal

Tangential Compliance: The lateral behavior is slightly different because there the effects of friction must be included. When simultaneous normal and tangential loads are applied then there is a central region, homothetic with the contact area, where no slip occurs, and a surrounding region with microslip [36, 14] (see also section 4, chapter 3). When the contact region is circular, with radius a, the relation between the tangential displacement, δ_x, and the tangential load, F_x is

$$\delta_x = \frac{1}{E_l^*} \frac{3F_z}{4a} \left[1 - \left(1 - \frac{F_x}{\mu_f F_z}\right)^{2/3}\right]. \tag{5.11}$$

Where $1/E_l^*$ is the combined lateral compliance, given by

$$\frac{1}{E_l^*} = \frac{(2-\nu_f)(1+\nu_f)}{2E_f} + \frac{(2-\nu_o)(1+\nu_o)}{2E_o} \tag{5.12}$$

where the subscript, f refers to the material properties of the finger, but o to that of the object. We note that if $E_f = E_o$ and $\nu_f = \nu_o$, then the ratio of normal compliance to lateral compliance is $2(1 - \nu)/(2 - \nu)$ which goes from 1 to 1.5 as ν goes from 0 to 0.5, i.e. lateral and normal compliances are comparable in this case.

For non-axisymmetric objects, i.e. when the contact area is an ellipse, similar relations have been derived and similarly there is a correction factor a function of the eccentricity, e, but the relations are not as simple as above and we confer the reader to [14] for details.

Table 5.9: Lists Exploratory procedures, sensor channels and sensor codes used for lateral compliance identification.

Exploratory Procedure	Sensor Channel	Sensor Code
Stretch Static touch	SA1, SA2 Strain gauge array Force sensors	Intensive Spatial Spatio-temporal

Layered Compliance: A variant of compliance identification is the case when we have an object that is composed of different layers that can slide relative to each other, e.g. skin over a bone or a muscle. The task is then to detect the shape and/or compliance of the deeper layer, e.g. finding lumps in tissue which is an important application of tactile sensing in medical practice [48]. One way of achieving that is to modify the transfer functions used in the decoding algorithms (see chapters 3 and 4) by increasing the parameter for sensor depth so that the signals estimates, the output, are the estimated displacements and loading distributions at the depth of the second layer. Its shape can then be identified and its compliance can also be estimated using the same relations as above.

Table 5.10: Lists Exploratory procedures, sensor channels and sensor codes used for layered compliance identification.

Exploratory Procedure	Sensor Channel	Sensor Code
Stretch Stroking	SA1, SA2 Strain gauge array Force sensors	Intensive Spatial Spatio-temporal

2.2 Identification of the State of Contact

Definition 5 *State-of-Contact Identification: the identification of the nature or mode of the interaction between the object and the fingerpad from sensor signals and estimation of the related parameters.*

As stated in the definition, then the concept state-of-contact refers to which mode the interaction between the object and the fingerpad is at the contact area. Is there adhesion, sliding with friction or something in-between? State of contact differs from the object properties delineated above, in that it is not strictly a property of the object only, but is rather an interface property. For example friction, which is very important in tactile sensing depends in reality on the load, sliding velocity, temperature, and surface texture in addition to individual and combined material properties [56, 4]. Identifying friction parameters, e.g. the friction coefficient μ_f, therefore has little meaning except as an interface property at that location and instant only.

Adhesion: Adhesion is mainly important for very soft and smooth objects[3] such as gels or gel-like materials. A clear cue for adhesion is obviously negative pressure in the contact area. It is however unknown if adhesion plays a role in human haptics as fingerpad irregularities, such as fingerprints prevent in most cases adhesion. Instead the finger ridges give better hold in wet and lubricated contact conditions, the same principle as is behind tiretracks.

Microslip: In section 4. chapter 3 we discussed in detail what happens when tangential loading is added to an object that is already under normal loading, assuming that Coulomb's law and axisymmetric Hertzian conditions are valid. For sake of completeness we will review those results here but refer the reader to chapter 3 or [36] for further details.

As one increases the tangential load, F_t from zero it turns out that slip does not occur instantaneously when the friction limit, $F_t = \mu_f F_z$ is reached. The object sticks to the fingerpad in a circular central region with radius, c, but microslip occurs in the surrounding region starting from the edge of the contact. In the microslip region the tangential loading is related to the normal loading through Coulomb's law but in the sticking region it follows load distribution giving uniform displacement. Figure 5-6 illustrates this phenomena, showing the loading situation in Fig. 5-6a, the stick and microslip areas superimposed on a grid showing the resulting tangential displacement in Fig. 5-6c. Profiles of the tangential and normal load distributions

---

[3]We exclude sticky films, glues etc. from our discussion here.

are shown in Fig. 5-6c and finally Fig. 5-6d shows the relation between the applied tangential load and the stick radius, which turns out to be given by

$$\frac{F_t}{\mu_f F_z} = 1 - (c/a)^3.$$

(5.13)

Since the tangential loading distribution has a sharp edge at the outer limits of the stick region ($r = c$) its extents can be inferred from the tangential load distribution and along with the contact radius used to calculate the friction coefficient from Eq. (5.13) without any global slip of the contact. This is a very valuable information that can be used to predict the onset of slip before it happens. More complicated but qualitatively similar behavior can be expected for more generally shaped object but will not be discussed further here, (cf. [67]).

Sliding: If the object is smooth so that Coulomb's law and Hertzian conditions are valid then during sliding the tangential and normal load distribution will be proportional to each other. In the absence of other spatial information, such as texture, the sliding velocity cannot be inferred from the sensors as μtexture will be based on a temporal code which cannot uniquely decide the sliding velocity. Hence, either kinesthetic information, texture, or shape variations that have smaller spatial wavelength than the fingerpad are needed to infer the sliding velocity.

3. Finger Control

In this section we will discuss what happens inside the *Finger Control* block in Fig. 5-1 and in Fig. 5-7 we have expanded that very block and shown its inside structure. In Fig. 5-7 we have divided the controller into two main paths, tangential controller and normal controller. We will first discuss the tangential controller as it is more involved and mainly consider stroking. Other exploratory procedures are, from the viewpoint of control, much simpler and can as such be considered special cases of stroking.

3.1 Tangential Control

During stroking the tangential controller must ensure that the fingerpad maintains contact and follows the shape of the object, while maintaining the contact area within the extents of the fingerpad. As discussed in section 1. we assume here that the desired direction of stroking, i.e.

the tangential velocity vector, is provided by an outside source (supervisor). However, in order to keep the contact region within the fingerpad area during stroking, the fingerpad will need to rotate as it moves over the surface. How this simultaneous rolling and sliding is combined is decided by the contact or stroking kinematics.

Stroking Kinematics

Equations describing the kinematics of an object and a finger in contact, subjected to simultaneous relative rolling and sliding have been available in the literature for some time [53]. They have recently been extended to include multiple fingers and contact dynamics [57, 55]. Here we will focus on the special and relatively simple case of stroking, i.e. when the center of contact does not move relative to the fingerpad. Figure 5-8 shows a fingerpad stroking an object and defines a coordinate system fixed in the fingerpad.

Contact kinematics then demand that the translation velocities v_x, v_y) and the rotational velocities, $(\dot{\theta}_x, \dot{\theta}_y)$ of the fingerpad be related through the curvature K_{obj} of the object at the contact location as follows

$$
\begin{bmatrix} \dot{\theta}_y \\ \\ \dot{\theta}_x \end{bmatrix} = K_{obj} \begin{bmatrix} v_x \\ \\ -v_y \end{bmatrix}
\tag{5.14}
$$

When the fingerpad is flat[4] K_{obj} is a 2×2 matrix of second spatial derivatives of the objects shape taken with respect to the coordinated system defined in Fig. 5-8. The relation in Eq. (5.14) is obtained under the assumption that the object's shape, as well as its first and second spatial derivatives vary smoothly in the contact area. Even if that is true, measurements of derivatives are always tricky, especially in the presence of imperfect measurements. Additionally, for our purpose, i.e. stroking, we are only interested in the average or overall curvature of the contact area.

Overall Curvature Estimation

The problem of finding the overall curvature of the contact area can equivalently be stated as fitting a constant curvature displacement distribution to the estimated surface displacements. The curvature should only be estimated within the contact area, defined here as being where

---

[4]Similar relations hold when the fingerpad is also curved, cf. [53] for details.

the normal load is positive (i.e. indicating pressure) and therefore we also need the estimated normal load distribution. An estimated distribution can be fitted to a constant curvature distribution using standard fitting techniques. Fitting in the least square sense can for example be obtained by matching the moments of the distributions and use those relations to solve for the parameters of the constant curvature distribution. A constant curvature displacement distribution can generally be described using six parameters

$$u_{z_0} = \delta - \left(\frac{A}{2}x^2 + \frac{B}{2}Y^2 + Cxy + Dx + Ey \right) \qquad (5.15)$$

We observe that the zeroth, first and second moments will give all six parameters, but the moments are defined as:

$$I_0 = \int_C u_{z_0} dx dy$$

$$I_x = \int_C x u_{z_0} dx dy \qquad I_y = \int_C y u_{z_0} dx dy \qquad (5.16)$$

$$I_{xx} = \int_C x^2 u_{z_0} dx dy \qquad I_{xy} = \int_C xy u_{z_0} dx dy \qquad I_{yy} = \int_C y^2 u_{z_0} dx dy$$

All the integrals are taken over the contact area C which is known from the surface load distribution as discussed above.

The entries in K_{obj} are then finally obtained by calculating each of the moments for both the constant curvature distribution in Eq. (5.15) and the estimated displacement distribution $\hat{u}_z$ and then solving for for the A, B and C values which are the values needed, since

$$K_{obj} = \begin{bmatrix} A & C \\ C & B \end{bmatrix}.$$

When viscous effects are negligible and quasi-static contact conditions are valid, we know that a Hertzian (i.e. ellipsoidal) load distribution will give a constant curvature displacement distribution. We can therefore work directly with the load distribution, i.e fit the estimated normal load distribution to a Hertzian distribution, and hence avoid the problem of explicitly estimating the area of contact. Hertzian load distribution can generally also be described using six parameters, e.g.

$$f_{z_0} = \phi_z \sqrt{1 - (A_f x^2 + B_f y^2 + C_f xy + D_f x + E_f y)} \qquad (5.17)$$

Similarly as above, the parameters of this relation can be estimated, in the least square sense. by matching the zeroth, first and second moments of the estimated and Hertzian distributions.

114

The entries for K_{obj} can then be obtained from known Hertzian load-displacement relations, cf. [36].

Example:

As an example we now show how the method delineated above can be used to estimate the overall curvature of a textured surface. Figure 5-9a shows the surface from a perspective view but Fig. 5-9c from above as a height-density plot. Figure 5-9b shows that part of the surface that contacts the fingerpad at this particular instant and similarly does Fig. 5-9d show the same from above as height-density plot. We note that the contact area is not a simply connected region and that one cannot reliably estimate the curvature from single location within that area.

As discussed above we use the six moments defined in Eq. (5.16) to obtain six equations that we use to solve for the parameters of interest in the constant curvature defined in Eq. (5.15). We combine this relations in a matrix equation

$$
\begin{bmatrix}
I_{0\delta} & I_{0A} & I_{0B} & I_{0C} & I_{0D} & I_{0E} \\
I_{x\delta} & I_{xA} & I_{xB} & I_{xC} & I_{xD} & I_{xE} \\
I_{y\delta} & I_{yA} & I_{yB} & I_{yC} & I_{yD} & I_{yE} \\
I_{xx\delta} & I_{xxA} & I_{xxB} & I_{xxC} & I_{xxD} & I_{xxE} \\
I_{yy\delta} & I_{yyA} & I_{yyB} & I_{yyC} & I_{yyD} & I_{yyE} \\
I_{xy\delta} & I_{xyA} & I_{xyB} & I_{xyC} & I_{xyD} & I_{xyE}
\end{bmatrix}
\begin{bmatrix}
\delta \\
A \\
B \\
C \\
D \\
E
\end{bmatrix}
=
\begin{bmatrix}
\hat{I}_0 \\
\hat{I}_x \\
\hat{I}_y \\
\hat{I}_{xx} \\
\hat{I}_{yy} \\
\hat{I}_{xy}
\end{bmatrix}
\tag{5.18}
$$

where, for example,

$$
I_{0A} = \int_C x^2 dxdy \qquad \text{and} I_{xxB} = \int_C y^2 x^2 dxdy
$$

and further

$$
\hat{I}_{xy} = \int_C \hat{u}_{z0} xy dxdy,
$$

where as before $\hat{u}_{z0}$ is the estimated surface displacement.

Figure 5-10 shows the results of the above applied to the surface show in Fig. 5-9. Figure 5-10a shows it as a surface plot with the fingerpad surface displacement superimposed onto the resulting constant curvature surface and Fig. 5-10b shows the same but from a profile view. We note that the constant curvature surfaces captures the overall curvature of the surface despite the widely varying curvature of the texture.

Fitting the estimated displacement distributions this way gives us an easily calculable and the estimate is robust since we avoid taking derivatives. However, care must be taken when the contact area becomes very small. The loads will the become concentrated and the effects of discrete sensors can then lead to inaccurate estimates of the overall curvature. It is however a different question how we should react to sharp points or corners and otherwise regulate the normal load so that the contact area is large enough but does not lead to overly high load concentrations that can damage the sensors.

3.2   Normal Control

The problem of maintaining a suitable normal force while moving along a surface has been under investigation in the field of robotics for some time [2] where the term *compliant motion control* has been used. Solution to this problem have been formulated in a number of ways using different control schemes. The most straightforward approach, in our case, is to directly control the total normal force, i.e. a force control scheme in the normal direction. A variant of this approach would be to control or regulate the maximum normal pressure or some other norm or measure of the normal load distribution. Other control schemes, such as impedance control can also be applied, but since we already have measurements of the contact force they may not be needed but one of its strengths is that force measurements are not needed [2, 26]. Impedance control might however prove useful during the phases when the hand is in free motion prior to or during contact [11].

4.   Conclusions

In this chapter we have discussed the computational aspects of exploration of objects and environments. We have analyzed exploration strategies in terms of the exploration procedures, sensor channels, codes and object properties that are available using tactile sensing. In addition to providing a general and common structure positioning exploration of objects relative to other aspects of tactile sensing, we have analyzed each of the above components in detail and explicitly stated related formulas where appropriate. We have finally discussed the implementation of proposed exploration strategies in terms of different control schemes.

A framework that organizes the different aspects that relate to computational theory of

haptics is a very important milestone – if it gains acceptance among researchers. We still must recognize, that we cannot claim that results presented here are based on the only viable or reasonable approach. For example, the intermediate step of *surface signal identification*, where we explicitly estimate both the surface load and surface displacement distributions, may not be necessary. Instead, the object properties could be identified directly from the sensor signals. We however believe that an explicit formulation like ours is needed first, and that our work has value in being a reasonable starting point and providing understanding useful for future work.
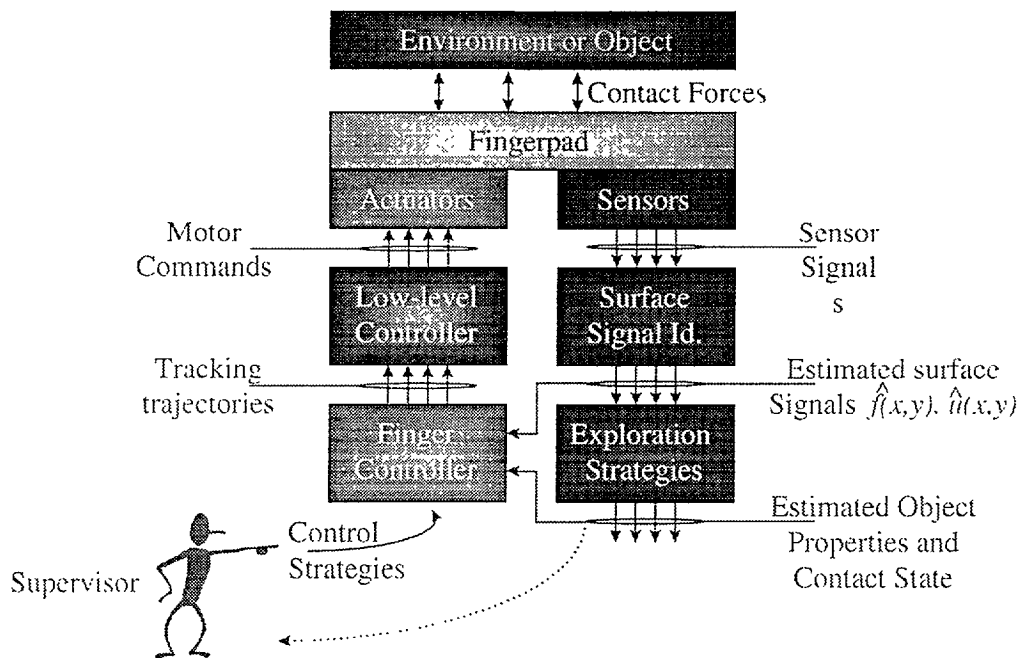
Figure 5-1: Shows a diagram that explains the structure and the relation between the various problems that constitute a computational theory of haptics. The *Surface Signal Identification* problem was treated in Chapters 3 and 4 but in this chapter we will discuss the *Exploration Strategy*, and *Finger Controller* blocks. The *Exploration Strategy* block refers to the problem of inferring object properties such as shape, texture and compliance or state of contact from the estimated surface signals. This involves determining, given a property that is to be explored, what kind of sensor information and what kind of action is needed for successful exploration. The *Supervisor* shown in the figure represents an external source that supplies additional information required to identify each object, e.g. the stroking direction for shape identification. The *Finger Controller* block represents the calculation of tracking trajectories for the fingerpad from a given desired action. local shape, and contact force distribution information.
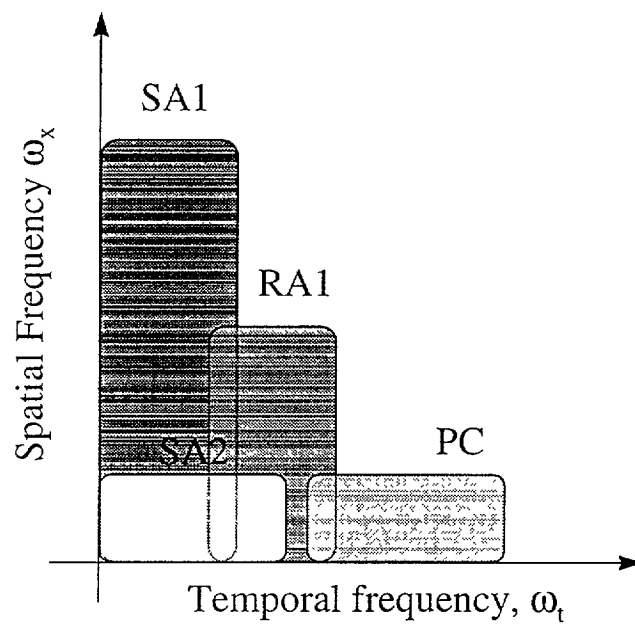
Figure 5-2: Schematically shows the temporal and spatial frequency characteristics of human receptors as ranges of sensitivity.

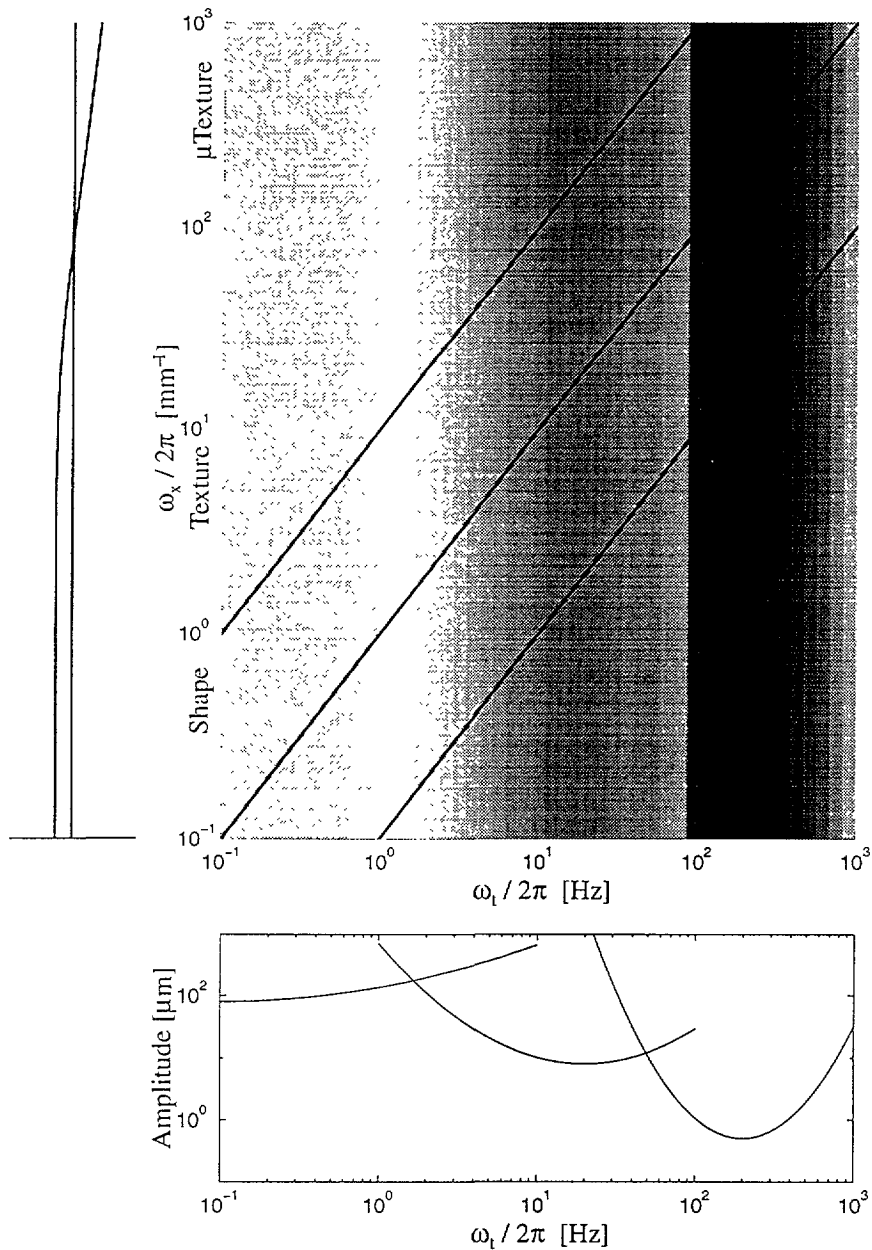Figure 5-3: Shows a typical spatial frequency distribution superimposed onto the temporal sensitivity properties of human receptors. The relation in Eq. (5.1) appears as a line on the loglog (ω_t, ω_x) plot (upper-right) and the line translates sideways by changing the stroking velocity v_t.
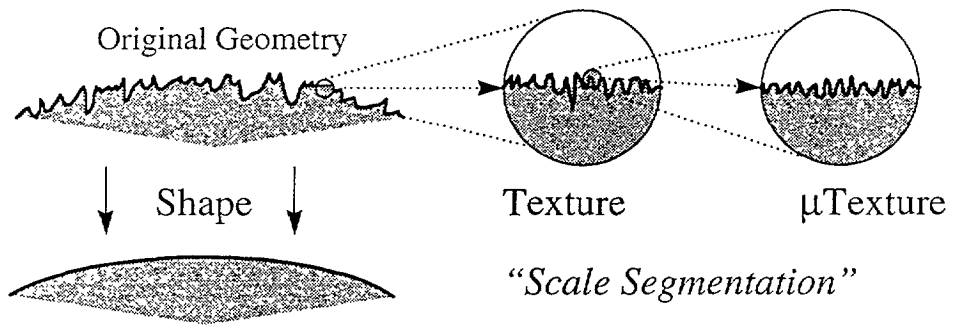
Figure 5-4: Shows scale segmentation schematically and how the original geometry is composed of Shape, Texture and μTexture.

Figure 5-5: Impact response trajectories for differently compliant materials. The trajectories are normalized with respect to that of the intermediate compliant material. We observe that there is a direct relation between the time to peak force and material compliance, as indicated in Eq. (5.10), and that it can be used for material discrimination.

(a) Configuration

(b) Tangential Displacement

(c) Load Distribution Profiles

(d) Load vs. Stick Area

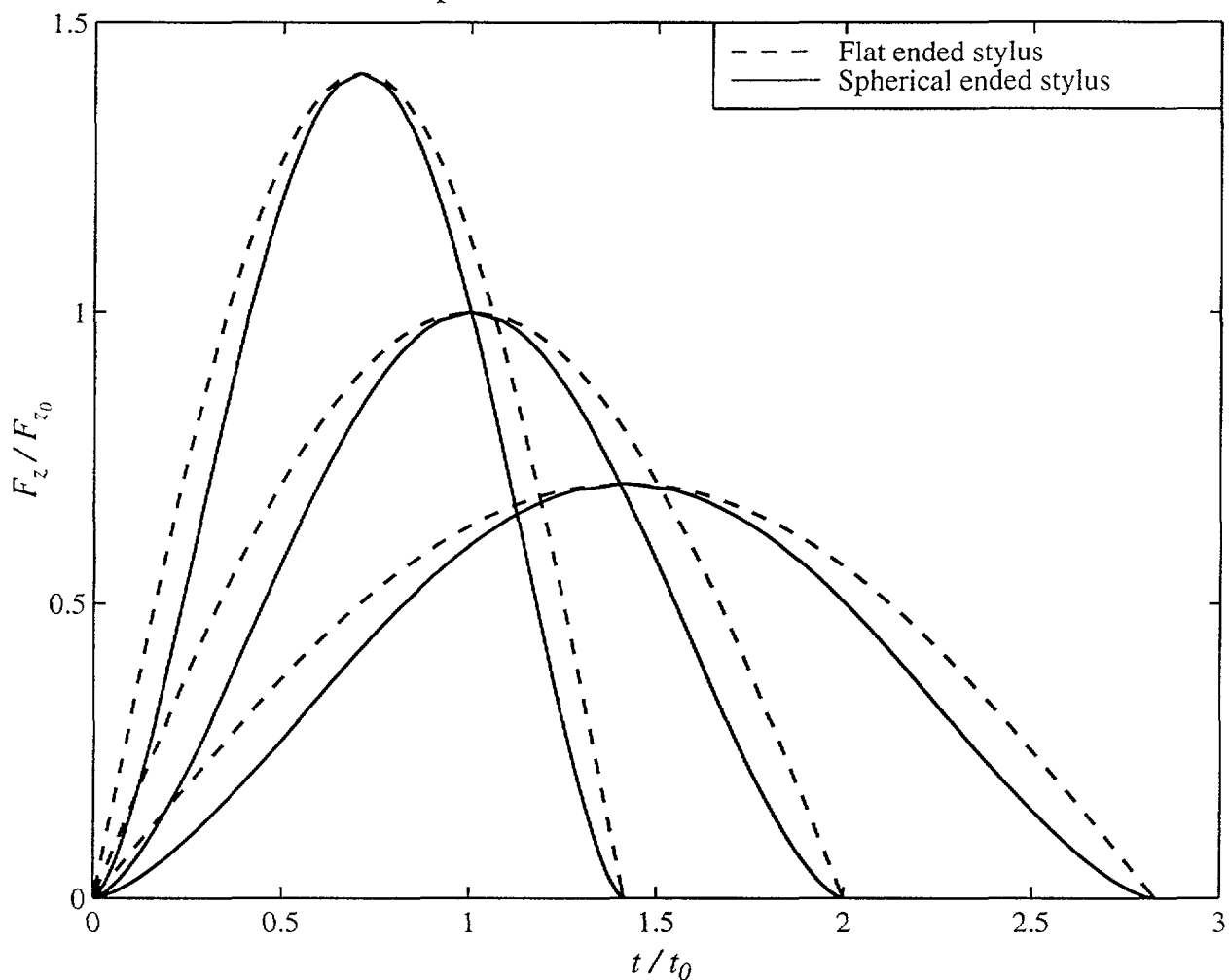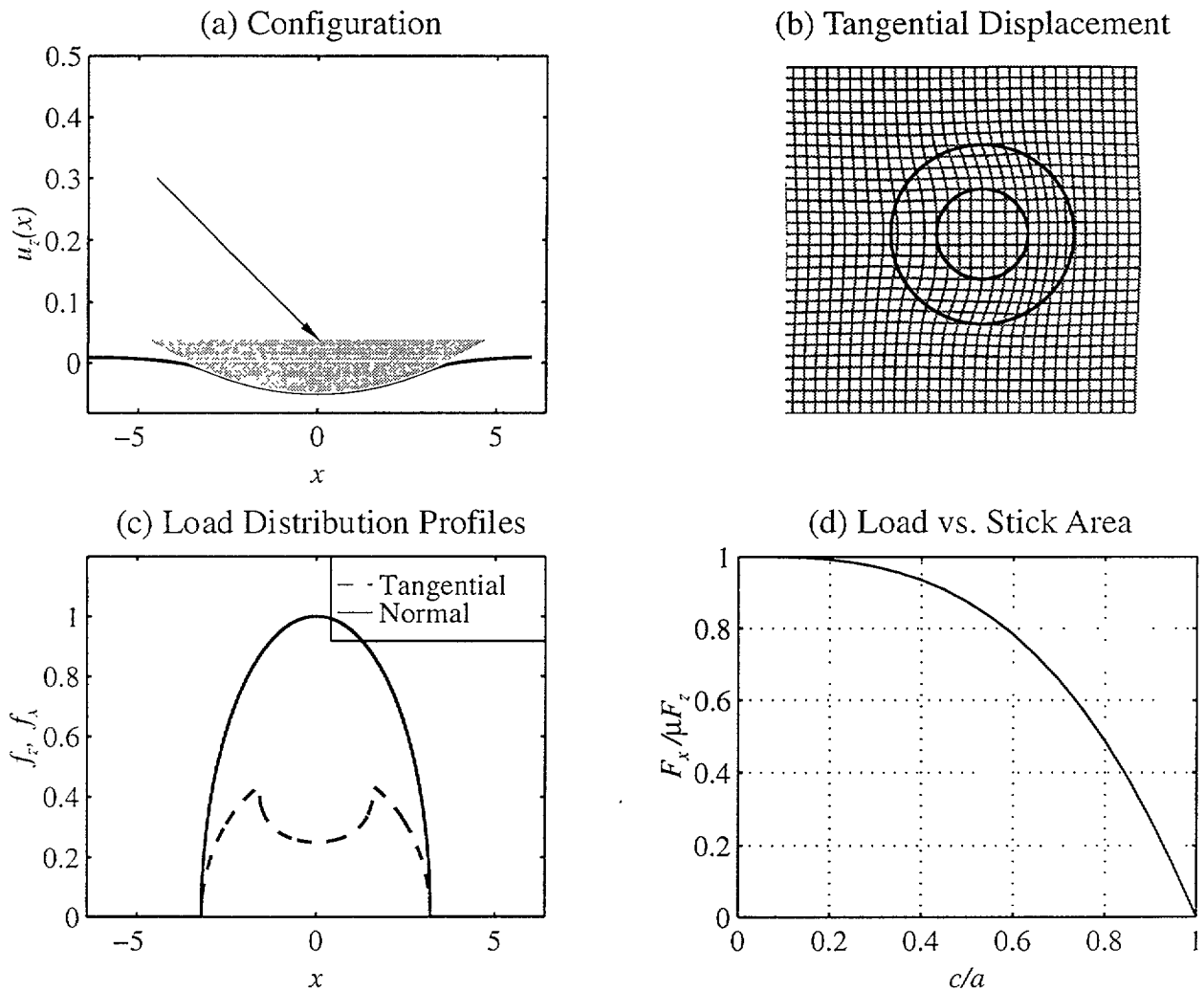Figure 5-6: Illustrates the behavior of axisymmetric Hertzian solid under simultaneous normal and tangential load. (a) shows the loading configuration, (b) shows the stick and microslip region superimposed onto a grid showing the resulting tangential displacement, (c) shows profiles of the tangential and normal load distributions and finally (d) shows the relation between normal load, tangential load, stick radius, contact radius and friction coefficient, i.e. Eq. (5.13).
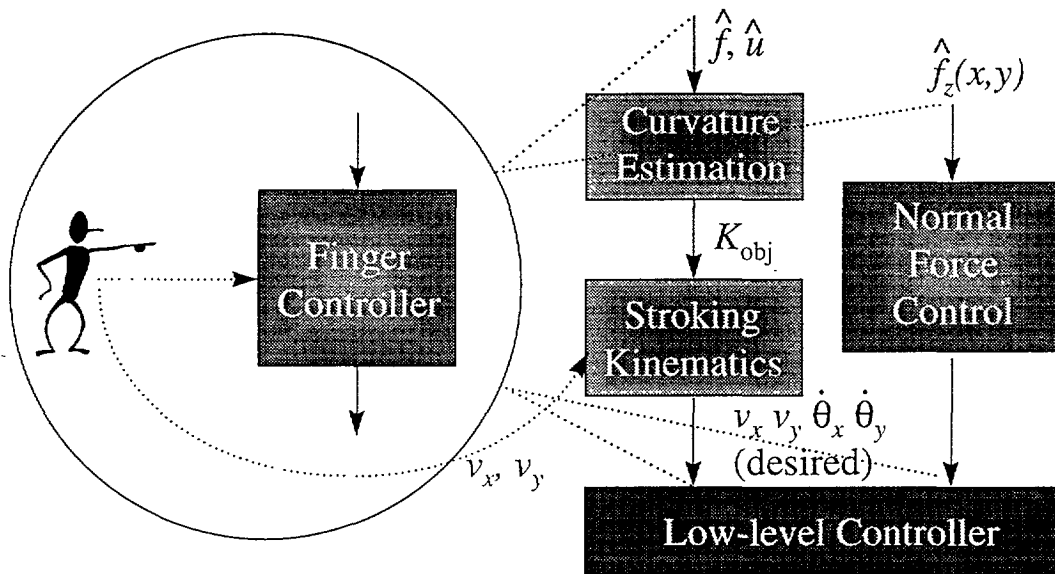
Figure 5-7: Shows a diagram that expands the Finger Controller-block in Fig. 5-1. There are two main paths: i) tangential control and ii) normal control. The tangential control takes as inputs estimated surface signals and stroking direction and velocity from a supervisor. It gives as output the desired tangential translation and rotation velocities $(v_x, v_y, \dot{\theta}_x, \dot{\theta}_y)$ after going through the steps of *Curvature Estimation* and *Stroking Kinematics*. The normal control path takes as input the estimated surface load distribution and gives as output desired total normal force. Both normal and tangential outputs are fed into a *Low-level Controller* which we assume is capable of tracking the desired signals with sufficient accuracy.
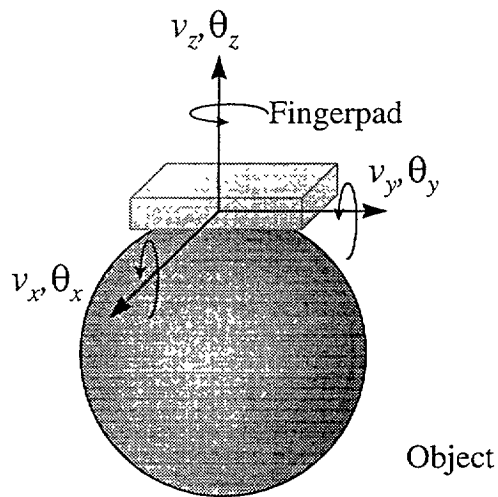
Figure 5-8: Shows a fingerpad stroking an object and defines a coordinate system fixed in the fingerpad. With the tangential velocities (v_x, v_y) and rotational velocities about the respective axes $(\dot{\theta}_x, \dot{\theta}_y)$.
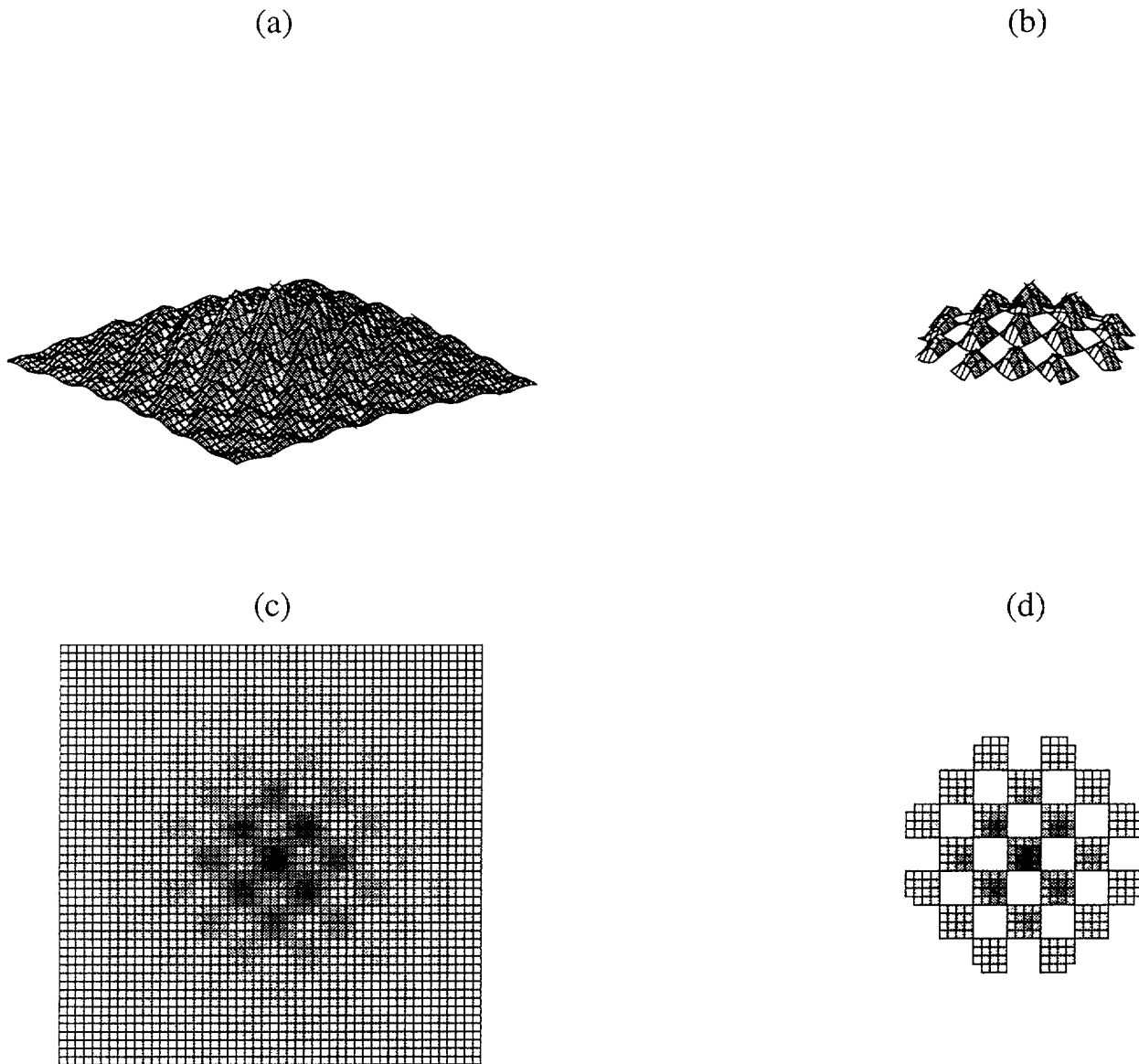
Figure 5-9: Shows a textured surface and the part of the surface that is in contact with the fingerpad. Figure (a) shows the actual surface from a perspective viewpoint, (c) from above as a height-density plot. Similarly, shows figure (b) the part in contact from a perspective but (d) from above. We note that the contact region is not a simply connected region, as there are areas where there is a gap between the object and the fingerpad.
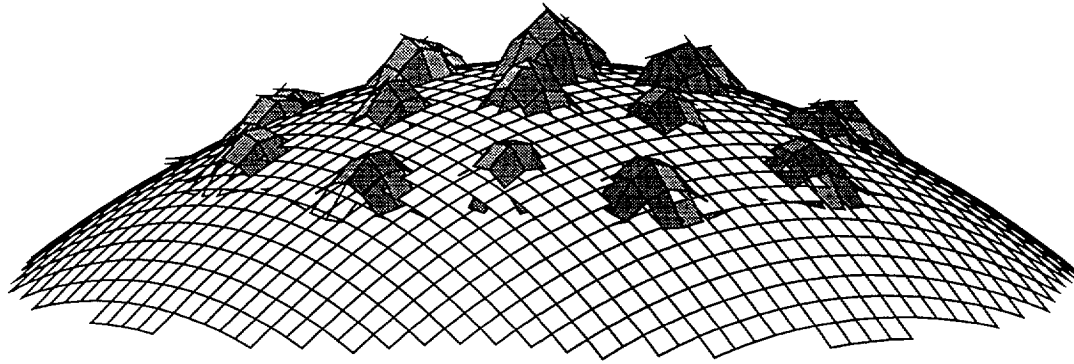
(a)
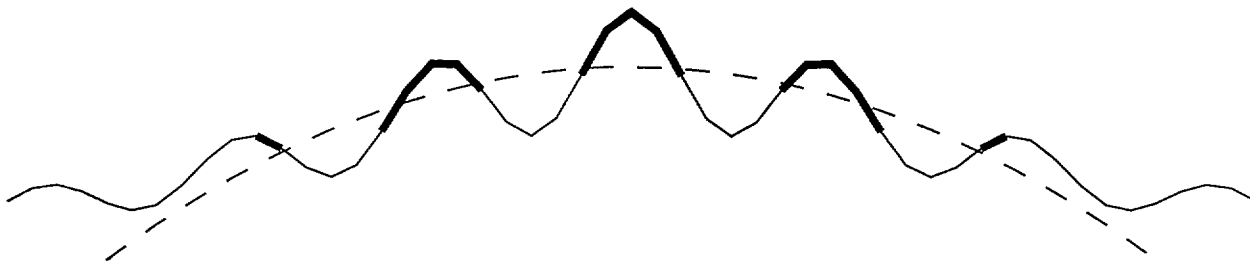
Figure 5-10: Shows a constant curvature surface superimposed on the texture surface in Fig. 5-9 obtained by matching the moments, defined in Eq. (5.16), of the constant curvature surface and the surface displacement within the contact area. Figure (a) shows it as a surface plot and (b) shows it from a profile view where the contact region is marked with thickened lines. We note that the constant curvature surface captures the overall curvature of the surface despite the widely varying curvature of the texture.

Chapter 6

Concluding Remarks and Suggestions for Future Work

1. Conclusions

In this thesis we have presented a basic computational theory of haptics. We divide the problem into *Identification* and *Control* problems. We further separate the identification problem into *Surface Signal Identification* and *Object Property Identification* problems as shown in Fig. 5-1. We have analyzed each of these problems and presented our results in four, by and large, independent chapters, each with their concluding remarks, but they can be summarized as follows:

1. In order to correctly decode a general 3D tactile signal from a sensor array, we need a minimum of three independent sensor signals, and we show that $(p_n, \varepsilon_{xz}, \varepsilon_{yz})$ is the only stress/strain signal combination without a directional bias.

2. We give solutions that are valid under static or quasi-static conditions as well as ones that include the effects of viscoelasticity and inertia and further give conditions under which the inertia can be ignored.

3. The transfer function approach developed in the thesis is shown to allow us to infer qualitative properties and behavior of the solution without specifying the inputs. The

transfer function approach further gives us access to powerful signal processing tools, such as the Wiener and Kalman filter which we evoke to solve the *decoding problem*. The decoding problem being the problem of reconstructing the surface signals from sensor signals, in a robust manner, in the presence of sensor noise.

4. We analyze exploration strategies in terms of exploration procedures, sensor channels, codes and the object properties that are available using tactile sensing and explicitly state related formulas where appropriate.

5. Finally, we discuss implementation issues in terms of different control schemes.

The above results are valid for homogeneous and linearly elastic materials and while infinitismal displacement assumptions hold. These are idealized conditions and it is therefore important to consider what happens when they are not completely satisfied. The tools and methods we apply have, however, been applied with good results to various problems where those assumptions may not always hold, most notably the methods developed around linear elasticity in mechanics and also the Kalman filter in navigation and control. We however cannot state unilaterally that the solutions given in this thesis will not fail under non-ideal conditions, but that can most likely only be assessed on case-by-case basis and then with the aid of experiments.

2. Suggestions for Future Work

The results presented here essentially provide a skeleton of a computational theory or an outline to which details need to be added. The encoding solutions are given for the infinite halfspace but solutions for other geometries, such as layered, finite thickness, finite size, cylindrical or spherical, might more accurately model real fingerpads and therefore prove more useful.

The decoding solution given here assumes that the sensor signal is linearly related to the components of the stress or strain tensor, but we might want to consider other nonlinear measures such as strain energy density or maximum compressive strain that experimental results indicate might constitute the relevant sensor stimulus in the human tactile system [13, 75]. In appendix F we state the decoding problem in general terms where we observe that the problem is then expressed in conditions regarding the integrability of the relevant PDEs. The integrability of general PDEs is an advanced mathematical problem beyond the scope of this thesis and we do not discuss that further here but refer the reader to [64].

130

The object identification problem has many possibilities for further work, such as experimental studies of human subject where the experimental paradigms and results are stated in terms of the concepts we have developed. As an example one could test the perception of texture in the terms of roughness measures or test the hypothesis that humans perceive texture and μtexture differently, the former being independent of stroking velocity.

Appendix A

Derivation of Static Transfer Function Matrices

We start with the differential equations of equilibrium[1]

$$\sigma_{ij,j} = 0 \quad i,j = x,y,z \tag{A.1}$$

and the linear stress strain relations according to Hooke's law

$$\sigma_{ij} = \lambda \varepsilon_{ij} \delta_{ij} + 2\mu \varepsilon_{ij} \quad i,j = x,y,z \tag{A.2}$$

where

$$\varepsilon_{ij} = \frac{1}{2} \left(u_{i,j} + u_{j,i} \right) \quad i,j = x,y,z$$

and $\delta_{ij} = 1$ if and only if $i = j$, and is zero otherwise. Further, the Lamè constants λ and μ (shear modulus) are in terms of Young's modulus and Poisson ratio:

$$\lambda = \frac{\nu E}{(1+\nu)(1-2\nu)}, \quad \mu = \frac{E}{2(1+\nu)}.$$

---

[1]Here we use tensor notation for compactness, where a ",j" in subscript means a partial derivative with respect to the independent variable represented by j and repeated symbols in subscript stand for summation over all indices.

In order to solve these nine partial differential equations we make use of the two dimensional Fourier transform defined by [5]

$$\bar{f}(\omega_x, \omega_y) = \iint_{-\infty}^{+\infty} f(x, y)e^{-j(\omega_x x + \omega_y y)} dx dy$$

$$f(x, y) = \frac{1}{4\pi^2} \iint_{-\infty}^{+\infty} \bar{f}(\omega_x, \omega_y)e^{j(\omega_x x + \omega_y y)} d\omega_x d\omega_y.$$

Assuming that all integrals are well behaved as $|x, y| \to \infty$, we apply this transform to each term in the equations in (A.1) and (A.2). Then the operator $\frac{\partial}{\partial x}$ is replaced by multiplication by $j\omega_x$, and $\frac{\partial}{\partial y}$ by $j\omega_x$. We further use D to notate $\frac{\partial}{\partial z}$. The 9 partial differential equations have now been transformed into ordinary differential equations in D ($\frac{\partial}{\partial z}$ becomes $\frac{d}{dz}$). We write (A.1) and (A.2) using matrix-vector notation as

$$K^T \bar{\sigma} = 0, \quad \gamma = Ku,$$

and

$$\bar{\sigma} = C\bar{\gamma}$$

where

$$K^T = \begin{bmatrix} j\omega_x & 0 & 0 & j\omega_y & D & 0 \\ 0 & j\omega_y & 0 & j\omega_x & 0 & D \\ 0 & 0 & D & 0 & j\omega_x & j\omega_y \end{bmatrix},$$

$$C = \begin{bmatrix} \lambda + 2\mu & \lambda & \lambda & 0 & 0 & 0 \\ \lambda & \lambda + 2\mu & \lambda & 0 & 0 & 0 \\ \lambda & \lambda & \lambda + 2\mu & 0 & 0 & 0 \\ 0 & 0 & 0 & \mu & 0 & 0 \\ 0 & 0 & 0 & 0 & \mu & 0 \\ 0 & 0 & 0 & 0 & 0 & \mu \end{bmatrix},$$

$\bar{\sigma} = [\bar{\sigma}_{xx}, \bar{\sigma}_{yy}, \bar{\sigma}_{zz}, \bar{\sigma}_{xy}, \bar{\sigma}_{xz}, \bar{\sigma}_{yz}]^T$, and $\bar{\gamma} = [\bar{\varepsilon}_{xx}, \bar{\varepsilon}_{yy}, \bar{\varepsilon}_{zz}, \bar{\gamma}_{xy}, \bar{\gamma}_{xz}, \bar{\gamma}_{yz}]^T$[2]. Eliminating $\bar{\sigma}$ and $\bar{\varepsilon}$ we get

$$K^T C K \bar{u} = 0 \tag{A.3}$$

where $\bar{u} = [\bar{u}_x, \bar{u}_y, \bar{u}_z]^T$ and

$$K^T C K = \begin{bmatrix} D^2 - \Omega^2 - \omega_x^2(\beta^2 - 1) & -\omega_x\omega_y(\beta^2 - 1) & j\omega_x(\beta^2 - 1)D \\ -\omega_x\omega_y(\beta^2 - 1) & D^2 - \Omega^2 - \omega_y^2(\beta^2 - 1) & j\omega_y(\beta^2 - 1)D \\ j\omega_x(\beta^2 - 1)D & j\omega_y(\beta^2 - 1)D & \beta^2(D^2 - \Omega^2) + \Omega^2\beta^2 \end{bmatrix}$$

---

[2]For the sake of simplicity in the definitition of K we use an alternative notation for strain: $\gamma_{ij} = 2\varepsilon_{ij}$ for $i \neq j$.

134

with $\Omega^2 = \omega_x^2 + \omega_y^2$ and $\beta^2 = (\lambda + 2\mu)/\mu$. The determinant of this matrix is

$$\det(K^T C K) = \beta^2 \mu^3 \left[D^2 - \Omega^2 \right]^3$$

and this system therefore has non-trivial solutions of the form

$$\bar{u}_i = (A_i + B_i z + C_i z^2) e^{-\Omega z} \quad i = x, y, z$$

where A_i, B_i, C_i are independent of z, and we have also used the condition that displacements stay finite as $z \to \infty$ to include only terms with negative exponents. Substituting this back into (A.3) we obtain

$$A_z = \frac{1}{\Omega} \left(j\omega_x A_x + j\omega_y A_y + B_z \frac{\beta^2 + 1}{\beta^2 - 1} \right)$$

$$B_x = -\frac{j\omega_x}{\Omega} B_z$$

$$B_y = -\frac{j\omega_y}{\Omega} B_z$$

$$C_x = C_y = C_z = 0$$

which gives

$$
\begin{bmatrix} \bar{u}_x \\ \bar{u}_y \\ \bar{u}_z \end{bmatrix} = e^{-\Omega z}
\begin{bmatrix}
1 & 0 & -\dfrac{j\omega_x z}{\Omega} \\
0 & 1 & -\dfrac{j\omega_y z}{\Omega} \\
\dfrac{j\omega_x}{\Omega} & \dfrac{j\omega_y}{\Omega} & \dfrac{1}{\Omega}\dfrac{\beta^2+1}{\beta^2-1} + z
\end{bmatrix}
\begin{bmatrix} \bar{A}_x \\ \bar{A}_y \\ \bar{B}_z \end{bmatrix} \tag{A.4}
$$

The three still unknown terms, A_x, A_y, B_z will be determined by boundary conditions at $z = 0$. Here, we will first pose the boundary conditions in terms of the load distributions on the surface of the infinite halfspace, defined by $z \geq 0$. The z-normal stress σ_{zz} at the surface $z = 0$ equals normal load on the surface, f_z. Similarly the shear stresses σ_{xz} and σ_{yz} at $z = 0$ equal the shear loads on the same surface, f_x and f_y respectively. The relevant stresses can be derived by substituting (A.4) into (A.2) which become

$$
\begin{bmatrix} \bar{\sigma}_{xz} \\ \bar{\sigma}_{yz} \\ \bar{\sigma}_{zz} \end{bmatrix} = \frac{\mu e^{-\Omega z}}{\Omega}
\begin{bmatrix}
-(2\omega_x^2 + \omega_y^2) & -\omega_x\omega_y & 2j\omega_x\left(\dfrac{1}{\beta^2-1} + \Omega z\right) \\
-\omega_x\omega_y & -(\omega_x^2 + 2\omega_y^2) & 2j\omega_y\left(\dfrac{1}{\beta^2-1} + \Omega z\right) \\
j\omega_x\Omega & j\omega_y\Omega & \Omega\left(\dfrac{\beta^2}{\beta^2-1} + \Omega z\right)
\end{bmatrix}
\begin{bmatrix} \bar{A}_x \\ \bar{A}_y \\ \bar{B}_z \end{bmatrix} . \tag{A.5}
$$

The unknown terms A_x, A_y, B_z can then be found by letting $z = 0$ and either invert Eq. (A.4) with $[\bar{u}_x, \bar{u}_y, \bar{u}_z] = [\bar{u}_{x0}, \bar{u}_{y0}, \bar{u}_{z0}]$ or Eq. (A.5) with $[\bar{\sigma}_{xz}, \bar{\sigma}_{yz}, \bar{\sigma}_{zz}] = \left[\bar{f}_x, \bar{f}_y, \bar{f}_z\right]$.

TFMs for Tractions as Inputs

It is convenient to solve for each load case separately and state the solution in terms of a Transfer Function Matrix (TFM) which after we have substituted for β and μ, finally becomes

$$\bar{u} = T_{uf} f,$$

with

$$T_{uf} = \frac{e^{-z\Omega}}{2\mu\Omega^3}
\begin{bmatrix}
2\Omega^2 - \omega_x^2(2\nu + \Omega z) & -\omega_x\omega_y(2\nu + \Omega z) & j\omega_x\Omega(1 - 2\nu - \Omega z) \\
-\omega_x\omega_y(2\nu + \Omega z) & 2\Omega^2 - \omega_y^2(2\nu + \Omega z) & j\omega_y\Omega(1 - 2\nu - \Omega z) \\
-j\omega_x\Omega(1 - 2\nu + \Omega z) & -j\omega_y\Omega(1 - 2\nu + \Omega z) & (2(1 - \nu) + \Omega z)\Omega^2
\end{bmatrix} \tag{A.6}$$

The strain and the stress field TFM's are obtained using the relations in (A.2) and results in

$$\bar{\varepsilon} = T_{\varepsilon f} f, \quad \text{where,} \quad \bar{\varepsilon} = [\varepsilon_{xx}, \varepsilon_{yy}, \varepsilon_{zz}, \varepsilon_{xy}, \varepsilon_{xz}, \varepsilon_{yz}]^T$$

with

$$T_{\varepsilon f} = \frac{e^{-z\Omega}}{2\mu\Omega^3}
\begin{bmatrix}
j\omega_x\left(2\Omega^2 - \omega_x^2(2\nu + \Omega z)\right) & -j\omega_x^2\omega_y(2\nu + \Omega z) & -\Omega\omega_x^2(1 - 2\nu - \Omega z) \\
-j\omega_x\omega_y^2(2\nu + \Omega z) & j\omega_y\left(2\Omega^2 - \omega_y^2(2\nu + \Omega z)\right) & -\Omega\omega_y^2(1 - 2\nu - \Omega z) \\
-j\Omega^2\omega_x(2\nu - \Omega z) & -j\Omega^2\omega_y(2\nu - \Omega z) & -\Omega^3(1 - 2\nu + \Omega z) \\
j\omega_y\left(\Omega^2 - \omega_x^2(2\nu + \Omega z)\right) & j\omega_x\left(\Omega^2 - \omega_y^2(2\nu + \Omega z)\right) & -\Omega\omega_x\omega_y(1 - 2\nu - \Omega z) \\
-\Omega^2\left(\Omega - \omega_x^2 z\right) & \Omega^2\omega_x\omega_y z & j\Omega^3\omega_x z \\
\Omega^2\omega_x\omega_y z & -\Omega^2\left(\Omega - \omega_y^2 z\right) & j\Omega^3\omega_y z
\end{bmatrix} \tag{A.7}$$

and $\bar{\sigma} = T_{\sigma f} f$, where, $\bar{\sigma} = [\sigma_{xx}, \sigma_{yy}, \sigma_{zz}, \sigma_{xy}, \sigma_{xz}, \sigma_{yz}]^T$

with

$$T_{\sigma f} = \frac{e^{-z\Omega}}{\Omega^3}
\begin{bmatrix}
j\omega_x\left(2\Omega^2 + 2\nu\omega_y^2 - \omega_x^2 z\Omega\right) & j\omega_y\left(2\nu\omega_y^2 - \omega_x^2 z\Omega\right) & -\Omega\left(2\nu\omega_y^2 + \omega_x^2(1 - \Omega z)\right) \\
j\omega_x\left(2\nu\omega_x^2 - \Omega\omega_y^2 z\right) & j\omega_y\left(2\Omega^2 + 2\nu\omega_x^2 - \omega_y^2 z\Omega\right) & -\Omega\left(2\nu\omega_x^2 + \omega_y^2(1 - \Omega z)\right) \\
j\Omega^3\omega_x z & j\Omega^3\omega_y z & -\Omega^3(1 + z\Omega) \\
j\omega_y\left(\Omega^2 - \omega_x^2(2\nu + z\Omega)\right) & j\omega_x\left(\Omega^2 - \omega_y^2(2\nu + z\Omega)\right) & -\Omega\omega_x\omega_y(1 - 2\nu - z\Omega) \\
-\Omega^2\left(\Omega - \omega_x^2 z\right) & \Omega^2\omega_x\omega_y z & j\Omega^3\omega_x z \\
\Omega^2\omega_x\omega_y z & -\Omega^2\left(\Omega - \omega_y^2 z\right) & j\Omega^3\omega_y z
\end{bmatrix} \tag{A.8}$$

We also calculate the TFM for the mean normal **stress** defined as

$$p_n = \frac{1}{3}\left(\sigma_x + \sigma_y + \sigma_z\right)$$

which gives

$$\bar{p}_n = T_{p_n f} f,$$

with

$$T_{p_n f} = \frac{2E}{3} \frac{e^{-z\Omega}}{2\mu\Omega} \begin{bmatrix} j\omega_x & j\omega_y & -\Omega \end{bmatrix}. \tag{A.9}$$

The relationship between $\bar{u}_0$ and $\bar{f}$ can be found by letting $z = 0$ in Eq. (A.6) obtaining

$$\bar{u}_0 = T_{u_0 f} f,$$

with

$$T_{u_0 f} = \frac{1}{2\mu\Omega^3} \begin{bmatrix} 2(\Omega^2 - \nu\omega_x^2) & -2\nu\omega_x\omega_y & j(1-2\nu)\omega_x\Omega \\ -2\nu\omega_x\omega_y & 2(\Omega^2 - \nu\omega_y^2) & j(1-2\nu)\omega_y\Omega \\ -j(1-2\nu)\omega_x\Omega & -j(1-2\nu)\omega_y\Omega & 2(1-\nu)\Omega^2 \end{bmatrix}. \tag{A.10}$$

We note that the z component decouples from the x and y components when the material is incompressible $\nu = 0.5$.

TFMs for Displacements as Inputs

The TFMs when the surface displacements are considered the inputs are found similarily as the ones in previous section:

$$\bar{f} = T_{fu_0}\bar{u}_0,$$

with

$$T_{fu_0} = \frac{\mu}{(3-4\nu)\Omega} \begin{bmatrix} \Omega^2(3-4\nu) + \omega_x^2 & \omega_x\omega_y & 2j(1-2\nu)\omega_x\Omega \\ \omega_x\omega_y & \Omega^2(3-4\nu) + \omega_y^2 & 2j(1-2\nu)\omega_y\Omega \\ 2j(1-2\nu)\omega_x\Omega & 2j(1-2\nu)\omega_y\Omega & 4(1-\nu)\Omega^2 \end{bmatrix}, \tag{A.11}$$

$$\bar{u} = T_{uu_0}\bar{u}_0,$$

with

$$T_{uu_0} = \frac{e^{-z\Omega}}{(3-4\nu)\Omega} \begin{bmatrix} (3-4\nu)\Omega - \omega_x^2 z & -\omega_x\omega_y z & -j\omega_x\Omega z \\ -\omega_x\omega_y z & (3-4\nu)\Omega - \omega_y^2 z & -j\omega_y\Omega z \\ -j\omega_x\Omega z & -j\omega_y\Omega z & (3-4\nu)\Omega + \Omega^2 z \end{bmatrix}. \tag{A.12}$$

For the strains

$$\bar{\varepsilon} = T_{\varepsilon u_0}\bar{u}_0,$$

with

$$T_{\varepsilon u_0} = \frac{e^{-z\Omega}}{(3-4\nu)\Omega}$$

$$\times \begin{bmatrix} j\omega_x\left((3-4\nu)\Omega - \omega_x^2 z\right) & -j\omega_x^2\omega_y z & \Omega\omega_x^2 z \\ -j\omega_x\omega_y^2 z & j\omega_y\left((3-4\nu)\Omega - \omega_y^2 z\right) & \Omega\omega_y^2 z \\ -j\Omega\omega_x\left(1-\Omega z\right) & -j\Omega\omega_y\left(1-\Omega z\right) & -\Omega^2\left(2(1-2\nu) + \Omega z\right) \\ \frac{1}{2}\omega_y\left((3-4\nu)\Omega - 2\omega_x^2 z\right) & \frac{1}{2}\omega_x\left((3-4\nu)\Omega - 2\omega_y^2 z\right) & \Omega\omega_x\omega_y z \\ -\frac{1}{2}\left((3-4\nu)\Omega^2 + \omega_x^2(1-2\Omega z)\right) & -\frac{1}{2}\omega_x\omega_y(1-2z\Omega) & j\Omega\omega_x(1-2\nu) + \Omega z) \\ -\frac{1}{2}\omega_x\omega_y(1-2z\Omega) & -\frac{1}{2}\left((3-4\nu)\Omega^2 + \omega_y^2(1-2\Omega z)\right) & j\Omega\omega_x(1-2\nu) + \Omega z) \end{bmatrix} \tag{A.13}$$

and for the stresses

$$\bar{\sigma} = T_{\sigma u_0}\bar{u}_0,$$

with

$$T_{\sigma u_0} = \frac{2\mu e^{-z\Omega}}{(3-4\nu)\Omega}$$

$$\times \begin{bmatrix} j\omega_x\left((3-2\nu)\Omega - \omega_x^2 z\right) & j\omega_y\left(2\nu\Omega - \omega_x^2 z\right) & -\Omega\left(2\nu\Omega - \omega_x^2 z\right) \\ j\omega_x\left(2\nu\Omega - \omega_y^2 z\right) & j\omega_y\left((3-2\nu)\Omega - \omega_y^2 z\right) & -\Omega\left(2\nu\Omega - \omega_y^2 z\right) \\ -j\Omega\omega_x(1-2\nu - \Omega z) & -j\Omega\omega_y(1-2\nu - \Omega z) & -\Omega^2\left(2(1-\nu) + \Omega z\right) \\ \frac{1}{2}\omega_y\left((3-4\nu)\Omega - 2\omega_x^2 z\right) & \frac{1}{2}\omega_x\left((3-4\nu)\Omega - 2\omega_y^2 z\right) & \Omega\omega_x\omega_y z \\ -\frac{1}{2}\left((3-4\nu)\Omega^2 + \omega_x^2(1-2\Omega z)\right) & -\frac{1}{2}\omega_x\omega_y(1-2\Omega z) & j\Omega\omega_x(1-2\nu + \Omega z) \\ -\frac{1}{2}\omega_x\omega_y(1-2\Omega z) & -\frac{1}{2}\left((3-4\nu)\Omega^2 + \omega_y^2(1-2\Omega z)\right) & j\Omega\omega_y(1-2\nu + \Omega z) \end{bmatrix} \tag{A.14}$$

Finally for the mean normal stress we obtain

$$\bar{p}_n = T_{p_n u_0}\bar{u}_0,$$

with

$$T_{p_n u_0} = \frac{2E}{3} \frac{e^{-z\Omega}}{(3 - 4\nu)} \begin{bmatrix} j\omega_x & j\omega_y & \Omega \end{bmatrix} \qquad (A.15)$$

.

Appendix B

Effects of Finite Sensor Size on a Stress Field

If the sensor is of a finite size, it will disturb the stress field around it and one may need to corrects for these effects at that sensor. There is also the possibility that the sensor will disturb the sensor field in such a way that it will effect other sensors close by. It is therefore appropriate to assess how close sensors of finite size can be placed without disturbing each other. We do that by investigating how a spherical inclusion with different elastic properties than the medium around it reacts to an external stressfield.

We assume that the stress field is uniform away from the inclusion or so slowly varying that it can be assumed to be uniform. It then follows from dimensional analysis that, under classical elasticity assumptions, the stress intensity factor[1] is independent of the absolute size of the inclusion and only depends on its geometrical form [24].

Here below we give the solutions for a cavity[2] under 3 different loading conditions, i.e. under (i) uniform stress, (ii) uniaxial stress, and (iii) pure shear.

---

[1] The *stress intensity factor* is defined as the ratio of the maximum stress to the uniform stress at a distance.

[2] If the inclusion is not a cavity but an inclusion of a different material, the behavior will be quite similar with slightly lower stress intensity factors [24].
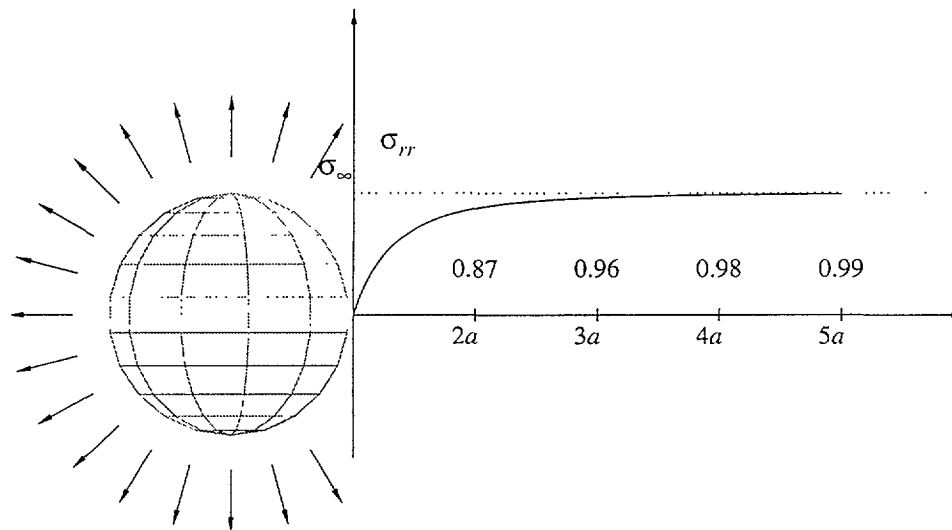
Figure B-1: Shows the effects of an inclusion on a uniform stress field. The plot shows the radial stress given by, $\sigma_{RR} = \sigma_\infty \left(1 - a^3/R^3\right)$.

1. Uniform Stress

In the case of a uniform stress, the radial stress, σ_{RR} and the hoop stresses $\sigma_{\theta\theta}$, $\sigma_{\phi\phi}$ are

$$\sigma_{RR} = \sigma_\infty \left(1 - \frac{a^3}{R^3}\right) \qquad \text{and} \qquad \sigma_{\phi\phi} = \sigma_{\theta\theta} = \sigma_\infty \left(1 + \frac{1}{2}\frac{a^3}{R^3}\right)$$

which means a stress intensity factor of 3/2 for the hoop stresses. The radial stress is plotted in Fig. B-1 and there we see that the error is 4% at $R = 3a$, and 1% at $R = 5a$ where R is the distance form the center of the inclusion and a is its radius. By that measure, sensors would have to be put 5 diameters apart for less than 2% cross-sensor error.

2. Uniaxial Stress

In the case when the external loading is a uniaxial tension σ_∞ applied at infinity in the z-direction then the most significant variations are observed in the normal stress on the plane perpendicular to the
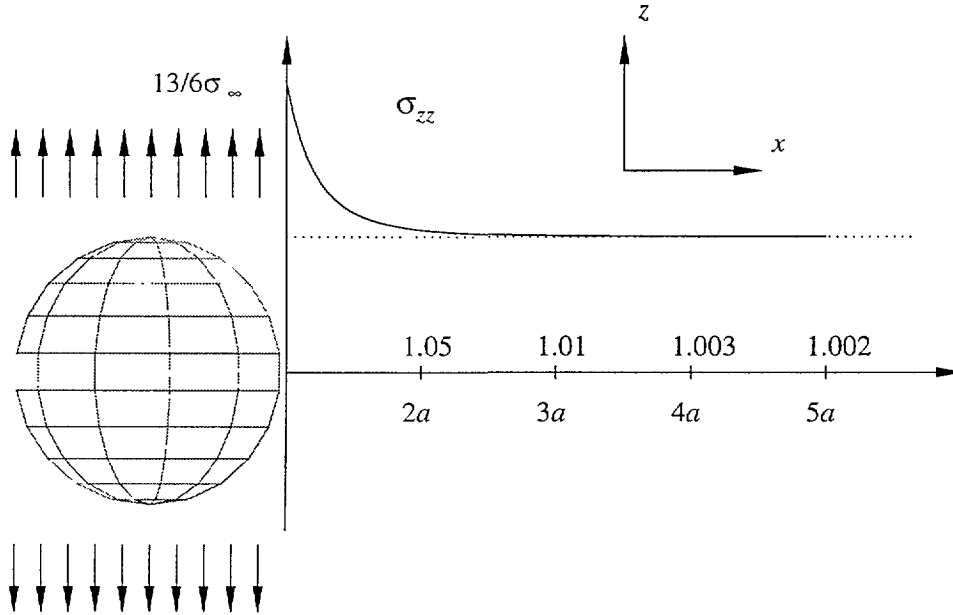
Uniaxial Tension

Figure B-2: Shows the effects of an inclusion on an uniaxial stress field. The plot shows the z-normal stress given by, $\sigma_{zz} = \left(1 + a^3/(6R^3) + a^5/R^5\right)$.

loading, i.e. σ_{zz}, which becomes

$$
\begin{aligned}
\sigma_{zz} &= \sigma_\infty \left(1 + \frac{1}{2}\frac{4-5\nu}{7-5\nu}\frac{a^3}{R^3} + \frac{9}{2}\frac{1}{7-5\nu}\frac{a^5}{R^5}\right) \\
&= \sigma_\infty \left(1 + \frac{1}{6}\frac{a^3}{R^3} + \frac{a^5}{R^5}\right) \qquad \text{for} \quad \nu = 0.5
\end{aligned}
$$

which means a stress intensity factor of 13/6. The σ_{zz} stress is plotted in Fig. B-2 and there it can be seen that the error is 1% for $R = 3a$ and 0.2% for $R = 5a$. The effect on the stressfield are therefore not spreading as far as in the case of a uniform stress.

3. Pure Shear

If uniform tension is applied in the z-direction and and uniform pressure is applied in x-direction the net effect is pure shear in the planes $x = \pm z$, ie. $\sigma_{xz} = \sigma_\infty$ [49]. It has a maximum at $x = z = 0, y = \pm a$
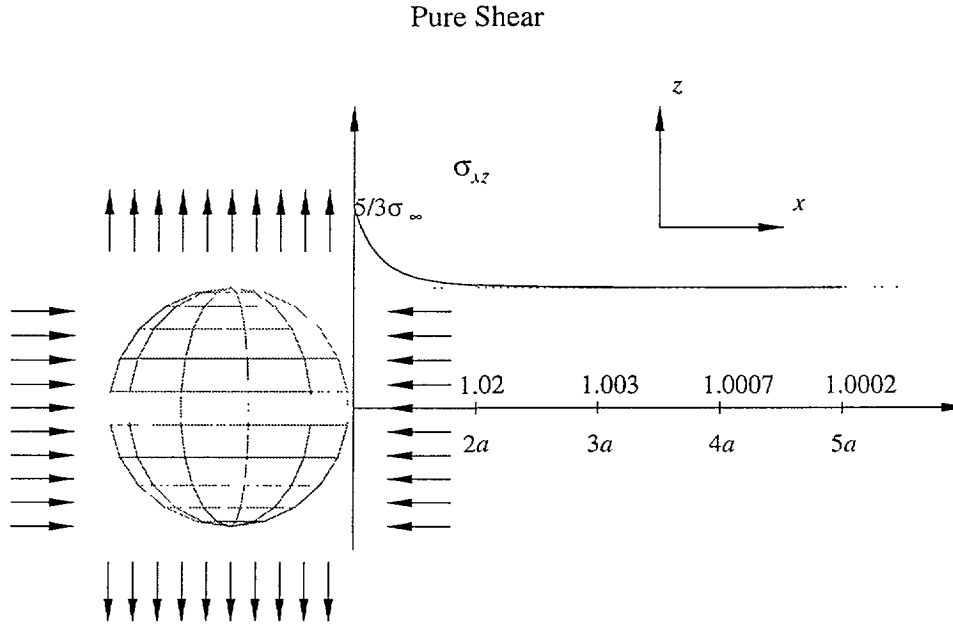
Figure B-3: Shows the effects of an inclusion on pure shear. The plot shows the xz-shear stress along the y-axis, given by $\sigma_{xz} = \sigma_\infty \left(1 + 2a^5/(3R^5)\right)$. We observe that the disturbance is more localized than the ones in Figs. B-2 and B-1

and along the y-axis the solution is

$$
\begin{aligned}
\sigma_{zz} &= \sigma_\infty \left(1 - \frac{5(1-2\nu)}{7-5\nu} \frac{a^3}{R^3} + \frac{3}{7-5\nu} \frac{a^5}{R^5} \right) \\
&= \sigma_\infty \left(1 + \frac{2}{3} \frac{a^5}{R^5} \right) \quad \text{for} \quad \nu = 0.5
\end{aligned}
$$

which means a stress intensity factor of $3/2$. The σ_{xz} stress is plotted in Fig. B-3 and there it can be seen that the error is only 0.3% for $R = 3a$ and 0.02% for $R = 5a$. These results indicate that under the assumptions given, shear sensors are less sensitive than normal stress sensors to disturbances caused by their own finite size. We note that this observation is analogous with the observations made in section 1 regarding the lowpass properties of the mean normal stress (spread out) and the bandpass properties of the shear strain (localized).

In summary the results of the above are that the disturbances of the stress field caused by finite size sensors estimated using solutions of spherical inclusions in an infinite medium have the following characteristics:

- The magnitude of the effect depends only on the geometry of the sensor, not on its dimension.

- Sensors from a material that is stiffer than the surrounding medium have generally a lesser effect than sensor made from softer materials.

- The effects on the mean normal pressure die out $\propto (a/R)^3$ where a is the radius of the sensor and R is the distance from its center.

- The effects on shear stress die out as $\propto (a/R)^5$, and shear sensors are therefore less likely to be sensitive to the effects of nearby sensors.

Appendix C

Derivation of Dynamic Transfer Function Matrices

In order to solve the nine partial differential equations given by Eqs. (4.1) and (4.2) in chapter 4 section 2.1, we make use of the triple Fourier-Laplace transform defined by

$$\bar{f}(\omega_x, \omega_y, s) = \int_0^{+\infty} \int\int_{-\infty}^{+\infty} f(x, y, \tau_1) e^{-j(\omega_x x + \omega_y y) + s\tau_1} dx dy d\tau_1$$

$$f(x, y, \tau_1) = \frac{1}{8\pi^3 j} \int_{\gamma - j\infty}^{\gamma + j\infty} \int\int_{-\infty}^{+\infty} \bar{f}(\omega_x, \omega_y, s) e^{j(\omega_x x + \omega_y y) + s\tau_1} d\omega_x d\omega_y ds.$$

(C.1)

Assuming that all the integrals are well behaved as $|x, y, \tau_1| \to \infty$, we apply this transform to each term in the equations in (4.1) and (4.2). Then the operator $\frac{\partial}{\partial x}$ is replaced by multiplication by $j\omega_x$, similarly $\frac{\partial}{\partial y}$ is replaced by multiplication by $j\omega_y$. We further use D to notate $\frac{\partial}{\partial z}$ and assuming zero initial conditions at $t = 0$, we replace $\frac{\partial}{\partial \tau_1}$ by s. The 9 partial differential equations have now been transformed into ordinary differential equations in D. ($\frac{\partial}{\partial z}$ becomes $\frac{d}{dz}$). We write (4.1) and (4.2) using matrix-vector notation as

$$K^T \bar{\sigma} = \beta^2 s^2 \bar{u}$$

and

$$\bar{\sigma} = C\bar{\varepsilon} \quad \bar{\varepsilon} = K\bar{u}$$

where

$$K^T = \begin{bmatrix} j\omega_x & 0 & 0 & j\omega_y & D & 0 \\ 0 & j\omega_y & 0 & j\omega_x & 0 & D \\ 0 & 0 & D & 0 & j\omega_x & j\omega_y \end{bmatrix},$$

147

$$C = \begin{bmatrix} \lambda + 2\mu & \lambda & \lambda & 0 & 0 & 0 \\ \lambda & \lambda + 2\mu & \lambda & 0 & 0 & 0 \\ \lambda & \lambda & \lambda + 2\mu & 0 & 0 & 0 \\ 0 & 0 & 0 & \mu & 0 & 0 \\ 0 & 0 & 0 & 0 & \mu & 0 \\ 0 & 0 & 0 & 0 & 0 & \mu \end{bmatrix},$$

$\bar{\sigma} = [\bar{\sigma}_{xx}, \bar{\sigma}_{yy}, \bar{\sigma}_{zz}, \bar{\sigma}_{xy}, \bar{\sigma}_{xz}, \bar{\sigma}_{yz}]^T$, $\bar{u} = [\bar{u}_x, \bar{u}_y, \bar{u}_z]^T$, and $\bar{\varepsilon} = [\bar{\varepsilon}_{xx}, \bar{\varepsilon}_{yy}, \bar{\varepsilon}_{zz}, \bar{\gamma}_{xy}, \bar{\gamma}_{xz}, \bar{\gamma}_{yz}]^T$ [1]. Eliminating $\bar{\sigma}$ and $\bar{\varepsilon}$ we get

$$\left[K^T C K - \beta^2 s^2 I\right] \bar{u} = 0 \qquad (C.2)$$

where

$$K^T C K = \begin{bmatrix} D^2 - \Omega^2 - \omega_x^2(\beta^2 - 1) & -\omega_x \omega_y(\beta^2 - 1) & j\omega_x(\beta^2 - 1)D \\ -\omega_x \omega_y(\beta^2 - 1) & D^2 - \Omega^2 - \omega_y^2(\beta^2 - 1) & j\omega_y(\beta^2 - 1)D \\ j\omega_x(\beta^2 - 1)D & j\omega_y(\beta^2 - 1)D & \beta^2(D^2 - \Omega^2) + \Omega^2\beta^2 \end{bmatrix}$$

with $\Omega^2 = \omega_x^2 + \omega_y^2$ and $\beta^2 = (\lambda + 2\mu)/\mu$. The determinant of this matrix is

$$\det(K^T C K - \beta^2 s^2 I) = \beta^2 \mu^3 \left(D^2 - n_1^2\right) \left(D^2 - n_2^2\right)^2$$

where

$$n_1 = \left(\Omega^2 + s^2\right)^{1/2} \quad n_2 = \left(\Omega^2 + \beta^2 s^2\right)^{1/2}$$

This system therefore has non-trivial solutions of the form

$$u_i = A_i e^{-n_1 z} + (B_i + C_i z)e^{-n_2 z} \quad i = x, y, z$$

where we have used the condition that displacements stay finite as $z \to \infty$ to include only terms with negative exponents. Substituting this back into (C.2) we further get that

$$\begin{aligned} A_z &= \frac{1}{\Omega}\left(j\omega_x A_x + j\omega_y A_y + B_z \frac{\beta^2 + 1}{\beta^2 - 1}\right) \\ B_x &= -\frac{j\omega_x}{\Omega} B_z \\ B_y &= -\frac{j\omega_y}{\Omega} B_z \\ C_x &= C_y = C_z = 0 \end{aligned}$$

---

[1] For the sake of symmetry we use the equivalent definition of strain: $\gamma_{ij} = 2\varepsilon_{ij}, \quad i \neq j$.

which gives

$$u_x = -A_z \frac{j\omega_x}{n_1} e^{-n_1 z} + B_x e^{-n_2 z}$$

$$u_y = -A_z \frac{j\omega_y}{n_1} e^{-n_1 z} + B_y e^{-n_2 z} \tag{C.3}$$

$$u_z = A_z e^{-n_1 z} + \frac{j}{n_2} \left(\omega_x B_x + j\omega_y B_y \right) e^{-n_2 z}.$$

The three still unknown constants, A_z, B_x, B_y will be determined by boundary conditions at $z = 0$.

TFMs with Tractions as Inputs

We will first pose the boundary conditions in terms of the load distributions on the surface of of the solid, defined as the infinite halfspace, defined as $z \geq 0$. The z-normal stress σ_{zz} at $z = 0$ equals normal load on the surface, $z = 0$, f_{z_0} and similarly the shear stresses σ_{xz} and σ_{yz} at $z = 0$ equal the shear loads on the same surface, f_{x_0} and f_{y_0} respectively. The relevant stresses can be derived by substituting (C.3) into (4.2) and then become

$$\frac{\sigma_{xz}}{\mu} = A_z 2j\omega_x e^{-n_1 z} - \frac{\omega_x \omega_y B_y + (n_2^2 + \omega_x^2) B_x}{n_2} e^{-n_2 z}$$

$$\frac{\sigma_{yz}}{\mu} = A_z 2j\omega_y e^{-n_1 z} - \frac{\omega_x \omega_y B_x + (n_2^2 + \omega_x^2) B_y}{n_2} e^{-n_2 z}$$

$$\frac{\sigma_{zz}}{\mu} = -A_z \frac{2\Omega^2 + s^2 \beta^2}{n_1} e^{-n_1 z} - 2j \left(\omega_x B_x + \omega_y B_y \right) e^{-n_2 z}.$$

It is convenient to solve for each load case separately and state the solution in terms of a Transfer Function Matrix (TFM) which finally becomes

$$T_{fu} = \begin{bmatrix} \omega_x^2 n_2 & \omega_x \omega_y n_2 & j\omega_x n_3^2 \\[2mm] \omega_x \omega_y n_2 & \omega_y^2 n_2 & j\omega_y n_3^2 \\[2mm] j\omega_x n_1 n_2 & j\omega_y n_1 n_2 & -n_1 n_3^2 \end{bmatrix} \frac{e^{-n_1 z}}{2\mu F_3}$$

$$+ \begin{bmatrix} \omega_y^2 (2n_1 n_2 - n_3^2) - n_3^2 n_2^2 & \omega_x \omega_y (n_3^2 - 2n_1 n_2) & j\omega_x n_1 n_2^2 \\[2mm] \omega_x \omega_y (n_3^2 - 2n_1 n_2) & \omega_x^2 (2n_1 n_2 - n_3^2) - n_3^2 n_2^2 & j\omega_y n_1 n_2^2 \\[2mm] -j\omega_x n_2 n_3^2 & -j\omega_y n_2 n_3^2 & n_1 n_2 \Omega^2 \end{bmatrix} \frac{e^{-n_2 z}}{2\mu n_2 F_3} \tag{C.4}$$

149

where $n_3 = (\Omega^2 + \beta^2/2s^2)^{1/2}$ and $F_3 = n_3^4 - n_1 n_2 \Omega^2$. The strains are obtained using Eq. (4.3) and hence the TFM is

$$
T_{f\varepsilon} = \frac{e^{-n_1 z}}{2\mu F_3}
\begin{bmatrix}
j\omega_x^3 n_2 & \omega_x^2 \omega_y n_2 & -\omega_x^2 n_3^2 \\
j\omega_x \omega_y^2 n_2 & j\omega_y^3 n_2 & -\omega_y^2 n_3^2 \\
-j\omega_x n_1^2 n_2 & -j\omega_y n_1^2 n_2 & n_1^2 n_3^2 \\
j2\omega_x^2 \omega_y n_2 & j2\omega_x \omega_y^2 n_2 & -2\omega_x \omega_y n_3^2 \\
-2\omega_x^2 n_1 n_2 & -2\omega_x \omega_y n_1 n_2 & -j2\omega_x n_1 n_3^2 \\
-2\omega_x \omega_y n_1 n_2 & -2\omega_y^2 n_1 n_2 & -j2\omega_y n_1 n_3^2
\end{bmatrix}
+ \frac{e^{-n_2 z}}{2\mu n_2 F_3} \times
$$

$$
\begin{bmatrix}
j\omega_x(2\omega_y^2 n_1 n_2 - n_3^2(2n_3^2 - \omega_x^2)) & j\omega_x^2 \omega_y(n_3^2 - 2n_1 n_2) & \omega_x^2 n_1 n_2^2 \\
j\omega_x \omega_y^2(n_3^2 - 2n_1 n_2) & j\omega_y(2\omega_x^2 n_1 n_2 - n_3^2(2n_3^2 - \omega_y^2)) & \omega_y^2 n_1 n_2^2 \\
j\omega_x n_2^2 n_3^2 & j\omega_y n_2^2 n_3^2 & -n_1 n_2^2 \Omega^2 \\
j2\omega_y(n_1 n_2(\omega_y^2 - \omega_x^2) + n_3^2(\omega_x^2 - n_3^2)) & j2\omega_x(n_1 n_2(\omega_x^2 - \omega_y^2) + n_3^2(\omega_y^2 - n_3^2)) & 2\omega_x \omega_y n_1 n_2^2 \\
2n_2 n_3^4 - 2\omega_y^2 n_1 n_2^2 & 2\omega_x \omega_y n_1 n_2^2 & j2\omega_x n_1 n_2 n_3^2 \\
2\omega_x \omega_y n_1 n_2^2 & 2n_2 n_3^4 - 2\omega_x^2 n_1 n_2^2 & j2\omega_y n_1 n_2 n_3^2
\end{bmatrix}
\quad \text{(C.5)}
$$

and the stresses are obtained using Hooke's law in Eq. (4.2), hence

$$T_{f\sigma} = \frac{e^{-n_1 z}}{2F_3} \times$$

$$
\begin{bmatrix}
-j\omega_x n_2((\beta^2-2)s^2-2\omega_x^2) & -j\omega_y n_2((\beta^2-2)s^2-2\omega_x^2) & -((\beta^2-2)s^2-2\omega_x^2 n_3^2) \\
-j\omega_x n_2((\beta^2-2)s^2-2\omega_y^2) & -j\omega_y n_2((\beta^2-2)s^2-2\omega_y^2) & -((\beta^2-2)s^2-2\omega_y^2 n_3^2) \\
-2j\omega_x n_2 n_3^2 & -2j\omega_y n_2 n_3^2 & 2n_3^4 \\
j2\omega_x^2\omega_y n_2 & j2\omega_x\omega_y^2 n_2 & -2\omega_x\omega_y n_3^2 \\
-2\omega_x^2 n_1 n_2 & -2\omega_x\omega_y n_1 n_2 & -j2\omega_x n_1 n_3^2 \\
-2\omega_x\omega_y n_1 n_2 & -2\omega_y^2 n_1 n_2 & -j2\omega_y n_1 n_3^2
\end{bmatrix}
$$

$$+\frac{e^{-n_2 z}}{2n_2 F_3} \times$$

$$
\begin{bmatrix}
j2\omega_x(2\omega_y^2 n_1 n_2 - n_3^2(2n_3^2-\omega_x^2)) & j2\omega_x^2\omega_y(n_3^2-2n_1 n_2) & 2\omega_x^2 n_1 n_2^2 \\
j2\omega_x\omega_y^2(n_3^2-2n_1 n_2) & j2\omega_y(2\omega_x^2 n_1 n_2 - n_3^2(2n_3^2-\omega_y^2)) & 2\omega_y^2 n_1 n_2^2 \\
2j\omega_x n_2^2 n_3^2 & 2j\omega_y n_2^2 n_3^2 & -2n_1 n_2^2 \Omega^2 \\
j2\omega_y(n_1 n_2(\omega_y^2-\omega_x^2)+n_3^2(\omega_x^2-n_3^2)) & j2\omega_x(n_1 n_2(\omega_x^2-\omega_y^2)+n_3^2(\omega_y^2-n_3^2)) & 2\omega_x\omega_y n_1 n_2^2 \\
2n_2 n_3^4 - 2\omega_y^2 n_1 n_2^2 & 2\omega_x\omega_y n_1 n_2^2 & j2\omega_x n_1 n_2 n_3^2 \\
2\omega_x\omega_y n_1 n_2^2 & 2n_2 n_3^4 - 2\omega_x^2 n_1 n_2^2 & j2\omega_y n_1 n_2 n_3^2
\end{bmatrix}.
$$

$$(C.6)$$

The mean normal stress defined as $p_n = (\sigma_{xx} + \sigma_{yy} + \sigma_{zz})/3$ is then

$$T_{fp_n} = \begin{bmatrix} -j\omega_x n_2 & -j\omega_y n_2 & n_3^2 \end{bmatrix} \frac{3\beta^2-4}{3} \frac{s^2 e^{-n_1 z}}{2F_3}. \tag{C.7}$$

TFMs with Displacements as Inputs

When the displacement distribution on the surface is taken as inputs, we use Eq. (C.3) to solve for (A_z, B_x, B_y) which gives:

The TFM giving the subsurface displacements, $\overline{u} = T_{uu_0}\overline{u}_0$, as being

$$T_{uu_0} = \begin{bmatrix} \omega_x^2 & \omega_x\omega_y & j\omega_x n_2 \\ \omega_x\omega_y & \omega_y^2 & j\omega_y n_2 \\ j\omega_x n_1 & j\omega_y n_1 & n_1 n_2 \end{bmatrix} \frac{e^{-n_1 z} - e^{-n_2 z}}{\Omega^2 - n_1 n_2} + \begin{bmatrix} 1 & 0 & 0 \\ 0 & 1 & 0 \\ 0 & 0 & 1 \end{bmatrix} e^{-n_2 z}, \tag{C.8}$$

the TFM for the strains, $\bar{\varepsilon} = T_{u\varepsilon}\bar{u}_0$, as being

$$
T_{\varepsilon u_0} = \begin{bmatrix}
j\omega_x^3 & j\omega_x^2\omega_y & -\omega_x^2 n_2 \\
j\omega_x\omega_y^2 & j\omega_y^3 & -\omega_y^2 n_2 \\
-j\omega_x n_1^2 & -j\omega_y n_1^2 & n_1^2 n_2 \\
2j\omega_x^2\omega_y & 2j\omega_x\omega_y^2 & -2\omega_x\omega_y n_2 \\
-2\omega_x^2 n_1 & -2\omega_x\omega_y n_1 & -2j\omega_x n_1 n_2 \\
-2\omega_x\omega_y n_1 & -2\omega_y^2 n_1 & -2j\omega_y n_1 n_2
\end{bmatrix} \frac{e^{-n_1 z}}{\Omega^2 - n_1 n_2}
$$

$$
+ \begin{bmatrix}
j\omega_x(\omega_y^2 - n_1 n_2) & -j\omega_x^2\omega_y & \omega_x^2 n_2 \\
-j\omega_x\omega_y^2 & j\omega_y(\omega_x^2 - n_1 n_2) & \omega_y^2 n_2 \\
j\omega_x n_1 n_2 & j\omega_y n_1 n_2 & \Omega^2 n_2 \\
j\omega_y(\omega_y^2 - \omega_x^2 - n_1 n_2) & j\omega_x(\omega_x^2 - \omega_y^2 - n_1 n_2) & 2\omega_x\omega_y n_2 \\
n_1(n_2^2 - \omega_y^2) - \omega_y^2 n_2 & \omega_x\omega_y(n_1 + n_2) & j\omega_x(\Omega^2 + n_2^2) \\
\omega_x\omega_y(n_1 + n_2) & n_1(n_2^2 - \omega_x^2) - \omega_x^2 n_2 & j\omega_y(\Omega^2 + n_2^2)
\end{bmatrix} \frac{e^{-n_2 z}}{\Omega^2 - n_1 n_2},
$$

(C.9)

the TFM for the stress $\bar{\sigma} = T_{u\sigma}\bar{u}_0$, as being

$$
T_{\sigma u_0} = \begin{bmatrix}
j\omega_x(2\omega_x^2 + s^2(\beta^2 + 2)) & j\omega_y(2\omega_x^2 + s^2(\beta^2 + 2)) & -n_2(2\omega_x^2 + s^2(\beta^2 + 2)) \\
j\omega_x(2\omega_y^2 + s^2(\beta^2 + 2)) & j\omega_y(2\omega_y^2 + s^2(\beta^2 + 2)) & -n_2(2\omega_y^2 + s^2(\beta^2 + 2)) \\
2j\omega_x n_3^2 & 2j\omega_y n_3^2 & -2n_2 n_3^2 \\
2j\omega_x^2\omega_y & 2j\omega_x\omega_y^2 & -2\omega_x\omega_y n_2 \\
-2\omega_x^2 n_1 & -2\omega_x\omega_y n_1 & -2j\omega_x n_1 n_2 \\
-2\omega_x\omega_y n_1 & -2\omega_y^2 n_1 & -2j\omega_y n_1 n_2
\end{bmatrix} \frac{\mu e^{-n_1 z}}{\Omega^2 - n_1 n_2}
$$

$$
+ \begin{bmatrix}
2j\omega_x(\omega_y^2 - n_1 n_2) & -2j\omega_x^2\omega_y & 2\omega_x^2 n_2 \\
-2j\omega_x\omega_y^2 & 2j\omega_y(\omega_x^2 - n_1 n_2) & 2\omega_y^2 n_2 \\
2j\omega_x n_1 n_2 & 2j\omega_y n_1 n_2 & 2\Omega^2 n_2 \\
j\omega_x(\omega_y^2 - \omega_x^2 - n_1 n_2) & j\omega_y(\omega_x^2 - \omega_y^2 - n_1 n_2) & 2\omega_x\omega_y n_2 \\
2n_3^2 n_1 - \omega_y^2(n_1 + n_2) & \omega_x\omega_y(n_1 + n_2) & j\omega_x(\Omega^2 + n_2^2) \\
\omega_x\omega_y n_1 n_2 & 2n_3^2 n_1 - \omega_x^2(n_1 + n_2) & j\omega_y(\Omega^2 + n_2^2)
\end{bmatrix} \frac{\mu e^{-n_2 z}}{\Omega^2 - n_1 n_2},
$$

(C.10)

and finally, the TFM for the mean normal stress, $\bar{p}_n = T_{p_n u_0}\bar{u}_0$, as being

$$
T_{p_n u_0} = \begin{bmatrix} j\omega_x & j\omega_y & n_2 \end{bmatrix} \frac{\mu e^{-n_1 z}}{\Omega^2 - n_1 n_2} \frac{3\beta^2 - 4}{3}.
$$

(C.11)

The variable s in the above equations is the Laplace variable corresponding to the scaled τ_1 time variable. To get the solution in terms of a Laplace variable corresponding to the actual time, t, we need only to replace s^2 everywhere with $c_p^{-2}s'^2$ so that we will get (after we drop the prime)

$$n_1 = \sqrt{\Omega^2 + c_p^{-2}s^2} \qquad n_s = \sqrt{\Omega^2 + c_s^{-2}s^2} \qquad n_3 = \sqrt{\Omega^2 + c_p^{-2}s^2/2}.$$

Appendix D

Retrival of the Static Solution

The dynamic solution should approach the static solution when $s \to 0$, but since both the denominator and the numerator vanish for $s = 0$ we use Taylor expansion for the denominator and also the $(e^{-n_2 z} - e^{-n_1 z})$ term around $s = 0$. Writing each step out explicitly we get

$$
\begin{aligned}
n_1 &= \sqrt{\Omega^2 + c_p^{-2} s^2} &&= \Omega(1 + \tfrac{1}{2} c_p^{-2} s^2) + O(s^4) \\
n_2 &= \sqrt{\Omega^2 + c_{sh}^{-2} s^2} &&= \Omega(1 + \tfrac{1}{2} c_{sh}^{-2} s^2) + O(s^4)
\end{aligned}
$$

and hence the denominator becomes

$$
\begin{aligned}
F_3 &= (\Omega^2 + \tfrac{1}{2} c_{sh}^{-2} s^2)^2 - \Omega^2 n_1 n_2 \\
&= \Omega^4 + \Omega^2 c_{sh}^{-2} s^2 - \Omega^2(\Omega^2 + \tfrac{1}{2} c_{sh}^{-2} s^2 + \tfrac{1}{2} c_p^{-2} s^2) + O(s^4) \\
&= \tfrac{1}{2} \Omega^2 s^2 (c_{sh}^{-2} - c_p^{-2}) + O(s^4),
\end{aligned}
$$

and the numerator term

$$
\begin{aligned}
(e^{-n_2 z} - e^{-n_1 z}) &= \exp\left(-\Omega z(1 + \tfrac{1}{2} c_{sh}^{-2} s^2 \Omega^{-2})\right) - \exp\left(-\Omega z(1 + \tfrac{1}{2} c_p^{-2} s^2 \Omega^{-2})\right) + O(s^4) \\
&= e^{-\Omega z} \left[\exp\left(-\tfrac{1}{2} c_{sh}^{-2} s^2 \Omega^{-1} z\right) - \exp\left(-\tfrac{1}{2} c_p^{-2} s^2 \Omega^{-1} z\right)\right] + O(s^4) \\
&= e^{-\Omega z} \left(1 - \tfrac{1}{2} c_{sh}^{-2} s^2 \Omega^{-1} z - (1 - \tfrac{1}{2} c_p^{-2} s^2 \Omega^{-1} z)\right) + O(s^4) \\
&= \tfrac{1}{2} e^{-\Omega z} s^2 \Omega^{-1} z (c_p^{-2} - c_{sh}^{-2}) + O(s^4).
\end{aligned}
$$

Substituting this into Eq. 4.5, we get for the mean normal stress

$$
\begin{aligned}
\lim_{s\to 0} T_{p_n f_z} &= \frac{3\beta^2 - 4}{3\beta^2} \frac{s^2}{c_{sh}^2} \frac{(\Omega^2 + \frac{1}{2}c_{sh}^{-2}s^2)e^{-n_1 z}}{\Omega^2 s^2 (c_{sh}^{-2} - c_p^{-2})} \\
&= \frac{3\beta^2 - 4}{3(\beta^2 - 1)} e^{-\Omega z} \\
&= \frac{2E}{3} \frac{1}{2\mu} e^{-\Omega z}
\end{aligned}
$$

and the shear strain

$$
\begin{aligned}
\lim_{s\to 0} T_{\epsilon_{xz} f_z} &= \frac{1}{2\mu} \frac{j\omega_x \Omega^3 \left(\frac{1}{2}s^2\Omega^{-1}e^{-\Omega z}z(c_p^{-2} - c_{sh}^{-2})\right)}{\frac{1}{2}\Omega^2 s^2 (c_{sh}^{-2} - c_p^{-2})} \\
&= \frac{1}{2\mu} j\omega_x z e^{-\Omega z}
\end{aligned}
$$

Appendix E

The Kalman Filter With Static Load

Since the Wiener filter given in chapter 3 and the Kalman filter given in chapter 4, minimize the same error measure, they should become identical when the (loads) signals become static. This can be seen, most easily, by using the discontinuous-time version of the Kalman filter under the assumption that the input is an unknown constant. In this case the Kalman filter estimate is given by

$$
\begin{aligned}
\widehat{\widetilde{\xi}} &= K\widetilde{\zeta} \\
K &= PC^*R^{-1} \\
P^{-1} &= P_0^{-1} + C^*R^{-1}C
\end{aligned}
\tag{E.1}
$$

We identify C as the static TFM $T(\omega_x, \omega_y, z)$, since it is the encoding solution relating the input and the state vector, which only contains the sensor output under static conditions. Similarly we note that in the static case the sensor noise intensity matrix $R(\omega_x, \omega_y)$ is the power spectrum matrix for the sensor noise, $\mathcal{P}_N(\omega_x, \omega_y)$, also the initial covariance estimate, $P_0(\omega_x, \omega_y)$ is the power spectrum matrix for the solution $\mathcal{P}_S(\omega_x, \omega_y)$, or $R = \mathcal{P}_n$ and $P_0 = \mathcal{P}_S$. Substituting the above into the equations in Eq. (E.1) and combining we finally obtain

$$
\begin{aligned}
\widehat{\widetilde{\xi}} &= \left[\mathcal{P}_S^{-1} + T^*\mathcal{P}_N^{-1}T\right]^{-1} T^*\mathcal{P}_N^{-1}\widetilde{\zeta} \\
&= \mathcal{P}_S\left[\mathcal{P}_N + T^*\mathcal{P}_S T\right]^{-1} T^*\widetilde{\zeta}
\end{aligned}
$$

which we recognize as the Wiener filter derived in [38, 80] and used for the static case in chapter 3.

Appendix F

General Statement of the Decoding Problem

Problem Statement: Given a 3D sensor signal $S = [S1, S2, S3]^T$, a function of the strain tensor at the sensor location, what conditions does it have to satisfy in order to be suitable[1] for decoding.

Remark: This approach, of assuming a 3D loading and a 3D sensor signal makes it necessary to consider strain measures in sets of three and one can therefore not answer questions such as: Is strain energy density suitable as relevant stimulus. (One will need to specify two additional strain measures.)

Assumptions

A1 The sensors form a continuous 2D sheet that is located in some sense parallel to the contact surface and both are anchored at an outer boundary where boundary conditions are known. (The boundary is at infinity for the infinite halfspace.)

A2 We further assume that the displacements and strains are parametrized everywhere by three variables (x, y, z), z being constant for both the surface and the sensor sheet (depth). We can then write the sensor signal as $S = S(u_i, u_{i,j})$ where $i, j = x, y, z$ and $u_{i,j}$ is the partial derivative of u_i wrt. j (e.g. $\partial u_x / \partial z = u_{x,z}$).

---

[1]By 'suitable for decoding' we mean that there is a one-to-one mapping between all allowable traction distributions and sensor distributions.

A3 Finally, we assume that the sensor sheet is sufficiently close to the surface so that there is a one-to-one relationship between surface displacements and the ones at the sensor depth.

Conditions: A sensor signal will be suitable for decoding if it satisfies the following conditions:

C1 The relation $S = S(u_i, u_{i,j})$ $\quad i,j = x,y,z$ can be integrated wrt. z using the encoding solution[2] so that it becomes $S' = S'(u_i, u_{i,k})$ $\quad i = x,y,z$ $\quad k = x,y$.

C2 The relation $S' = S'(u_i, u_{i,k})$ is integrable wrt. x,y giving $S'' = S''(u_i)$ $i = x,y,z$.

C3 This relation, S'', has to invertable, i.e. there exists a function, S''^{-1}, such that $u = [u_x, u_y, u_z]^T = S''^{-1}(u)$.

Remark: Condition C2 is different from C1 as does not need the encoding solution, but utilizes the fact that the integrand is known over all the integration domain and at the boundary. It is therefore a condition on the sensor signal independent of the particular shape or mechanical composition of the fingerpad.

---

[2]By "the encoding solution" we mean the model of the fingerpad that given the displacements at one depth gives the displacements and also strains at all depths and hence the sensor signal S for all z.

Bibliography

[1] F. Arman and J.K. Aggarwal. "Model-Based object recognition in dense-range images - a review". *ACM Computing Surveys*, 24(1):5–43, 1993.

[2] H. Asada and J.E. Slotine. *"Robot analysis and control"*. John Wiley and Sons, 1986.

[3] P.J. Besl and R.C. Jain. "Three-Dimensional object recognition". *Computing Surveys*, 17(1):75–145, 1985.

[4] F.P. Bowden and D. Tabor. *"Friction and lubrication of solids, parts I-II"*. Oxford University Press, London, 1964.

[5] R.L. Bracewell. *"The Fourier Transform and Its Applications"*. McGraw-Hill Book Company, New York, 1978.

[6] R.G. Brown and P.Y.C. Hwang. *"Introduction to random signals and applied kalman filtering"*. John Wiley and sons, New York, 1992.

[7] M. Buss, H. Hashimoto, and J.B. Moore. "Dextrous hand grasping force optimization". *IEEE transactions on robotics and automation*, 12(3):406–417, 1996.

[8] H.H. Calvit. "Numerical solution of the problem of impact of a rigid sphere onto a linear viscoelastic half-space and comparison with experiment". *International Journal of Solids and Structures*, 3:951–966, 1960.

[9] A. Cameron, R. Daniel, and H. Durrant-Whyte. "Touch and motion". In *Proceedings of IEEE Conference on Robotics & Automation*, pages 1062–1067, Philadelphia, PA, 1988.

[10] K.R. Castleman. *"Digital Image Processing"*. Prentice-Hall, New Jersey, 1979.

[11] J.E. Colgate and N. Hogan. "Robust control of dynamically interacting systems". *International Journal of Control*, 48:65–88, 1988.

[12] C.E. Connor, S.S. Hsiao, J.R. Phillips, and K.O. Johnson. "Tactile roughness: Neural codes that account for psychophysical magnitude estimates". *The Journal of Neuroscience*, 10(12):3823–3836, 1990.

[13] K. Dandekar. *"Role of Mechanics in Tactile Sensing og Shape"*. PhD thesis, MIT, 1995.

[14] H. Deresiewicz. "Oblique contact of non-spherical bodies". *Trans. ASME, Journal of Applied Mechanics*, 24, 1957.

[15] G. Eason. "Dynamical problems of the theory of elasticity". In *"Application of Integral Transforms in the Theory of Elasticity"*, Wien, 1975. Springer - Verlag.

[16] G. Eason, J. Fulton, and I.N. Sneddon. "The generation of waves in an infinite elastic solid by variable body forces". *Phil. Trans. A.*, 248:548–607, 1956.

[17] R.E. Ellis and M. Qin. "Singular-Value and finite-element analysis of tactile shape recognition". In *Proceedings of IEEE Conference on Robotics & Automation*, pages 2529–2535, 1994.

[18] R.S. Fearing. "Tactile sensing mechanisms". *The International Journal of Robotics Research*, 9:3–23, 1990.

[19] R.S. Fearing. "Planar elasticity for tactile sensing". In *Advanced Tactile Sensing for Robotics, Editor: H.R. Nicholls*. World Scientific, 1992.

[20] R.S. Fearing and J.M. Hollerback. "Basic solid mechanics for tactile sensing. *Int. J. of Robotics Res*, 4(3):40–54, 1984.

[21] N.P. Galatsanos and R.T. Chin. "Digital restoration of multichannel images". *IEEE Transactions on Accoustics, Speech, and Signal Processing*, 37:415–421, 1989.

[22] N.P. Galatsanos, A.K. Katsaggelos, R.T. Chin, and A.D. Hillery. "Least squares restoration of multichannel images". *IEEE Transactions Signal Processing*, 39:2222–2252, 1991.

[23] G.M.L. Gladwell. *"Contact Problems in the Classical Theory of Elasticity."*. Sijthoff and Noordhoff, Alphen aan den Rijn, 1980.

[24] J.N. Goodier. "Concentration of stress around spherical and cylindrical inclusions and flaws". *Trans ASME*, 55:39–44, 1933.

[25] J.A. Greenwood. "A unified theory of surface roughness". *Proceedings, Royal Society*, A393:133–157, 1984.

[26] N. Hogan. "Impedance control: An approach to manipulation, parts i-iii". *Journal of Dynamic Systems, Measurement and Control*, 107:1–24, March 1985.

[27] B.K.P. Horn. *"Robot Vision"*. MIT Press, Cambridge, Massachusetts, 1986.

[28] R. D. Howe and M. R. Cutkosky. "Dynamic tactile sensing: Perception of fine surface features with stress rate sensing". *IEEE Transactions on Robotics and Automation*, 9:140–151, 1993.

[29] S.S. Hsiao, K.O. Johnson, and L.A. Twombly. "Roughness coding in the somatosensory system". *Acta Physiologia*, 84:53–67, 1993.

[30] S.C. Hunter. "The hertz problem for a rigid spherical indenter and a viscoelastic half-space". *J. Mech. Phys. Solids*, 8:219–234, 1960.

[31] R.C. Jain and A.K. Jain. *"Analysis and Interpretation of Range Images"*. Springer-Verlag, New York, 1990.

[32] B.V. Jayawant. "Tactile sensing in robotics". *Journal of physics E: Scientific Instruments*, 22:604–692, 1989.

[33] K. O. Johnson and S.S Hsiao. "Neural mechanisms of tactual form and texture perception". *Annu. Rev. Neurosci.*, 315:227–250, 1992.

[34] K. O. Johnson and G. D. Lamb. "Neural patterns evoked by braille-like dot patterns in the monkey". *Journal of Physiology (London)*, 310:117–144, 1981.

[35] K. O. Johnson and J. R. Phillips. "Tactile spatial resolution. iii. a continuum model of skin predicting mechanoreceptor responses to bars, edges and gratings". *Journal of Neurophysiology*, 46:1204–1225, 1981.

[36] K.L. Johnson. *"Contact Mechanics"*. Cambridge University Press, Cambridge, 1985.

[37] T. Kailath. "A view of three decades of linear filtering theory". *IEEE Transactions on Information Theory*, IT-2:141–181, 1974.

[38] N.B. Karayiannis and A.N. Venetsanopoulos. "Regularizing theory in image restoration - the stabilizing functional approach". *IEEE Transactions on Accoustics, Speech, and Signal Processing*, 38:1155–1179, 1990.

[39] R.L Klatzky, S.J. Lederman, and V. Metzger. "Identifying objects by touch: An "expert system"". *Perception and Psychophysics*, 37(4):299–302, 1983.

[40] G.D. Lamb. "Tactile discrimination of textured surfaces: Peripherial neural coding in the monkey". *Journal of Physiology*, 338:567–587, 1983.

[41] R.H. Lamotte. Unpublished communication. 1996.

163

[42] S.J. Lederman. "Hand movements: A window into haptic object recognition". *Cognitive Psychology*, 19, 1987.

[43] S.J. Lederman, R.L. Klatzky, and D.T. Pawluk. "Lessons from the study of biological touch for robotic haptic sensing". In *Advanced Tactile Sensing for Robotics, Editor: H.R. Nicholls*. World Scientific, 1992.

[44] E.H. Lee and J.R.M. Radok. "The contact problem for viscoelastic bodies". *Trans. ASME Series E: Journal of Applied Mechanics*, 27, 1960.

[45] L. Ljung. *"System Identificaction: theory for the user"*. Prentice-Hall, New Jersey, 1987.

[46] M.S. Longuet-Higgins. Statistical properties of an isotropic random surface. *Philosophical Transactions of the Royal Society*, 250A, 1956.

[47] M.S. Longuet-Higgins. The statistical analysis of a random moving surface. *Philosophical Transactions of the Royal Society*, 249A, 1956.

[48] J.M. Loomis and S.J. Lederman. "Tactual perception". In *"Handbook of perception and human performance. Eds: K.R. Boff and J.P. Thomas"*, New York, 1986. John Wiley and Sons.

[49] A.E.H. Love. *"A Treatise on the mathematical theory of elasticity"*. Dover, New York, 1944.

[50] T. Mcinerney and D. Terzopoulos. "A finite element model for 3d shape reconstruction and nonrigid motion tracking". In *"ICCVP"*, 1993.

[51] G.F. Miller and H. Pursey. "The field and radiation impedance of mechanical radiators on the surface of a semi-infinite isotropic solid". *Proceedings, Royal Society*, A223:521–541, 1954.

[52] S.K. Mitter. *"Filtering and Stochastic Control: A Historical Perspective"*. Center for Intelligent Control Systems: Report No. 470, 1996.

[53] D.J. Montana. "The kinematics of contact and grasp". *The International Journal of Robotics Research*, 7(3):17–31, 1988.

[54] D.J. Montana. "Contact stability for two-fingered grasps". *IEEE transactions on robotics and automation*, 8(4):421–430, 1992.

[55] D.J. Montana. "The kinematics of multi-fingered manipulation". *IEEE transactions on robotics and automation*, 11(4):491–503, 1995.

[56] D.F. Moore. *"The friction and lubrication of elastomers"*. Pergamon Press, Oxford, 1972.

[57] R.M. Murray and S.S. Sastry. "Grasping and manipulation using multifingered robot hands". In *Proceedings of Symposia in Applied Mathematics: Volume 41 Robotics*, pages 91–128, Louisville, KY, 1990.

[58] P.R. Nayak. "Random process model of rough surfaces". *Transactions of the ASME: Journal of Lubrication Technology*, 93:398–407, 1971.

[59] H.R. Nicholls. "Tactile sensor design". In *"Advanced Tactile Sensing for Robotics, Editor: H.R. Nicholls"*, London, 1992. World Scientific.

[60] E.J. Nicolson and R.S Fearing. "Sensing capabilities of linear elastic cylindrical fingers". In *Proceedings of IEEE/RSJ Conference on Intelligent Robots & Systems*, pages 1062–1067, Yokohama, Japan, 1993.

[61] W. Nowacki. "Dynamics of elastic and viscoelastic systems". In *"Application of Integral Transforms in the Theory of Elasticity"*, Wien, 1975. Springer – Verlag.

[62] K. Ogata. *"Modern Control Engineering"*. Prentice-Hall, New Jersey, 1997.

[63] Y.C. Pati, D. Friedman, P.S.Krishnaprasad, C.T. Yao, and M.C. Peckerar. "Neural networks for tactile perception. In *Proceedings of IEEE Conference on Robotics & Automation*, pages 135–139, Philadelphia, PA, 1988.

[64] J. Rauch. *"Partial Differential Equations"*. Springer-Verlag, New York, 1991.

[65] D. De Rossi, A. Caiti, R. Bianchi, and G. Canepa. "Fine-Form tactile discrimination through inversion of data from a skin-like sensor. In *Proceedings of IEEE International Conference on Robotics & Automation*, pages 398–403, Sacramento, CA, 1991.

[66] A. Salisbury and D.A. Hills. "Some useful results in the classical hertz contact problem". *Journal of Strain Analysis*, 18:101–105, 1983.

[67] A. Salisbury and D.A. Hills. "Some useful results in the tangentially loaded hertzian contact problem". *Journal of Strain Analysis*, 18:107–110, 1983.

[68] K.B. Shimoga. "Finger force and touch feedback issues in dexterous telemanipulation". In *Proceedings of the NASA-CIRSSE International Conference on Intelligent Robotic Systems for Space Exploration*, Troy, New York, 1992.

[69] K.B. Shimoga. "Robot grasp synthesis: A survey". *The International Journal of Robotics Research*, 14(3):230–266, 1992.

[70] I. N. Sneddon. *"Fourier Transforms"*. McGraw-Hill, New York, 1951.

[71] I.N. Sneddon. "Integral transform methods for the solution of mixed boundary value problems in the classical theory of elastostatics". In *"Application of Integral Transforms in the Theory of Elasticity"*, Wien, 1975. Springer - Verlag.

[72] T.H. Speeter. "Three-dimensional finite element analysis of elastic continua for tactile sensing". *The International Journal of Robotics Research*, 11:1–19, 1992.

[73] M.A. Srinivasan. "Tactile sensing in humans and robots: Computational theory and algorithms". In *Newman Laboratory Technical Report*, Departmental of Mechanical Engineering, MIT, 1988.

[74] M.A. Srinivasan. "Haptic interfaces". In *Virtual Reality: Scientific and Technical Challenges, Eds: N.I. Durlach and A.S. Mavor, Report of the Committee on Virtual Reality Research and Development*. National Research Council,National Academy Press, 1994.

[75] M.A. Srinivasan and K. Dandekar. "An investigation of the mechanics of tactile sense using two dimensional models of the primate fingertip". *Journal of Biomechanical Engineering*, 118:48–55, 1996.

[76] S.S. Stevens and J.R. Harris. "The scaling of subjective roughness and smoothness". *Journal of Experimental Psychology*, 5, 1962.

[77] M.M. Taylor and S.J. Lederman. "Tactile roughness of groved surfaces: A model and the effect of friction". *Perception and Psychophysics*, 17(1), 1975.

[78] D. Terzopoulos. "Regularization of inverse visual problems involving discontinuities". *IEEE PAMI*, PAMI-8, 1986.

[79] T.R. Thomas. *"Rough Surfaces"*. Longman, New York, 1982.

[80] A. N. Tikhonov and V. Y. Arsenin. *"Solutions of Ill-Posed Problems."*. John Wiley and Sons, New York, 1977.

[81] S. P. Timoshenko and J.N. Goodier. *"Theory of Elasticity"*. McGraw-Hill, New York, 1970.

[82] T.C.T. Ting. "The contact stresses between a rigid indenter and a viscoelastic half-space". *Trans. ASME, Series E, Journal of applied mechanics*, 33, 1966.

[83] N.W. Tschoegl. *"The phenomenological theory of linear viscoelastic behavior: an introduction"*. Springer-Verlag, New York, 1989.

[84] C. L. van Doren. "A model of spatiotemporal tactile sensitivity linking psychophysics to tissue mechanics". *Journal of the Acoustic Society of America*, 85:2065–2080, 1989.

[85] W.H. Yang. "The contact problem for viscoelastic bodies". *Trans. ASME Series E: Journal of Applied Mechanics*, 33, 1966.

[86] D.C. Youla. "On the factorization of rational matrices". *IRE Trans. Inf. Th.*, IT-7, 1961.